# RECENT AND CONTEMPORARY CRUSTAL DEFORMATION IN EASTERN IRAN

A THESIS
SUBMITTED BY
ARSALAN MOHAJER-ASHJAI B.Sc., M.SC.

FOR THE DEGREE OF
DOCTOR OF PHILOSOPHY
OF
THE UNIVERSITY OF LONDON

THE DEPARTMENT OF GEOPHYSICS
IMPERIAL COLLEGE OF SCIENCE AND TECHNOLOGY
LONDON

JANUARY, 1975

## Abstract

Iran lies in a zone of active mountain building which forms a complex boundary between the Arabian and Eurasian crustal plates. In an attempt to gain a better understanding of current tectonic processes, and to investigate the applicability of the crustal micro-plate concept, geodetic, microearthquake and geological field studies have been made of certain major faults in the eastern part of the country, supplemented by studies of aerial photographs and ERTS 1 satellite imagery.

On geological and seismological grounds, attention was concentrated on the Dasht-e-Bayaz and Great Kavir (Doruneh) faults, which form the northern boundary of the Lut Block, a proposed micro-plate. A small number of geodetic networks, consisting of lines a kilometer or so in length spanning these faults, were constructed and measured in October 1971, May 1972 and November 1974 with a Mekometer, a highly accurate electro-optic distance-measuring instrument. Siting of these networks was aided by a complementary study of microearthquake activity, using portable smoked drum seismographs. This revealed considerable activity, exceeding 15 events per day in places, with a tendency for the greatest activity to be associated with the ends of the strike slip faults, where a concentration of stress might be expected on theoretical grounds. Eight well recorded shocks were located with accuracy of better than 1 km. in N. Kashmar and seven similar shocks in the Dasht-e-Bayaz areas. These plus other less accurately located shocks seem to be associated with a newly found fault in N. Kashmar and the Dasht-e-Bayaz fault respectively. Two composite fault plane solutions are also presented for these microearthquakes and low b values (about 0.5) were found from the recurrence curves obtained for different stations.

To provide a basis for interpreting these results, a detailed map of recent and former fault traces has been prepared, based on aerial and satellite photographs. The angular relationship of the recent fault trends revealed by these photographs, together with available information on Neogene folding and the source mechanisms of the major earthquakes occuring in the area, suggest a consistent NE-SW compression of the crust and an almost uniform strain distribution. This is consistent with the results of the geodetic study, where measurements across the Dasht-e-Bayaz fault revealed left-lateral displacement combined with extension in the NW-SE direction, also with a composite fault plane solution showing a dominant left-lateral movement with a N46E axis of compression.

Regional seismicity, internal deformation, dislocation lines cutting across the Lut Block, and low b values obtained from microearthquake studies, imply non-rigid behaviour of this proposed plate and, therefore, throw doubt on the micro-plate concept as an explanation of the observed recent and contemporary crustal deformation taking place in eastern Iran. Three regions near Birjand, Zahedan and Tabas are tentatively classified as the tectonic knots where major earthquakes might be expected in the future.

CONTENTS


| | | Page Nos. |
|---|---|---|
| ABSTRACT | ..... | 2 |
| CONTENTS | ..... | 3 |
| CHAPTER I | INTRODUCTION | |
| 1.1 | Presentation of the problem ..... | 6 |
| 1.2 | Methods of Investigation ..... | 13 |
| 1.3 | Brief outline of the chapters in this thesis .... | 20 |
| CHAPTER II | BACKGROUND INFORMATION ON THE AREA | |
| 2.1 | Regional introduction ..... | 23 |
| 2.2 | Physiography ..... | 24 |
| 2.3 | Previous studies ..... | 28 |
| 2.4 | A brief tectonic history ..... | 31 |
| CHAPTER III | GEODETIC MEASUREMENTS | |
| 3.1 | Introduction ..... | 35 |
| 3.2 | Advantages of the direct distance measurement used in this work ..... | 39 |
| 3.3 | Instrumentation : the Mekometer and its operation | 43 |
| 3.4 | Corrections applied to the Mekometer results ... | 47 |
| 3.5 | Geodetic data analysis ..... | 51 |
| 3.6 | The geodetic networks ..... | 56 |
| | 3.6.1 The Dasht-e-Bayaz network ..... | 57 |
| | 3.6.2 The Khalilabad network ..... | 61 |
| 3.8 | Results from the Dasht-e-Bayaz network ..... | 62 |

Page Nos.

CHAPTER IV MICROEARTHQUAKE STUDIES

4.1 Introduction ..... 71

4.2 Programme of microearthquake studies in eastern Iran ..... 77

4.3 Instrumentation ..... 81

4.4 Data analysis ..... 87

4.5 Microearthquake occurrence rates ..... 90

4.6 Estimation of magnitudes and regional seismicity curves ..... 100

4.7 Location methods for microearthquakes ..... 118

4.8 Hypocentre determination in eastern Iran ..... 121

4.9 Composite fault plane solution in eastern Iran ..... 129

CHAPTER V GEOMORPHIC STUDIES

5.1 New evidence on the extent and the nature of movement of the Great Kavir Fault ..... 138

5.2 The pattern of faulting of the Great Kavir Fault system ..... 140

5.3 Variations in the relative sense of movement along the Great Kavir Fault ..... 148

5.3.1 Sense of movement in the western section ..... 148

5.3.2 Longitudinal and shear strain components in the Quaternary alluvial deposits west of Dorumeh ..... 149

5.3.3 Sense of movement in the central section of the Great Kavir Fault ..... 162

Page Nos.

5.3.4 Sense of movement in the eastern section of the Great Kavir Fault ..... 166

5.4 Strike of the Great Kavir Fault ..... 179

5.5 The observed trend on the satellite imageries ..... 180

5.6 Evidence on a fossil plate boundary ..... 180

5.7 Discussion and conclusion ..... 181

CHAPTER VI DISCUSSIONS

6.1 Reflections on the rigidity of the Lut Block ..... 185

6.2 Dislocation theory and analysis of after-shocks in eastern Iran ..... 189

6.3 Significance of the observed low b values in the area ..... 194

6.4 A new interpretation of the seismicity of eastern Iran ..... 196

6.5 Variations of the maximum horizontal shortening and recent crustal deformation in eastern Iran .. 202

CHAPTER VII SUMMARY OF CONCLUSIONS, AND SUGGESTION FOR FURTHER STUDY

7.1 Conclusions ..... 208

7.2 Suggestions for further work ..... 211

APPENDIX 1 ..... 213

ACKNOWLEDGEMENTS ..... 217

CITED REFERENCES ..... 220

# CHAPTER I

# INTRODUCTION

## 1.1 Presentation of the problem

The concepts of plate tectonics have principally been established by the study of oceanic plate boundaries. The seismicity of such boundaries is confined to a zone no wider than a few tens of kilometers or less, whereas continental tectonics are more complicated. Many authors have remarked that the distribution of epicentres on continents is quite different from that of those beneath the oceans. This difference is clearly shown in Figure1.1 where the epicentres along mid-oceanic ridge follow a thin strip, whereas those in the Mediterranean,and in Iran in particular, are distributed over a broad belt. This difference shows that it is not in general possible to describe the tectonics of continents in terms of the motion of a few large aseismic plates.

Two possible explanations for the difference between the deformation of continents and oceans have been suggested (McKenzie 1972). The first depends on the existence of many older faults which act as lines of weakness. Such faults do not exist on ridge axes because they are the sites of sea-floor production and thus are young and quite rigid.

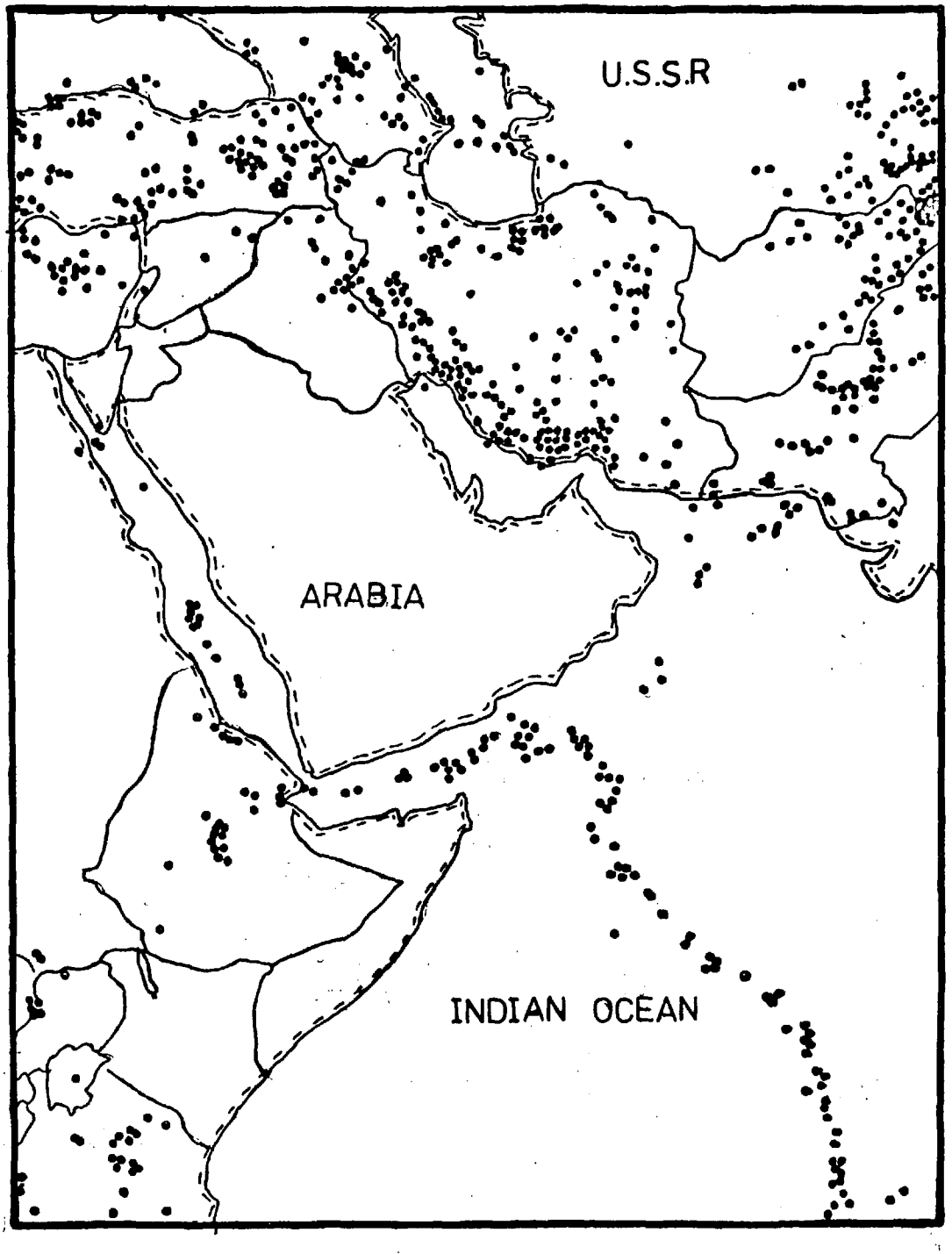



Fig.1.1. Position of all epicenters of earthquakes in the Middle East and part of the Indian Ocean located by the U.S. Coast and Geodetic Survey between 1961 and 1972. Note the dispersed seismicity of the continental area relative to that of the oceanic crust.

The other possible explanation of the difference between oceanic and continental seismicity is that the rocks which form continental plates behave in a different way from oceanic plates when subjected to shearing stresses. Such a difference would not be unexpected because continents contain rocks with more silica than those of the oceans (Ringwood 1968). Silica-rich rocks such as granite deform at low temperatures more easily than basalts, and this may lead to differences in the behaviour of continental and oceanic regions.

The principal problem with which this thesis is concerned is whether the simple concepts of plate tectonics, or its new version in terms of microplates, which has recently been adopted by McKenzie (1970, 1972) and Nowroozi (1972), can usefully be applied to the continents, and in particular to the east Iranian area.

Nowroozi (1972) advances a model of plate boundaries for the Middle East based on seismological and tectonic data for which there is very little field evidence. His neotectonic model has lately been very readily adopted by geologists to elucidate the tectonics of much earlier times (Takin 1972 and Vialon et al. 1972). Nevertheless, it should be kept in mind that the field evidence for the existence of tectonic plates is not yet established in Iran. As an example, Nowroozi (1972) has inferred a northward moving plate in central eastern Iran which he has named the Lut plate. However, his model of small plate tectonics for this area is based on a very dispersed

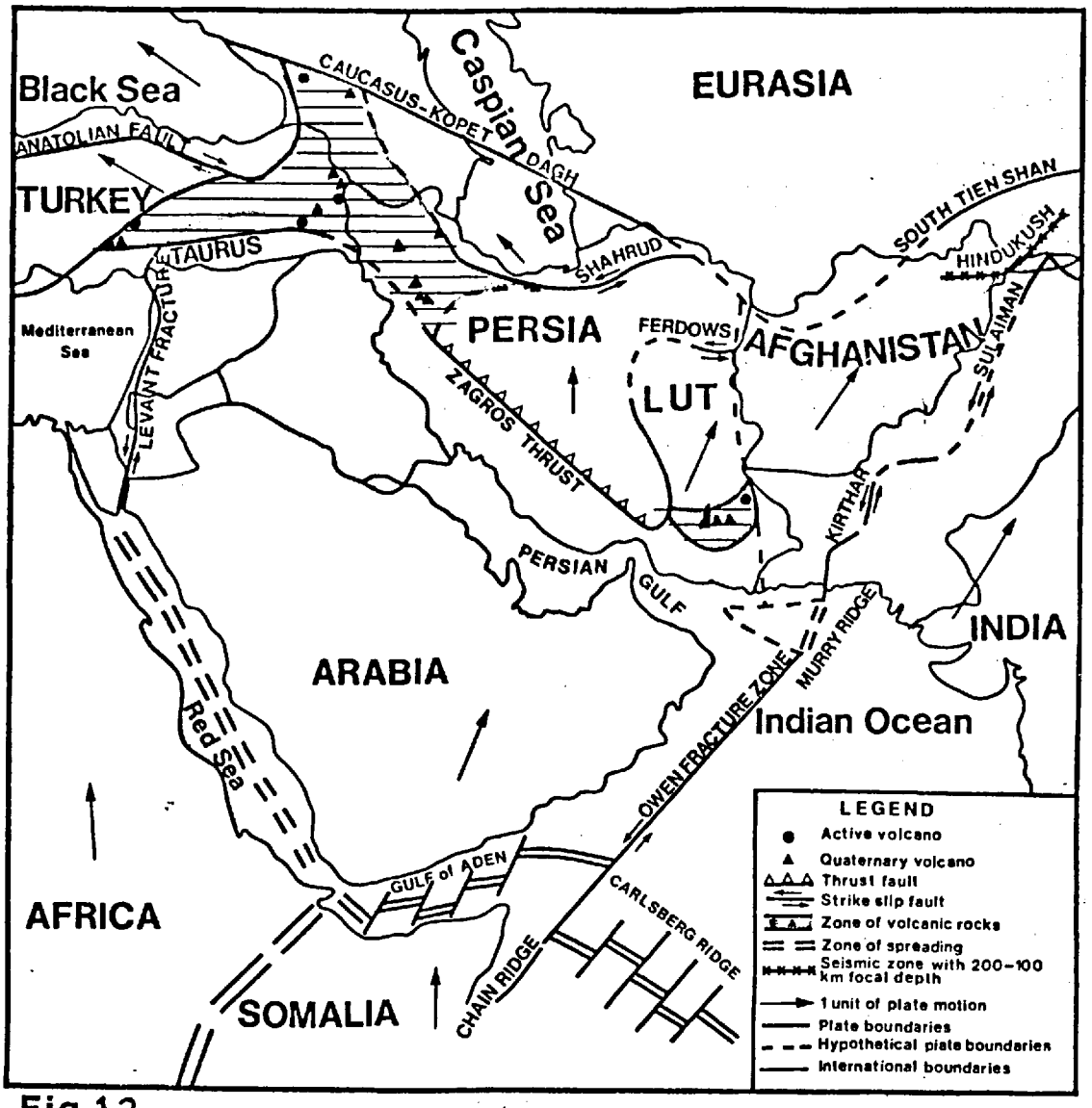
seismicity and only five fault plane solutions. Nowroozi's suggested plate boundaries and directions of motion contradict the recent findings of the present author who has carried out extensive field work in the northern part of the concerned area (see Chapter V).

McKenzie (1972) also expresses his views on neotectonics of the Mediterranian, based on the seismicity and the fault plane solutions for the major shocks of the area. Although his available data is similar to that of Nowroozi's, his proposed model of plate tectonics is different, particularly for the east Iranian area. A close inspection of the seismicity map of Iran (Figure 1.1) shows that the deformation is occurring at present over most of Iran, and the boundaries of the plates that Nowroozi and McKenzie have adopted (Figures 1.2 and 1.3) are marked by fault systems rather than by single faults, so the concept of plates in this region should be used with some caution. Comparison of the plates in the Middle East suggested by the above-mentioned authors, in Figures 1.2 and 1.3, shows a clear ambiguity in the neotectonic interpretations of the seismicity maps, particularly as regards the senses of relative motion of the plates.

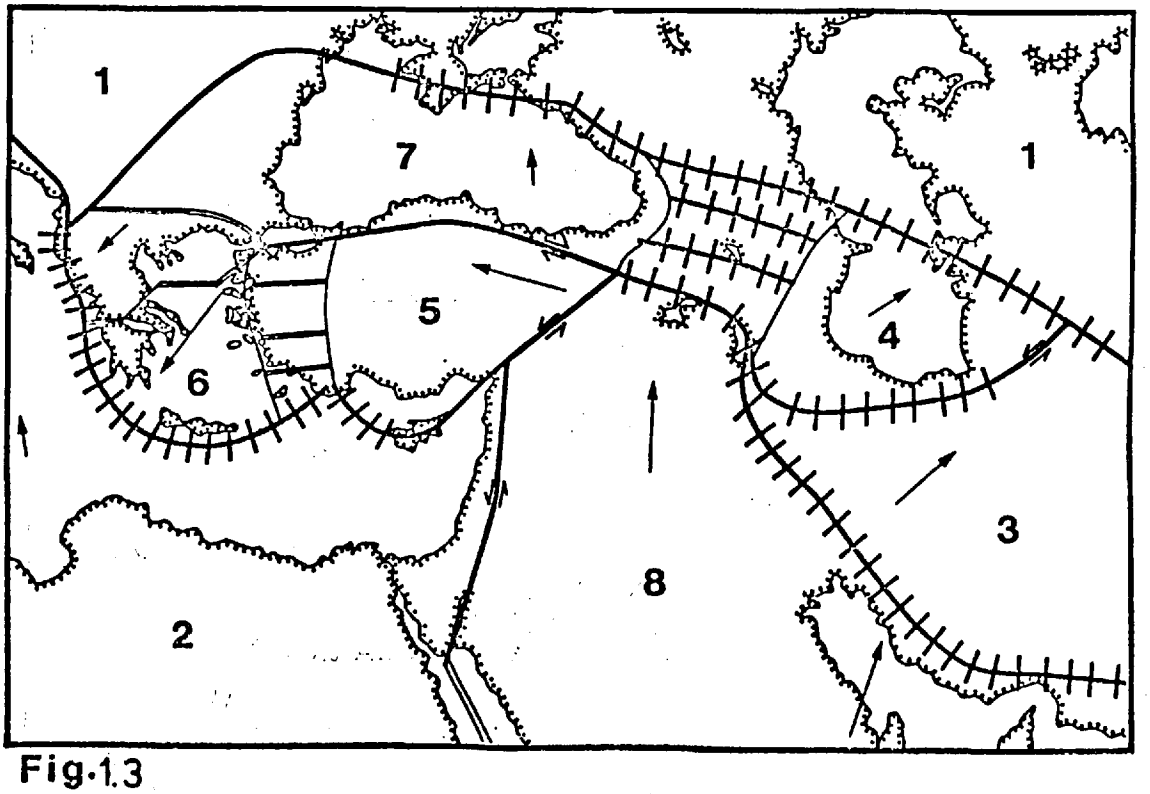
For example, the Lut, a north-east moving plate on Nowroozi's model is not accepted by McKenzie at all (Figures 1.2 and 1.3) and the senses of movement of the bordering faults of this plate, inferred from the relative lengths of the slip vectors, are in contradiction with a recent detailed study by the author (see Chapters

Fig. 2. Nowroozi's sketch map of plates of the Middle East and their direction of motion. The lengths of vectors are in an arbitrary unit. Thick lines denote the proposed plate boundaries and thinner lines the border limits. Quaternary and recently active volcanoes are shown, with solid triangles and circles respectively, in zones of suggested continental spreading, which are hachured. Small arrows represent the direction of relative movements, and denteritic lines under thrusting in Zagros. (After Nowroozi, 1972)

Fig. 3. McKenzie's sketch of plate boundaries and motion. The arrows show the directions of motion relative to Eurasia, and their lengths are approximately proportional to the magnitude of the relative velocity. Plate boundaries across which extension is occurring are shown by a double line, transform faults by a single heavy line, and boundaries across which shortening is occurring by a solid line crossed by short lines at right angles. The plates are assigned the following numbers: 1 Eurasian, 2 South Caspian, 3 Iranian, 4 Arabian, 5 Aegean, 7 Turkey, 8 Black Sea. (After McKenzie, 1972.)


Black Sea
CAUCASUS-KOPET DAGH
Caspian Sea
EURASIA
ANATOLIAN FAULT
TURKEY
TAURUS
SHAHRUD
SOUTH TIEN SHAN
HINDUKUSH
SULAIMAN
Mediterranean Sea
LEVANT FRACTURE
PERSIA
FERDOWS
AFGHANISTAN
LUT
ZAGROS THRUST
KIRTHAR
PERSIAN GULF
MURRY RIDGE
INDIA
ARABIA
Red Sea
OWEN FRACTURE ZONE
Indian Ocean
GULF of ADEN
CARLSBERG RIDGE
AFRICA
CHAIN RIDGE
SOMALIA
LEGEND
Active volcano
Quaternary volcano
Thrust fault
Strike slip fault
Zone of volcanic rocks
Zone of spreading
Seismic zone with 200–100 km focal depth
1 unit of plate motion
Plate boundaries
Hypothetical plate boundaries
International boundaries

Fig·1.2


1
7
1
5
4
6
3
8
2

Fig·1.3

V and VI). Also, McKenzie suggests that both the South Caspian (4) and Iranian (3) plates are moving north-eastward with a proposed higher speed for the latter, whereas Nowroozi takes the South Caspian to be moving north-west and the Iranian plate toward the north. Disagreements be tween the directions of motion of the Black Sea and the Arabian plates are also evident from the presented models. Furthermore, there are two crustal spreading zones in Nowroozi's map which manifest extensional features in the earth's crust and through which volcanoes continued their activity to the present time. These zones of possible opening through the crust are shown as crustal shortening or compressional features on McKenzie's neo-tectonic model for the same area. The above-mentioned discrepancies open the question as to how valid the inference of the boundaries and direction of movements of the plates might be when based solely on a relatively short observation time of dispersed seismicity, a few fault plane solutions, and limited geological information. Geophysical methods in general, compared with other earth sciences, are thought to be an exact science, relatively free from personal description and judgement. But the fact that two different models based on similar data have been proposed for one area introduces the possibility that personal judgement might interfere with the actual facts in some cases such as the present.

Thus, it should be emphasised that adequate field evidence and detailed observational data are always required to refine the

results obtained from the study of major shocks and present day crustal deformation in a structurally complicated area such as Iran. This task entails the application of many available techniques, of which the most accessible and suitable ones are discussed here.

## 1.2 Methods of investigation

In addition to the three major methods of investigation which have been utilized in this thesis, all the available geophysical, geomorphic and geological information has been assembled as an aid to determining the nature of recent and sub-recent crustal deformation in eastern Iran.

The new data presented here resulted from a detailed field study in conjunction with aerial and satellite photographs, geodetic measurement using the Mekometer, and microearthquake surveys along the major active faults.

The interpretation of aerial and satellite photographs of the major fault zones and their adjacent region has been used in order to infer the relation between the main fault trend and the often complicated pattern of minor faulting associated with it. There have also been attempts to differentiate between recent or sub-recent active faults and older geological movement, and when possible, to deduce the sense of motion along the presently active faults.

The author has personally made, for the first time, a detailed field study through many traverses of, and along, the Great Kavir (Doruneh) fault from Rushtkhar, near the Iran border, all the way to the west, in central Kavir, some distance beyond Doruneh village. New evidence on the sense of movement in different segments of the Great Kavir fault in recent and older time intervals has been found. Statistical studies of the dominant trends of fracturing and other lineaments have been made, based on the actual field measurements and also from the aerial and satellite photo-interpretations. The results are compared, to show the degree of confidence in the techniques and to infer the direction of the principal axis of stress and its variations in different localities along the Great Kavir Fault. This type of analysis, based on satellite photographs, in conjunction with the available geological information, was extended to other parts of eastern Iran (Mohajer-Ashjai et al., in press). Published and unpublished field reports, mostly by geologists from the Geological Survey of Iran, and others, in addition to the satellite photographs, have been used to assess the neotectonic framework of the area under study.

Measurement of crustal deformation is another pertinent and most promising way to investigate the presently dynamic features of the earth's crust in the area. Geodetic surveys, in particular, could substantially reveal the amount and direction of relative movements in adjacent blocks of the crust (e.g. Hofman 1968, Savage and Burford 1973).

An electro-optic distance measuring device, which was recently developed by the National Physical Laboratory in the United Kingdom (Froome and Bradsell,1966), proved successful as an accurate ($10^{-6}$ ppm ) and dependable tool to perform repeated measurement on lines up to 3 km in length (Brander 1973). The technique provided useful information concerning the present mode of movements, at least at the upper part of the crust, in the Imperial Valley (California), (Brander and Mason, personal communications) in Iceland (Brander 1973) and on Mount Etna (Wadge 1974).

It was decided to use the Mekometer to study the nature and the amount of relative movements of the possible small plates in eastern Iran.

Selecting the sites for the geodetic networks, which should fundamentally cross a plate boundary, is the first step. This is normally done, according to the basic concepts of plate tectonics, on the basis of the historical earthquakes and the available seismicity records associated with a major fault zone. In preparation for the geodetic field work, the present author compiled all the available information on the major earthquakes which occurred in recent years and in historical times for eastern Iran. As is shown in Figure 6.6 (Chapter VI), the epicentres are too dispersed to suggest any definite trend as a plate boundary. Also, there is an apparent migration of epicentres over a larger time span, which

prevents any conclusions being drawn on the most suitable site for constructing the geodetic network. However, it was blindly chosen to make the initial measurements somewhere on the Dasht-e-Bayaz (Ferdows) Fault,because the most recent major shock occurred on this fault in 1968.

During the course of the field work it became apparent that one of the most important practical problems concerning the geodetic measurements was where to site the benchmarks. This is particularly serious, considering the length of the suspected fault zone,which often runs into hundreds of kilometers, and the cost of making observations based on blind guesses.

Thus, as a tentative alternative, the author has put emphasis on the usefulness of microearthquake studies to delineate the trace of the currently active faults, or the extent of a dilatant area in which stresses are reaching a critical phase before a major shock occurs. In particular, there are many active faults which might not show a clear surface expression, or where a high rate of erosion would sweep their fresh signs away. Meanwhile, numerous field studies within the past few years have indicated that both continuous fault creep and surface displacements during small earthquakes are much more prevalent than had been suspected before. Allen (1968) distinguishes three distinct active zones along the San Andreas Fault system with which are associated the great bulk of the small and moderate earthquake activity. It is significant,

moreover, that it is only in this area that fault creep has been recognized (Figure 1.4). This was later on confirmed by Healy et al. (1972), whose microearthquake activity data recorded in 1969 clearly revealed patterns of faulting that coincide with zones where the fault is creeping. Other interesting features of the data presented by Healy et al. (1972) include the linear trends of earthquakes that branch from the main trends, and may reflect the distribution of the strain concentrations between locked and creeping portions of the fault (Figure 1.5). They also found that at some locations the earthquake patterns are defining fault trends that have not been identified by geologic mapping. This is a good example of how the application of microearthquake studies may directly be used to decide the most suitable locations for geodetic networks, as suggested here.

The use of microearthquakes to define the boundaries of the major tectonic elements is also regarded as a first step toward earthquake prediction. A major part of the earthquake prediction effort in the United States has been directed toward study of the distribution of microearthquakes in the transition zones between locked and creeping portions of the San Andreas Fault.

In an attempt to find a physical basis for earthquake prediction, Nersesov et al. (1969) succeeded in using the microtremors that preceeded the larger shocks in the Garm region of central Asia. This was done using the observed premonitory changes in the ratio

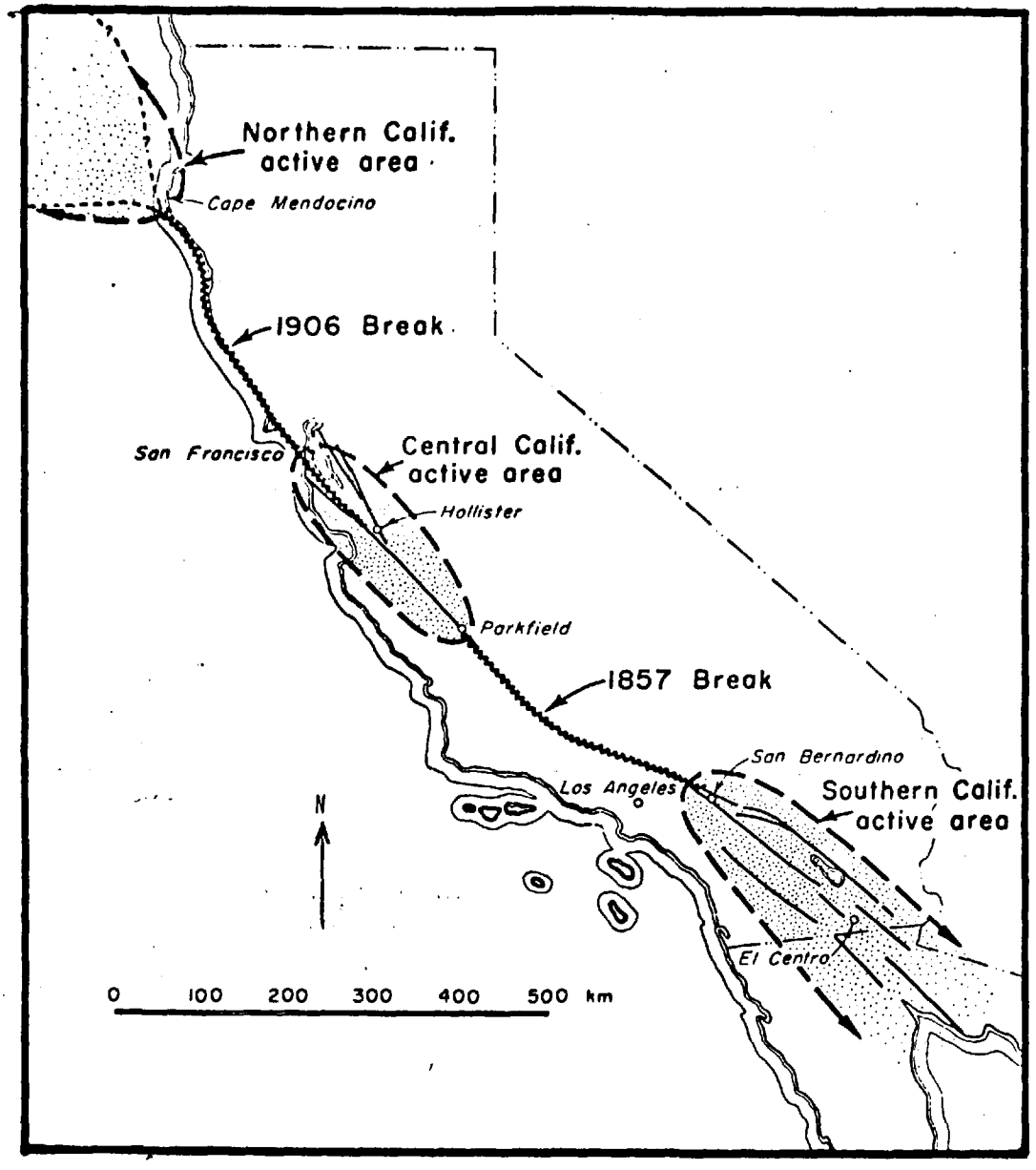



Fig. 1.4. Areas of contrasting seismic behavior along the San Andreas fault zone in California. (After Allen, 1968).

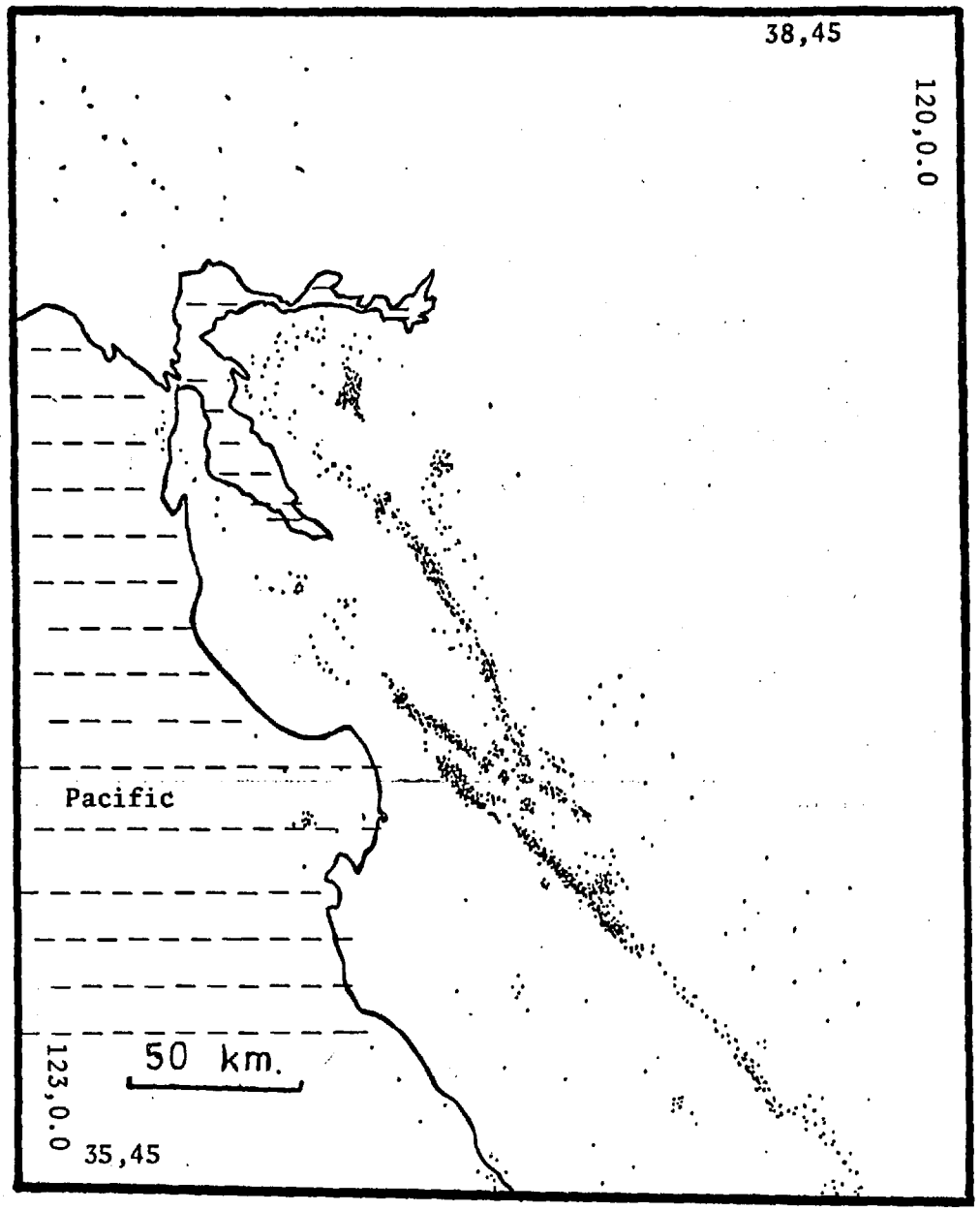



Fig. 1.5. Central California microearthquakes( $<$3.5 magnitude) in 1970. Note branchings from the main linear trends.(After Healy et al.,1972)

of the seismic compressional velocity to that of the seismic shear velocity ($V_p/V_s$) prior to a series of earthquakes of moderate magnitude. Nearly identical results were reported recently for somewhat smaller earthquakes in the Adirondack region of New York State by Aggrawal et al. (1973). These discoveries of a similar anomaly in velocity of the small foreshocks in different regions leaves little doubt on the potential applicability of precursory features of microearthquakes in the prediction of at least certain classes of large and destructive earthquakes.

## 1.3 A brief outline of the chapters in this thesis

The main objectives of this study are presented in Chapter I, following a brief survey of controversial conclusions of different authors concerning the neotectonic models in the Middle East. An introduction to the techniques used in the work for this thesis, their justification, and relevance, is also included in Chapter I.

Chapter II deals mainly with general background information about eastern Iran, where most of the detailed regional studies have been made.

Geodetic measurements were conducted in east Iran using the Mekometer. A detailed account of the network, the measurement performance and the results are presented in Chapter III.

In Chapter IV the significance of microearthquake studies is discussed, using examples from other parts of the world. New insights into the relevance of the statistical observation of the small earthquakes are also given,and this is suggested as a tool for the systematic study of crustal deformation and neotectonics of an area.

Interpretation of the data resulting from microearthquake surveys along some major faults in eastern Iran,and a comparison with a typical study, by the author, in central Scotland are dealt with in Chapter IV.

Geomorphic studies are thought to be crucial to a better understanding of the geophysical phenomena, so the report of the field observations in conjunction with a detailed interpretation of the aerial and satellite photographs are presented in Chapter V. This data is used to refine the inferences of nature of movements along the major structural features which had been deduced from the geophysical data, and also to modify the subsequent suggested and proposed models of the eastern Iranian neotectonics.

Details of all the available data appears in Chapter VI, and an attempt has been made to construct and discuss several possible models of deformation presently active in eastern Iran which best fit the data.

Chapter VII, the final one, includes a summary of the conclusions reached in this study and suggestions for further research in the area.

# CHAPTER II

## BACKGROUND INFORMATION ON THE AREA

### 2.1 Regional introduction

The area under study lies mainly in the Khorassan province of eastern Iran between $30^{o}$ and $36^{o}$ N. latitude and $57^{o}$ and $62^{o}$ E. longitude. The major portion of the area lies in the extremely arid desert region of central-eastern Iran, where summer temperatures in the plains may be as high as $50^{o}C$, while during winter, mountain temperatures can fall below $-40^{o}C$. The annual rainfall is less than 10 cm and water, therefore, is very scanty. Human life depends entirely on an artificial irrigation system called Ghanat (a traditional Persian underground tunnel dug into the alluvial fan, rising at a gradient of about 1:1000 or higher towards the mountain front . They tap the aquifer and by using less slope for the tunnel than that of the surface of the fan, water is eventually led to the open).

Access to the region is mainly by the Mashad-Torbat-e-Heidarieh-Gonabad-Ghain-Birjand highway, which crosses the central part of the area under study, or via the Gonabad to Ferdows-Tabas-Yazd highway, a route through the western part of the area. These highways have motorable connections to other small towns and villages of the area and to reach certain outcrops one has to drive along

dry stream beds, on uncultivated plains or even over small hills.

## 2.2 Physiography

Physiographically, this area of Iran is divided into five major zones, four of which trend approximately north-south and coincide with four main tectonic zones, the western desert region or Tabas Basin, the Shotori Range, the eastern desert region or Lut Desert, and the Eastern Iranian Range. The fifth zone consists of the east-west trending structures of Kuh-e-Sorkh and Dasht-e-Bayaz on the northern limit of the Lut Desert, which also includes the northwest striking mountains of the Ferdows area (Figure 2.1).

The Tabas basin is an intermontane depression with an elevation of about 600 m a.s.l. The centre of the basin is occupied by a "kavir" (salt flat), from which the whole basin has received the name Kavir-e-Tabas. Only the gravel-covered eastern margin of the basin, which receives sufficient fresh water from the Shotori Range, is inhabited. Here lies the town of Tabas (about 8,000 inhabitants), the largest centre of population in the basin.

The Shotori Range is a narrow (10 km in the south, 30 km in the north) north-south running feature which is sharply limited by important fault lines. It is part of a more extensive range that continues south to Nayband and north to Ozbak-kuh. The highest elevation is Kuh-e-Shotori proper, a peak east of Tabas, with an elevation of 2,700 m.

Fig. 2.1. Physiographical and structural map of eastern central Iran.

LEGEND

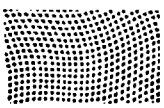
① ① The western desert region( Tabas Basin ).

② ② The Shotori Range.

③ ③ The eastern desert region( Lut Basin.

④ ④ The Eastern Iranian Range.

⑤ ⑤ The nortern limit of the Lut Zone( E-W running Kuh-e-Sorkh, The Great Kavir Fault and the Dasht-e-Bayaz structures ).



Proposed Tabas and Lut Blocks( Stocklin, 1968 ).



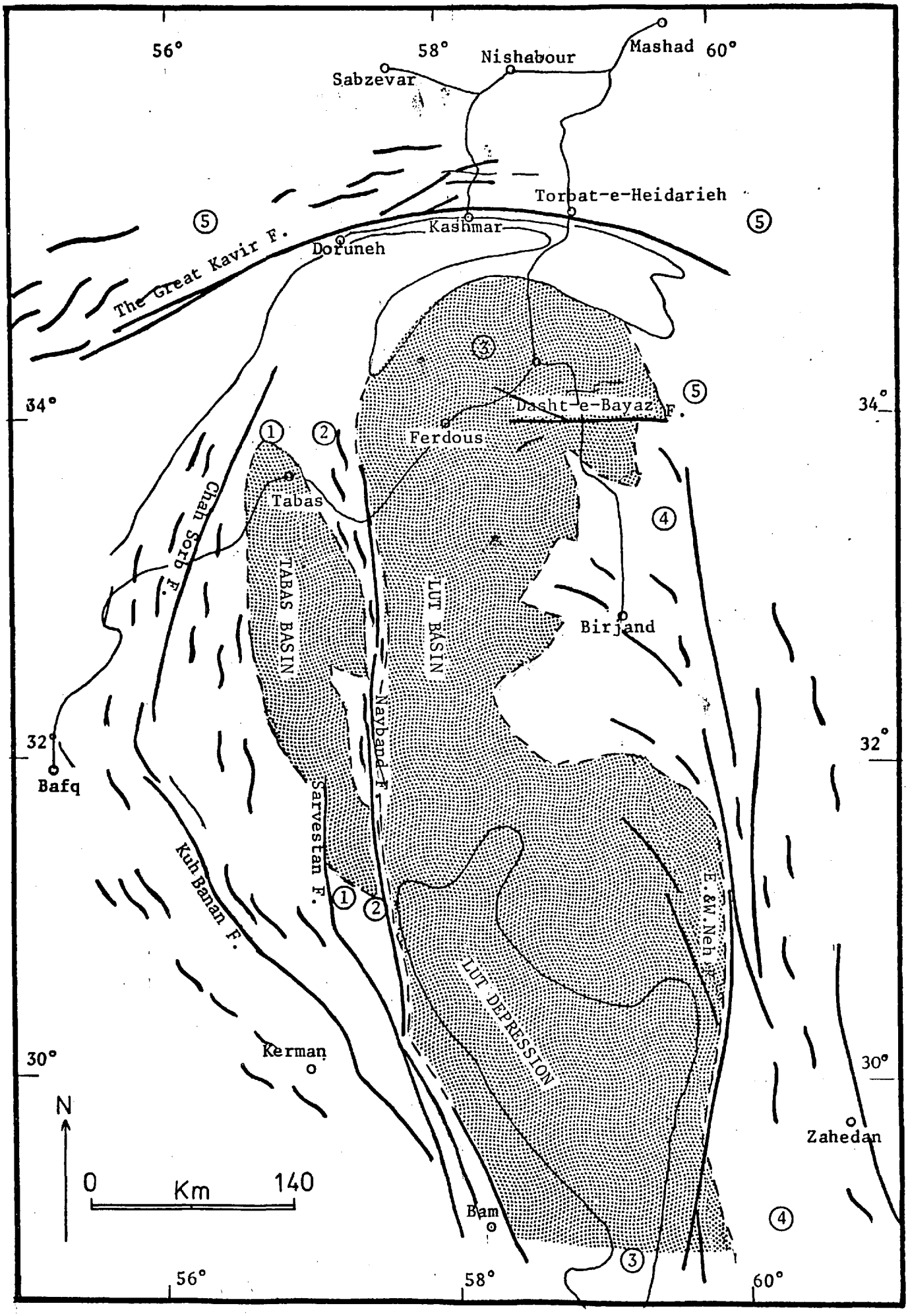
Axes of foldings.



Major faults.



Main roads.


56°
58°
60°
Mashad
Nishabour
Sabzevar
Torbat-e-Heidarieh
Kashmar
Doruneh
The Great Kavir F.
Dasht-e-Bayaz F.
Ferdous
Tabas
Chah Sorb F.
TABAS BASIN
LUT BASIN
Nayband F.
Sarvestan F.
Kuh Banan F.
LUT DEPRESSION
E. & W. Neh F.
Birjand
Bafq
Kerman
Bam
Zahedan
34°
32°
30°
N
0
Km
140

The Lut Desert, with its northern and southern extensions, is nearly 1000 km long and occupies as a distinct north-south trending geographic unit the greater part of eastern Iran. The northern sector of it is a country of low-weathering hills and several intervening large gravel plains and salt flats. Among the latter, the most extensive ones are the Kavir-e-Namak in the north and the Kavir-e-Robat in the east, which are covered by extensive sand belts on their eastern side. The lowest point in this zone is Boshruyeh (675 m ) and the highest is 1300 m near Khur.

The main branch of East Iranian Ranges, which represent the easternmost part of the area under consideration, trends north-south and follows the Iranian-Afghanistan border, and consists of strongly folded, very thick flysch-type and partly volcanic material. This zone of extreme mobility, with its high mountains, is particularly distinct from the apparently stable and depressed Lut desert to the west. The highest elevation in this zone is 2930 m near Birjand, the most important city in the eastern Lut area.

All these north-south trending structures terminate by joining east-west running ranges such as the Kuh-e-Sorkh and Kuh-e-Bakharz (around latitude 35.5) or Dasht-e-Bayaz and Ferdous (latitude 34) to the north. These ranges, with their exceptional trend in the area, are associated with many faults showing different senses of movements and moderate to tight foldings. Highest points in this zone are 2200 m and 2720 m near Akbarabad (N. Kashmar), and Ferdous

respectively, and low lands have an average altitude of 900 m. The three most destructive earthquakes of Iran: Kashmar 1903, Torbat-e-Heidarieh 1923 and Dasht-e-Bayaz 1968, (Ambraseys and Tchalenko 1969, Niazi 1969, Nabavi 1972 and Tchalenko 1974) originated in this zone and provided the main motivation for the author to concentrate his effort in this zone, to study the nature of present-day activity through instrumentation of Dasht-e-Bayaz and the Great Kavir Faults.

## 2.3 Previous studies

As mentioned earlier, the major portion of the area under study is desert and hardly accessible, which might explain why geological and geophysical information was extremely scarce before 1965. In 1906 Tabas and its surroundings were visited by Sven Hedin (1918, 1927) (a Swedish explorer) on his expedition to India. However, Furon (1941) was the first to report on the occurrence of paleozoic rocks in the Shotori Range. Further reconnaissance work in the Shotori Range, in the mountains west and south of the Tabas basin, in the East Iranian Range, and northern Lut, was undertaken by the National Iranian Oil Company, and the results were compiled on the Geological Map of Iran, scale 1:2,500,000 (National Iranian Oil Co., 1959), and two papers by Gansser (1955) and Stocklin (1961) briefly treated some aspects of the geology of this area.

In 1963 the Geological Survey of Iran began systematic mapping in the Shotori Range as part of an extensive mapping project

to cover the entire Shotori - Shirgesht - Ozbak-kuh Range. This work resulted in three geological maps on a scale of 1:100,000, two of which have been published together with detailed reports (Stocklin et al. 1965, Ruttner et al. 1968). These maps, in addition to compilation of other unpublished geological reports in adjacent regions, constitute the basis of the Boshruyeh Quadrangle Map, scale 1:250,000, with explanatory text (Stocklin and Nabavi 1971). Other maps published by the Geological Survey of Iran covering parts of East Iranian Range, Ferdous and west Kashmar regions are the Kashmar Quadrangle Map, scale 1:250,000, Eftekhar-Nezhad (in press), and The Geological Reconnaissance Map of Central Lut, scale 1:500,000, Stocklin et al. (1972). Geophysical information other than seismological data is extremely scarce and is limited to some gravity and magnetic data. The gravity data is in the form of a Bouguer anomaly map of Iran (25 mgal contours) which is given in publication No. 22, Institute of Geophysics, Tehran University, 1965 (see Figure 2.2). This map shows a regional gravity low of about -175 mgal which runs in a south-west direction from latitude $34^{o}$N at the eastern Iranian frontier. This strongly oriented gravity feature appears to be related to the basement structures, since the general trend of surficial structures are north-south or east-west in direction. The gradient and low value of this gravity anomaly suggest a relatively thick crust, in the order of 40km.

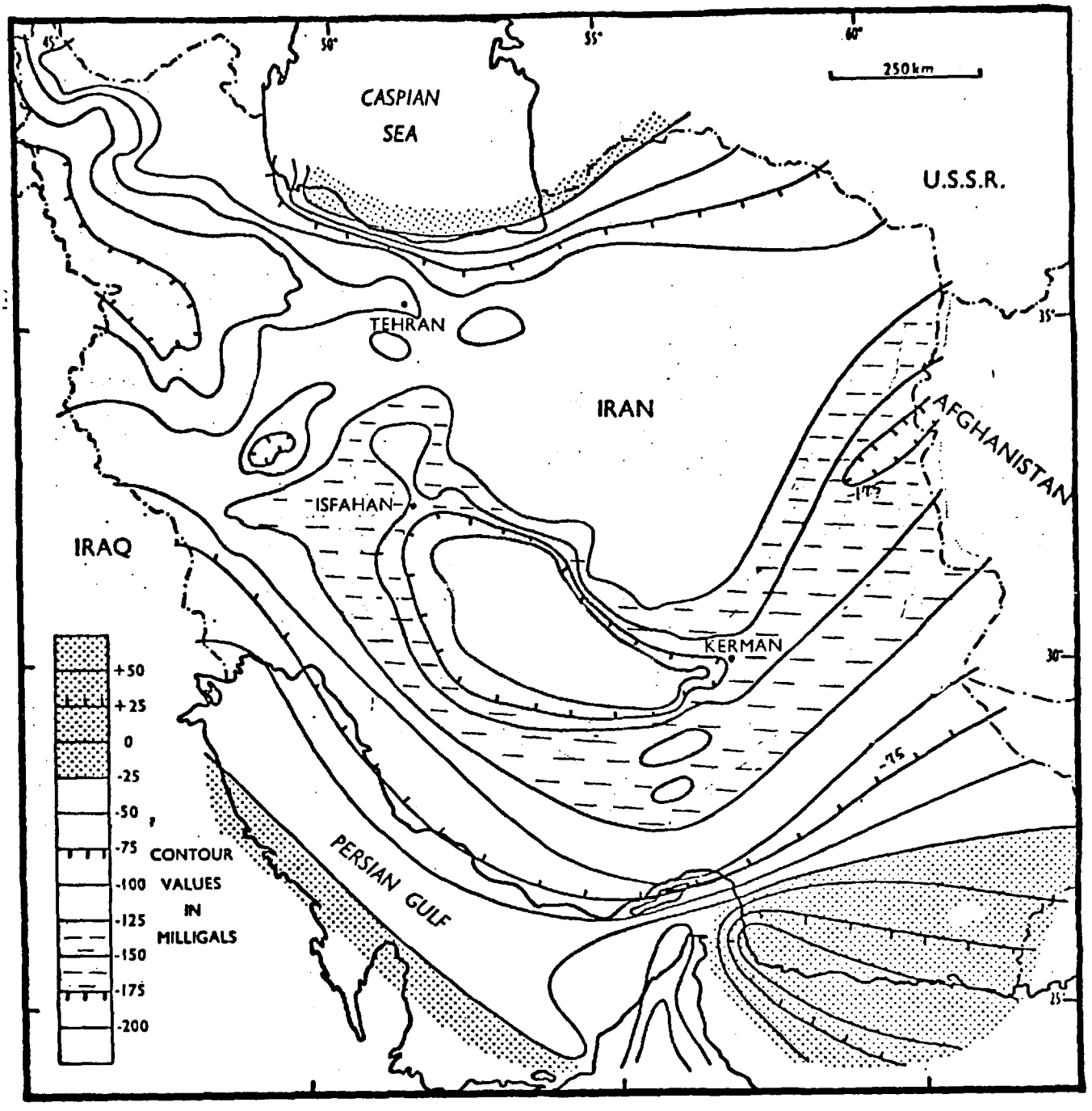



Fig. 2.2. Bouguer gravity anomaly map of Iran. (Published by Institute of Geophysics, Tehran University, 1965).

There is a brief report by Kaveh and Salehi (1972) on the ground measurements and aeromagnetic surveys undertaken by Oil Companies in certain isolated parts of Iran. This surveys cover an area of 61,000 sq.km of the Dasht-e-Lut centred at about $58^{\circ}$ $50'$ E longitude and $30^{\circ}$ $20'$ N latitude. Magnetically, the area shows uniform, tight fold anomalies which exceed 200 gammas in amplitude, trending vaguely north-south to northeast-southwest

A magnetic map of the country was also published by the Institute of Geophysics, Tehran University (No. 12 in 1963) which is based on limited data points (38 station across the Iranian plateau), and does not reveal much information pertinent to the present study.

## 2.4 A brief tectonic history

As revealed by the available geological reports, mainly by the Geological Survey of Iran, a Late-Precambrian diastrophism was responsible for the consolidation of the Precambrian basement and most probably for a prevailing north-south trend in the basement configuration, a trend that has persisted throughout the later history of this part of Iran (Stocklin and Nabavi 1971). However, the map of the Bouguer anomaly of Iran (Figure 2.2) does not readily support this view and, as mentioned earlier, it suggests a north-east trend for the lower crust in this area.

Geologists further suggest that the Paleozoic was a time of relative

tectonic calm. This conclusion is not necessarily valid for the eastern part of Iran, east of Shotori Ranges, because outcrops of Paleozoic, in particular pre-Permian,rocks in this eastern region are scarce and so far insufficiently studied.

With more certainty, it has been postulated that Late-Triassic faulting and folding movements have played an important role in the report area. They created an early "Shotori horst" along an important north-trending fracture zone. As suggested by Stocklin (1968) the horst persisted as a swell and a facies divider during Jurassic time, whereas the areas west and east of it became further consolidated by Late-Triassic movements into highly rigid blocks (Tabas and Lut Blocks) and during the Jurassic were subjected to strong subsidence. At the end of the Jurassic or in Early-Cretaceous,general uplift and possibly some folding affected the whole area. The Cretaceous was probably a period of relative tectonic calm until near the end, when local basaltic volcanism announced the beginning of the main Alpine diastrophism. This severe tectonic activity can be dated to the Early-Tertiary, Pre-Middle-Eocene, and was characterized by strong compression and thrusting in the area. At least two subsequent phases of gentle folding and strong faulting and fracturing were accompanied by powerful volcanism in the eastern desert area, and finally, Stocklin and Nabavi (1971) concluded that the Tertiary movements on the whole accentuated the pre-existing situation; faulting, thrusting and further uplift converted the Late-Triassic - Jurassic Shotori horst into the present Shotori Range and the mobile belt

of the East Iranian Ranges (Stocklin et al. 1972), while the adjoining Tabas and Lut Blocks persisted as relatively rigid elements and as areas of subsidence, to become the Tabas and Lut depressions of today.

In recent attempts to invoke the plate tectonic concept to explain the geology of Iran, Takin (1972) assumed a micro-continent comprising central and east central Iran, which was produced in the Mesozoic, surrounded by narrow Red Sea type ocean basins, the remnants of which are assumed to be the coloured Melange Ophiolites around the central and east Iranian micro-continent.

Crawford (1972) examined the International Tectonic Map of Eurasia (Yanshin 1966) and concluded that some unity of tectonic style exists in the Lut area east of the Oman line (Furon 1941) and west of the Chaman fault system in Pakistan, with marked differences from the areas to east and west. Crawford admits the conspicuous internal divisions in his so called Lut-Helmand-Oman Block, but regards it neither as part of the Arabian-Iranian platform nor as part of peninsular India. Instead, as he suggested, the block could have been an island of sub-continental size in Tethys.

Whatever the mechanism of movements, the history of tectonic activity in eastern Iran definitely continues to Quaternary and even to the present time.

On August 31, 1968, a magnitude 7.5 earthquake occurred in the Dasht e-Bayaz region which killed nearly 11,000 people and devasted almost all the villages within an area of 150 by 60 km. The city of Ferdous was also totally destroyed by a strong aftershock on September 1, 1968. Different aspects of the phenomena related to the earthquake and its aftershocks are covered in the following publications: General field observation and fracture pattern analysis, by Ambraseys and Tchalenko (1969), Source dynamics of the shock and some field observations, by Niazi (1969), and Immediate aftershock studies, by Crampin (1969). A preliminary geological map of the Dasht-e-Bayaz area was also prepared by Behzadi (1972).

As discussed earlier, the general trend of structural units changes sharply both in the upper and lower crust in eastern Iran. The area where this drastic change occurs (near $34^{o}$-$35^{o}$N. latitude) is marked by severe earthquakes in the 20th century and is quite distinct from an adjacent aseismic area between 100-200 km to the east along the Iranian-Afghan border (see Seismicity Map of the World, Dorman and Barazangi 1969).

These features attracted a special interest in the area, internationally, and at present there are several programmes of geological and geophysical investigation in progress other than those presented in this study, and reference will be given to them in the appropriate discussions in the following chapters.

# CHAPTER III

# GEODETIC MEASUREMENTS

## 3.1 Introduction

The dynamic view of the earth, in terms of large horizontal movements, is now well established in the light of recent hypotheses of the sea floor spreading (Hess 1962), continental drift (Wegener 1922, Bullard et al. 1965), and the plate tectonics (McKenzie and Parker, 1967 Morgan 1968).

Although the ground displacements associated with major earthquakes have been observed in many parts of the world since early times, and some of them are well documented in historical books, it was not until the present century that the unifying elastic rebound theory was proposed by Reid (1910), after detailed field observations and geodetic measurements across the fresh fractures left behind by the major 1906 shock in California. Reid proposed that strain accumulates across a fault zone until the shear strain exceeds the static friction on the pre-existing fault surface, or the shear strength of the rock, if there is no previous faulting, when the fault moves suddenly, releasing most of the accumulated strain.

If this is so, a knowledge of the way in which strain accumulates along the fault is fundamental to an understanding of the process by which earthquakes are generated, and how they can be predicted.

Whitten (1948, 1955, 1958, 1960), Burford (1968), Scholtz and Fitch (1969), Savage et al. (1973) and many other research workers computed displacement fields from triangulation resurveys along the San Andreas Fault and concluded that, in times of quiescence between large earthquakes, substantial displacements take place in the vicinity of the fault that may reflect a steady accumulation of strain as predicted by the elastic rebound theory. In general, this theory, when modified to take into account what is now known about frictional sliding, may explain most, if not all, observations of tectonic crustal deformation. This is illustrated in Figure (3.1), which shows an example of the way in which strain accumulates and is released by elastic rebound along a major fault zone or plate boundary.

The elastic rebound theory has been supported by the experimental work in the rock mechanic laboratories at confining pressures in the range 2 to 10 K.bar. Brace and Byerlee (1970) have substantially clarified the mechanism of earthquakes on shallow faults by showing the fact that slip on previously faulted surfaces of rock occurs rather frequently with intermittent slow episodic build up of stress, followed by rapid slip and a near instantaneous drop of stress. This mechanism,which is called the stick-slip concept,overcomes the vagueness of Reid's original concept of slow healing of a fault following an earthquake, and demonstrates that fracture-like instabilities are possible on existing faults.

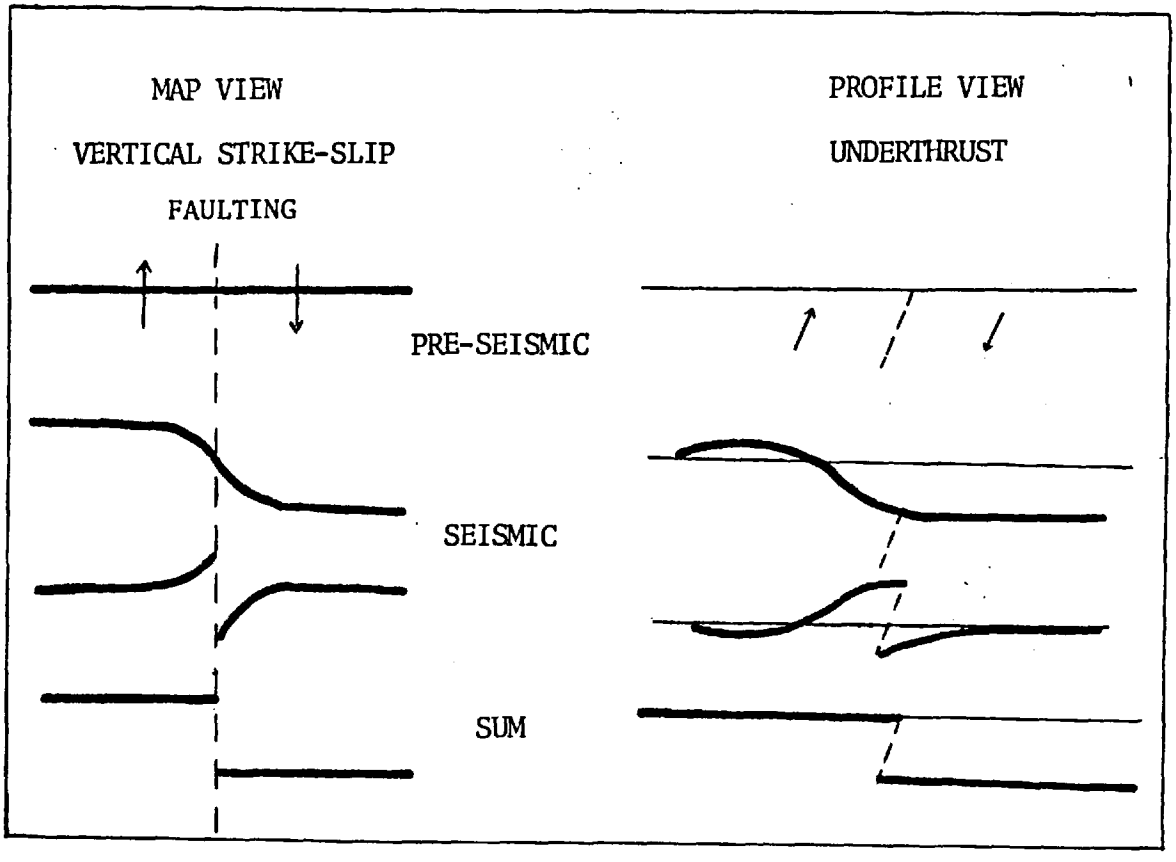



Fig. 3.1 Elastic rebound models of plate boundaries. (After Scholz, 1972.)

Left. Transcurrent boundary: map view showing horizontal deformation, on a greatly exaggerated scale, of a line (solid curve) initially normal to the fault trace (dashed line). The pre-seismic curve gives deformation of such a line during a period of strain accumulation, the seismic shows deformation by an earthquake, and the sum is the total deformation for the entire earthquake cycle. The arrows give the long-term motion of one side of the fault with respect to the other

Right. Thrust boundary: vertical section, arrows indicate long-term relative plate motion. Vertical deformation (on a greatly exaggerated vertical scale) of an initially horizontal surface is shown by the heavy curves, whereas the fine lines give the initial configuration of that surface. Dashed line is the fault.

In more complex seismic zones, such as the Iranian Plateau (Alpine-Himalayan belt in general), where crustal deformation and seismicity occur over a broader region, the elastic rebound process is much more complex than in the example given above. The geodetic measurements reported in this thesis are one of the few attempts to study the crustal deformation in a structurally complicated area with predominant thrust faulting and active folding.

Geodetic data is also thought to be useful in predicting earthquakes by estimating the normal and the shear strain rates on the surface trace of a plane of potential slip. The thesis is that when these strains and the forces associated with them reach some critical ratio, an earthquake will occur. Two shortcomings of this hypothesis as pointed out by Howard (1968) are:

1. The condition of strain at the times of the first geodetic survey are not normally known.

2. Geodetic data reveal the strain at the earth's surface but not at depth, as is shown by Chinnery (1961).

Since the Dasht-e-Bayaz network was constructed less than three years after the magnitude 7.3 earthquake, which might have relieved a major portion of the accumulated strain in the area, we have had hopes to monitor the gradual strain build-up, starting from a nearly unstrained condition. In addition, changes in strain

rates when measured on the ground surface in a direction normal to the fault may enable one to study the mechanism of fault movement. Figure (3.2) is an example illustrating two different types of motion, stable sliding in the lower figure and stick-slip in the upper figure, as suggested by Savage and Burford (1970). These models indicate the shear-strain profiles which should be expected along a line on the surface drawn perpendicular to the strike of the fault.

To test whether or not the above-mentioned models fit the case of the Dasht-e-Bayaz and the Great Kavir faults it was decided to extend the geodetic networks in a direction normal to the fault traces rather than along them.

## 3.2 Advantages of the direct distance measurements used in this work

The problem of measuring small horizontal movements on the surface of the earth in areas of seismic activity has generally been solved by re-observing a triangulation network. If there have been changes, the difference in the observations will indicate the magnitude of the movement. The usual practice for calculating these shifts of position has been to compute geographic coordinates of the points for each set of observations and then to compare the coordinates. There is always the possibility that errors of observation or weaknesses in the network itself may produce accumulated

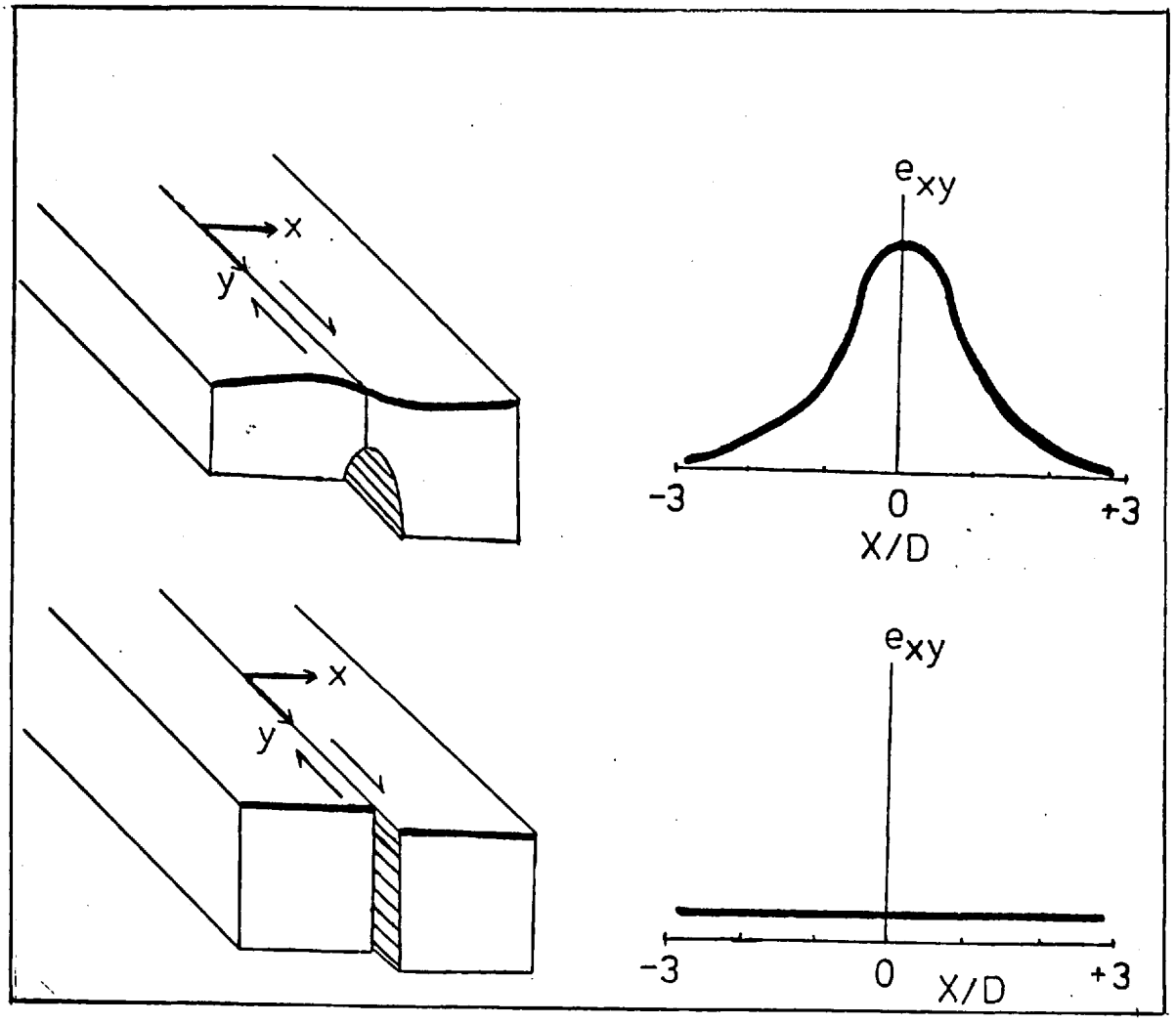



Fig. 3.2. Two models of block motion along the San Andreas Fault with a sketch of the shear strain $e_{xy}$, that should be observed at the surface on a profile normal to the fault strike. (After Savage and Burford, 1970.)

effects, and these often exceed any conceivable ground movement. Also, a stable base line must always be available as reference for the network. Any small shift in one of the reference points can produce fictitious shifts in position of all the other points.

A better method for determining crustal movements from repeated triangulation measurements is to calculate a displacement field referred to a fixed line. Many investigators have used this method on the assumption that deformation could be considered homogeneous within a small area (e.g. Whitten and Claire 1960). Others have found that random measurement errors lead to such large errors in the displacement vectors as to completely mask the actual strains when computed in this way. The assumption is that all displacements are parallel to the neighbouring fault (neither generally applicable nor necessarily true) and it also uses the changes of angle of one triangle, which is related to uniformity of the distributed strain over the polygon defined by all stations. Frank (1966) has developed a method that avoids this problem. He pointed out that the shear components of the surface strain could be calculated from changes in the observed angles in re-surveyed triangulation networks. He defined the shear components $\gamma_1$ and $\gamma_2$ in terms of the usual tensor strains

$$e_{ij} = 1/2 \left(\delta u_i/\delta x_j + \delta u_j/\delta x_i\right) \quad \text{as}$$

$$\gamma_1 = e_{11} - e_{22}$$

$$\gamma_2 = e_{12} + e_{21}$$

This method is widely accepted and used by many investigators because it avoids many problems associated with other available methods already mentioned. But even Frank's method has its own deficiencies. For example, using this method one loses all information on dilatational strains, which are very important for a complete strain analysis.

Many attempts have been made to develop a better method of calculation for the crustal deformations based on triangulation data, but all of them have their own limitations. There is, however, an alternative to these methods, which consists in measuring the distances between two points directly and accurately, using an instrument such as a Geodimeter or Mekometer. With these instruments, the above-mentioned difficulties of interpretation are avoided and translation of the stations are easily recorded.

An additional advantage of the Mekometer, which makes it of particular interest to studies such as the ones carried out here, is its great accuracy and range (of the order of 0.2 parts per million, over a distance up to 3 kilometer).

## 3.3 Instrumentation : the Mekometer and its operation

Measurements of the earth strain along certain faults in eastern Iran reported in this thesis is based on the prototype Mekometer developed at the National Physical Laboratory in the United Kingdom by Froome and Bradsell (1961, 1966, 1971).

The Mekometer is a precise electro-optic distance measuring device which uses a pulsed light source, modulted at a frequency of around 500 MHz to achieve a sensitivity of 0.1mm over a maximum range of 3kms. Use of UHF modulation has the advantage that the distance can be measured in terms of an internal variable light path instead of by the electrical circuits used in other electro-optic distance measuring devices, such as the Geodimeter.

The light source is a xenon flash-tube arranged to produce an intense spark of 1μsec duration at a repetition frequency of 100 Hz. The light is plane polarized by means of a polaroid disc before it passes through modulating crystal of potassium dihydrogen phosphate (KDP). The process of demodulation (or detection) is achieved by means of a second KDP crystal, and both crystals are placed at the high impedance end of a quarter-wave tunable cavity, resonant at about 492 MHz and pulsed into operation for a duration of 40 μsec. In this time the light must pass twice, once out and once back, through the crystal, so that the maximum possible distance of travel of the light is

$$3 \times 10^{8} \times 40 \times 10^{-6} \text{ m} = 12 \text{ kms}$$

giving a maximum range of the instrument of 6 kms. However, in order to allow the induced oscillations time to stabilise, the light does not leave until half-way through the pulse, reducing the maximum range to 3kms.

The optic axis of each crystal is arranged to be parallel to the electric field in the cavity so that the light emerging from it is elliptically polarized at the resonant frequency of this cavity. This light is transmitted to a cube-corner reflector located at the far end of the line to be measured. The light returned from this far-point, traverses an internal variable light path, passes through a second KDP crystal and onto the cathode of photo-multiplier. Between this demodulating crystal and the photo-detector is a second polaroid crossed relative to the first.

Crystals of the KDP type exhibit the linear electro-optic effect, so that after passage through the second crystal the ellipticity of the polarized light is either enhanced or cancelled, depending upon the instantaneous phase of the electric field relative to the phase of the modulation of the light returned from the far-point. In practice, the phase-measuring process consists of adjusting the variable light path until the photo-multiplier 'sees' a minimum. Attached to the variable light path is a scale used to measure the displacement of the variable optical element. The measuring procedure is as follows.

The modulator is adjusted to produce a modulation wavelength of 2 ft so that the pattern from the far-point repeats every 1 ft.

The variable light-path is set to a detector minimum and the fraction of a foot in the required distance read-off directly from the tape scale attached to it. A scheme involving discrete changes of modulation frequency allows the measurement of the number of tens and of hundreds of half-wavelengths in the distance to be obtained. From a map, the number of thousands of these half-wavelength units can be found, and the distance from Mekometer axis to reflector axis accurate to $\pm$ 6 ppm established after subtraction of an instrumental correction. Such a measurement takes about ten minutes.

A second advantage of the Mekometer is the use of a wavelength standard instead of a frequency standard to maintain the accuracy of the modulation wavelength. The standard is a microwave cavity resonator (frequency nine times that of the basic modulation frequency) constructed of fused quartz and filled with dry air but so arranged within the instrument that it acquires atmospheric temperature and pressure. Output from the modulating cavity is fed, via a frequency multiplier, into a coupling loop in the side of the quartz standard cavity. A second coupling loop takes power from the standard to a diode detector, which indicates when the modulating cavity frequency is exactly one-ninth of the frequency of the standard cavity.

A further advantage of the Mekometer is the use of elliptical polarisation in the modulation. This is a great improvement over the amplitude modulation usually used in electro-magnetic distance measuring

devices, such as the Geodimeter, because phase distortion by random atmospheric fluctuations is very much less than the corresponding emplitude distortion, making the Mekometer inherently less susceptible to atmospheric influences than are other similar instruments.

The coefficients, fortunately linear, governing the dependence of reference cavity frequency on temperature and pressure are now very well known, but must nevertheless be regularly checked in the field. This helps define their behaviour under peculiar circumstances, and also indicates when the reference cavity drying agent needs changing.

Since the intended frequency versus refractive index compensation is not perfect, better accuracy of measurement can be achieved by correcting for both independently. This complicates the measuring process considerably, as several temperatures and pressures must be recorded simultaneously with the distance readings, of which never fewer than six, and often fifteen or more, are made for each line. A reading here is a setting of the movable mirrors, not a complete setup, which is done usually only once on each line. The ten or so readings will then be averaged later. The number taken will depend on the prevalent atmospheric conditions, which controls the scatter among them. If the scatter is low, less than 0.001m, six readings will suffice; if it is between 0.001 and 0.003m, ten readings should be made; for scatters between 0.003 and 0.010, twelve to fifteen are necessary, and if the scatter is greater than 0.010m, measuring should be stopped. With a little practice one can soon tell what weather will produce good and bad measurements.

The description of the Mekometer is not intended to be complete. A fuller description can be found in the relevant papers by Froome and Bradsell, and in the Ph.D theses of R.W. Calvert (1970) and J. Brander (1973).

## 3.4 Corrections applied to the Mekometer results

There are two instrumental, one atmospheric, and one topographic corrections which can be applied to the Mekometer results in order to improve its accuracy and make it more suitable for geophysical applications.

The first instrumental correction is concerned with the modulating frequency of the Mekometer, which is a function of the temperature and pressure of the air in the reference cavity. Effects of these parameters have been determined experimentally, by measuring the frequency at constant temperature and varying pressure, and vice versa. The experiment has been repeated several times during each field trip and a linear relationship of the general form of $F = F_o + \alpha T$ was established in which $F_o$ signifies modulating frequency at $0^oC$ and F at $T^oC$, $\alpha$ representing the constant of the linear equation. The pressure characteristic resulted in a similar relationship and thus, the correction for modulating frequency which is applied to the Mekometer measurements is a linear function of the temperature and pressure pertaining to the time of the measurements, and normally comes to about $\pm$ 3 ppm.

The second instrumental correction is a constant, which is independent of temperature, pressure or any of the usual variables

and its value depends upon the target reflector used. This value is simply subtracted from the measured distance and is usually about half a centimeter or less.

The correction involving atmospheric parameters is that for refractive index. This is a function of temperature, pressure and to a small extent, water vapour pressure. Thus the atmospheric correction is obtained by substituting measured values of air temperature and pressure into the empirical formula of Barrel and Sears (1939), and comes to about 1 pp m for each $^{o}C$ temperature variation.

$$(n-1) = (n_{st} - 1) \frac{P.(1 + b_T \cdot p)(1 + 15 \cdot a)}{760.(1 + b15 \cdot 760).(1 + aT)}$$

where

P = the atmospheric pressure in mmHg

T = the effective atmospheric temperature in $^{o}$ c

a = .003661

b = $(1.049 - 0.015 . T) \times 10^{-6}$

$n_{st}$ = the refractive index at S.T.P. (as above)

The final correction for topography is particularly important in rugged (undulating) terrain as in Iran, where the mekometer is often sited at a different altitude relative to the reflector, as illustrated in Figure (3.3). This has a significant effect in two possible situations, a) where the relative height of Mekometer and reflector varies in successive measurements and b) where relative

changes take place in the elevation of the stations.

a) Suppose that the line joining reflector and the Mekometer is inclined at an angle $\theta$ to the horizontal, that the horizontal distance between the two points is D, and the point-to-point distance as measured by the Mekometer, is d. Then $D = d \cos\theta$, also if the difference in height above the ground between instrument

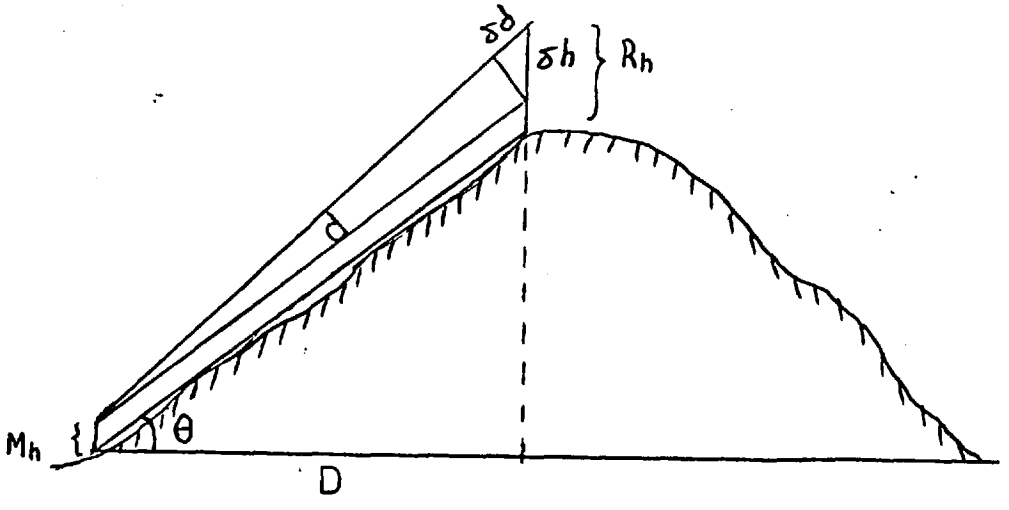



Figure 3.3. Effect of the height difference between Mekometer ($M_h$) and reflector ($R_h$).

---

and reflector is $\delta h$ this will lead to an error $\delta d$ in the measured distance given by $\delta d = \delta h \sin\theta$

Consequently, the height difference of the tripods in each set of measurements will lead to an error $\delta D$ in the computed horizontal distance D given by,

$$\delta D = \delta d \cos\theta$$

But $$\delta d = \delta h \sin\theta$$

Thus $$\delta D = \delta h \sin\theta \cdot \cos\theta$$

i.e. $$\delta D = \delta h \cdot \frac{\sin 2\theta}{2}$$

Thus a change of 100 mm (about 4") in the relative height of instrument and reflector will, for a slope of $2^{o}$ (about 1 in 25), lead to an error in D of about 4 mm. This example illustrates the importance of measuring accurately the height of instrument and reflector above the ground as well as the slope of the terrain between them. However, in most of the cases when only the point-to-point comparison of the ground distance in successive measurement is required, the measured distances are not reduced to horizontal lines and, therefore, the only correction applied is in the form of:

$$\delta d = \delta h \sin\theta$$

This source of error tends to be relatively high in the rugged area of the Dasht-e-Bayaz network, and that was the reason the initial analysis of the data, before considering the topographic correction, was unsuccessful. (See section 3.7).

b) Another significant effect of the topographic correction is on the change in length of a line, caused by vertical movement of one of the stations. The previous formulation also hold for this case and, therefore, it is almost impossible to detect or rule out the possibility

of any vertical movement from the mekometer measurements alone. Thus it is necessary to keep the lines in the mekometer network as nearly as possible horizontal and/or to eliminate the consequences of topographic variations or vertical movements either by measuring vertical angle with a theodolite or precise levelling.

## 3.5 Geodetic data analysis

In the discussion presented in Section 3.2, it was pointed out that the classical method of analysis of repeated survey data faces considerable difficulties. This, briefly, involves the establishment of two or three dimensional cartesian coordinate systems for all the stations in each survey, and then the comparison of the coordinates to give information on station displacements on earth strain. These coordinates are calculated from the adjusted survey angles and an assumed stable base line. To make this physically justifiable the base-line has to be a long way from any areas of activity, in the order of 50 kilometers from the fault trace (Savage and Burford 1970), which is not, of course, a readily practical condition.

Another difficulty is the accumulated observational errors, which are introduced by using all of the angles between the stations and the base-line (origin). Thus, after a few network stages these accumulated observational errors may easily become large enough to mask the possible ground movements.

The technique of analysis of the displacement vectors also suffers from the same unjustified assumption of two fixed stations (or a base-line) in that, in order to define a displacement vector, there must be a reference whose motion is either known separately or ignored. Violation of this requirement means that artificial displacements and rotations will be introduced into the station coordinates. In a very confused situation where there is no well-defined tectonic direction, and almost every line has undergone some change of length, the choice of a suitable base-line from which to make a displacement vector analysis becomes impossible, and the only approach to analysing the results seems to be through the homegeneous strain assumption. Especially when a large number of faults are involved, it is probably true to say that the movements in such an area will approximate to a homogeneous strain state.

Two preferred ways of formulating the strain analysis based on the mekometer results are mentioned in the following, which have been derived from the theory of infinitiesimal strain in two dimension.

The first method resembles Frank's (1966), which derives local shear strain information from the angle changes within a triangle (also see Mohajer-Ashjai 1974).

If an infinitesimal strain, represented mathematically in two dimensions by the tensor

$$\begin{matrix} \varepsilon_{11} & \varepsilon_{12} \\ \varepsilon_{21} & \varepsilon_{22} \end{matrix}$$

acts upon a line of original length r and azimuth with respect to a given direction of $\varphi$, then the change of length of that line, $\delta r$, is given by the equation.

$$\frac{\delta r}{r} = \frac{\Delta}{2} + \frac{\gamma_1}{2} \cos 2\varphi + \frac{\gamma_2}{2} \sin 2\varphi$$

where $\Delta$, $\gamma_1$ and $\gamma_2$ are described in terms of the tensor by the equations

$$\Delta = 1/2 \ (\varepsilon_{11} + \varepsilon_{22})$$

$$\gamma_1 = \varepsilon_{11} - \varepsilon_{22}$$

$$\gamma_2 = \varepsilon_{12} + \varepsilon_{21}$$

The fourth component, rotation, unfortunately does not appear directly in the expression for the change of length, which is to be expected, and can be determined only by measuring astronomical bearings.

The terms $\Delta$, $\gamma_1$ and $\gamma_2$ are, respectively, the dilatation, right-lateral shear on a NW-SE striking plane, and right lateral shear on an E-W striking plane.

The two shear components, which will vary according to the axis used to define $\varphi$, may be easily combined to give a resultant direction of maximum shear and its associated magnitude. These last mentioned quantities are independent of the axis used to define $\varphi$, as also is the dilatation.

Also from these components, $\gamma_1$ and $\gamma_2$, the principal strain pattern responsible for the movements, may be calculated.

The second method used here utilizes a simple equation expressing the state of finite longitudinal strain with reference to the angle they make with the x-coordinate axis in the strained state.

$$\frac{1}{\lambda} = \frac{1}{\lambda_1} \cos^2\theta' + \frac{1}{\lambda^2} \sin^2\theta' \qquad (3.1)$$

(From Ramsay 1967, p. 66)

since $\lambda = (1 + e)^2$, this becomes

$$1/(1 + e)^2 = \cos^2\theta' /(1 + e_1)^2 + \sin^2\theta' /(1 + e_2)^2$$

Now we are normally dealing with changes of only a few mm in lines a few kilometers long, i.e. strains of the order $10^{-6}$. Thus the infinitesimal strain theory applies and we can ignore second and higher order terms. Re-writing the above equation in the form:

$$(1 + e)^{-2} = (1 + e_1)^{-2} \cos^2\theta' + (1 + e_2)^{-2} \sin^2\theta'$$

and expanding by the binomial theorem, ignoring second and higher order terms, we arrive at:

$$e = e_1 \cos^2\theta' + e_2 \sin^2\theta' \qquad (3.2)$$

One can now make three such simple equations using three re-measured lines of the Mekometer trilateration network, solving these equations simultaneously. Values of $e_1$ and $e_2$ the principal longitudinal strains, and the angle between $e_1$ and e in the strained state can, therefore, be calculated. To reduce the number of unknown variables ($\theta'_1$, $\theta'_2$ and $\theta'_3$) in these equations, a common unknown such as $\theta'_i = \varphi \pm \alpha_i$ is, of course, adopted, where $\alpha i$ signifies the azimuth of the line measured. Also, the maximum value of the shear strain is easily determined using $\gamma = \pm (e_1 - e_2)$ which is derived by converting the equation for finite shear strain ( $\gamma = \pm \frac{\lambda_1 - \lambda_2}{2(\lambda_1 \lambda_2)^{\frac{1}{2}}}$ after Ramsay 1966, p. 69) to infinitesimal strain conditions with the usual approximations.

Nevertheless, for quick assessment of the state of strain in a simple fault zone, particularly when the direction of general movement in the area is roughly known from other data, application of the displacement vector analysis could be useful. This is simply done by using three stations forming the apices of a triangle, one of whose stations has moved. Thus there will be observable length changes on two of three sides. The third side, which has not changed length, is chosen as the base line, and both stations are taken to be fixed. The components of the displacement vector of the moving station are the changes of length on the two lines, in the direction of the two lines. Knowing two components of a vector makes it possible to calculate its magnitude and direction, so that the displacement may be determined.

## 3.6 The geodetic networks

There are two geodetic networks in eastern Iran constructed for the Mekometer measurements. These are the Dasht-e-Bayaz and the Doruneh networks which were both designed with two major considerations in mind, 1) both networks are extended perpendicular to the fault trace in order to detect the variations of strain with distance from the fault, as predicted by the stick-slip model of faulting (see section 3.1), 2). Both networks are built up of doubly-braced quadrilaterals arranged end to end. The reason for this is that such

figures are the simplest which provide a check of the self-consistency of the measured distances. In angle measurement networks, the simplest figure that may be used is the triangle, where the condition that the three angles must sum to $180^{o}$ is a check on the consistency of the observations. However, this figure is not suitable for distance measurements, in that it provides no check of self consistency.

The bench marks are constructed on the principle of least disturbance of the surrounding ground. They are all placed in alluvium, in places unlikely to be affected by ground water, and where topographic gradients are insufficient to cause slippage, except in the event of a major earthquake. Each one consists of a concrete slab about six inches thick, flush with the ground surface and set around the top three or four inches of a metre long angle iron stake hammered completely into the ground. There is in each concrete block a small non-ferrous metal mark, onto which the tripods are centred. They have all been painted yellow. Some of them are unfortunately rather uncomfortably near cultivated land, though outside the existing limits, which will hopefully not change in the next few years.

### 3.6.1 The Dasht-e-Bayaz network

There are sixteen benchmarks in the Dasht-e-Bayaz network,

forming seven quadrilaterals, in each of which Mekometer measurements are made on six lines giving a total therefore of thirty-six distances. They are arranged so that eight are north of the main fault break, and eight south. They are numbered from the south, in two rows, east and west. The total span of the network is about six km in a north-south direction and around one km east-west (Figure 3.4).

The pairs of stations numbered one to four are in the gently undulating ground south of the fault, and the two stations 5 are on small hills overlooking the village of Boskababak. The two stations 6 are on the larger central hills which command the whole valley, and the four remaining stations lie in the complicated ridge and gulley system between the central hills and the mountains.

Of the four lines which actually cross the fault, two at least are fairly well inclined to it, and any movement occurring on it should be detected quite easily if sufficient measurements are made. For strain accumulation away from the fault, the ease of detection will depend entirely on its magnitude.

Except for East and West 6, which must be reached on foot, all stations are accessible by vehicle, a feature which may help in their relocation, as there are now quite well developed tracks to each one. From the village of Dasht-e-Bayaz, the road which leads to the North Western corner of the plain should be followed,

until the turning left off to Karashk. This road then immediately crosses first a dry water course and then a Ghanat line. On the ridge on which the first ghanat well stands are East and West 8. There are well developed tracks to both, and both are marked with piles of stones.

East and West 7 are on the ridge which overlooks the cultivated valley of the village of Karashk. This is further along the road from East and West 8. East and West 6 both are on the hills between the villages of Boskabad and Karashk. There is a footpath around the highest of these, which crosses their axis at a kal (dry water course) about 20m west of West 6. East 6 is on the second height east of West 6, about 400m away.

West 5 is on a flat ridge south of the village of Boskabad. Leaving the village there is a fork in the road, the right turning of which goes towards the south. This south road, from which one can go on to the University of Mashad's creepmeter, crosses a ridge soon after the fork, at a rather difficult piece of driving. By turning right here one can drive up onto the ridge where West 5 is situated. East 5 is further on along the left branch of the road fork, towards Faizbad from Boskabad. It is on a small knoll between which and the road there is a dry water course. In the bottom of this knoll some of the Quaternary deposits are well exposed, exhibiting a striking unconformity.

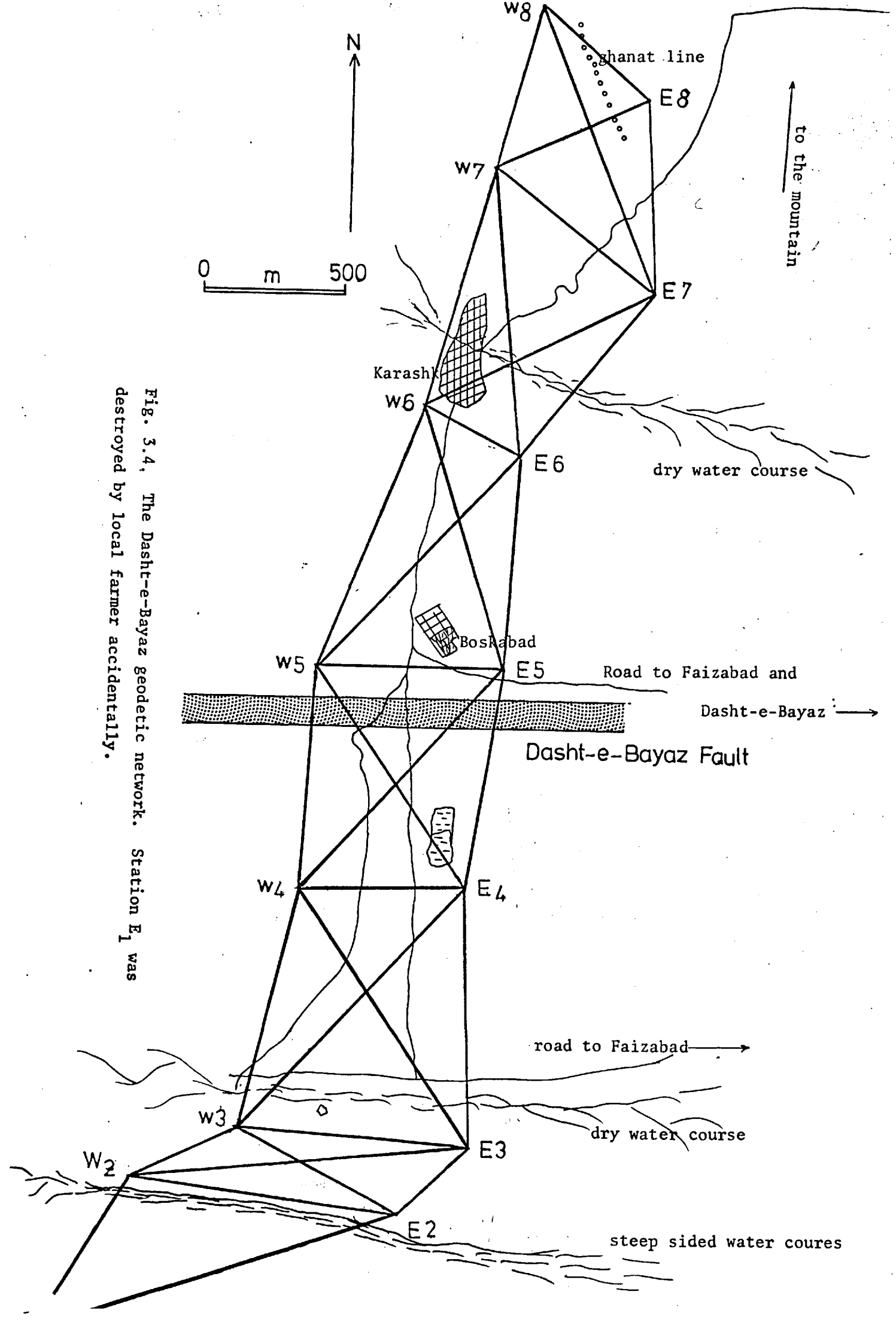



Fig. 3.4, The Dasht-e-Bayaz geodetic network. Station $E_1$ was destroyed by local farmer accidentally.

After the West 5 ridge, the southward road branches again. Both branches continue southwards, but displaced east and west. The east branch passes close by a deserted farm, which the west branch misses by about two hundred meters. East 4 is to be found about 100m south-east of the deserted farm. West 4 is west of the other road and rather south of the farm.

Continuing southwards from West 4, the westerly road reaches and crosses with some tortuousness, a wide water course on whose southern bank is a ruined house. Behind this, a road running east to Faizabad crosses the westerly road. West 3 is about thirty meters south of the cross-roads. East 3 is on the southern bank of the dry water course, some way east of some cultivated land.

The next two stations, East and West 2, are very close to the last two, in positions dictated by the topography. Both are on the northern bank of a very steep-sided water course. The last two stations, East and West 1, are both on a ridge some way south of the steep sided water course, in sight of a second ruined house.

### 3.6.2 The Great Kavir (Doruneh) Fault network

This network, of eight steel and concrete stations, was built near Kalib abad (west of Kashmar) in the foothills of a large mountain and first measured in May 1972. Unfortunately, in December 1974, it was found that seven of the eight stations had been

methodically destroyed, with certain features of the destruction strongly suggesting premeditated sabotage.

It is unlikely to have been the work of local peasants because there was nothing of particular value in the construction, and because only a few of the steel angle irons (which were the most valuable part) were missing. There were pick axe marks in the concrete fragments, and the only station not destroyed lay apart from the others across a small river gulley.

If these stations had not been destroyed, and suppose a rapid rate of movement would have been measured along this fault, some conclusions of the thesis would have had to be modified. However, four triangulation networks built by the Cambridge team on the same fault in 1971, and remeasured in three occasions until 1974, (with the accuracy of $\pm$ 5mm) did not reveal any appreciable movement (G. King and D. McKenzie personal communication). This apparent lack of creep along the Great Kavir Fault, if true, supports the conclusion derived from microearthquake studies in this area, as presented in Chapter IV.

## 3.7 Results from the Dasht-e-Bayaz network

Distance measurements have been made with the prototype N.P.L. Mekometer on all the lines of the network on two occasions, in November 1971 and April 1972, and with a commercial Kern Mekometer

in November 1974. Results of these three successive measurements are presented in Table 3.1.

Their analysis through the displacement vector method did not reveal any consistant movement at the first try. However, as discussed earlier (Section 3.3), in order to obtain maximum precision from these distance measurements it is found necessary to measure also the vertical angles between the stations, which was done for only one quadrilateral in 1973, that which actually crosses the fualt break (Figure 3.5)near the village of Boskabad and for other quadrilaterals in 1974.

Using these vertical angles it has been possible to correct the distance measurements to about $\pm$ 2mm so that distance changes of more than about 3mm can be considered significant.

The results from the one quadrilateral have been analysed on the assumption that the observed changes represent homogeneous strain across the entire area of the quadrilateral; they show that in the period concerned there was left-lateral shear strain across the quadrilateral amounting to 8 $\pm$ 5mm and extension of 4 $\pm$ 4mm. The error limits indicate that the former of these should be considered significant, although the latter should not. The results also show that the direction of maximum extension is N124 ($\pm$15)E. Such a system of compression and extension suggests a left-lateral shear movement along the surface break in this area, which strikes at N85° E. However, the strain and slip pattern in the periods

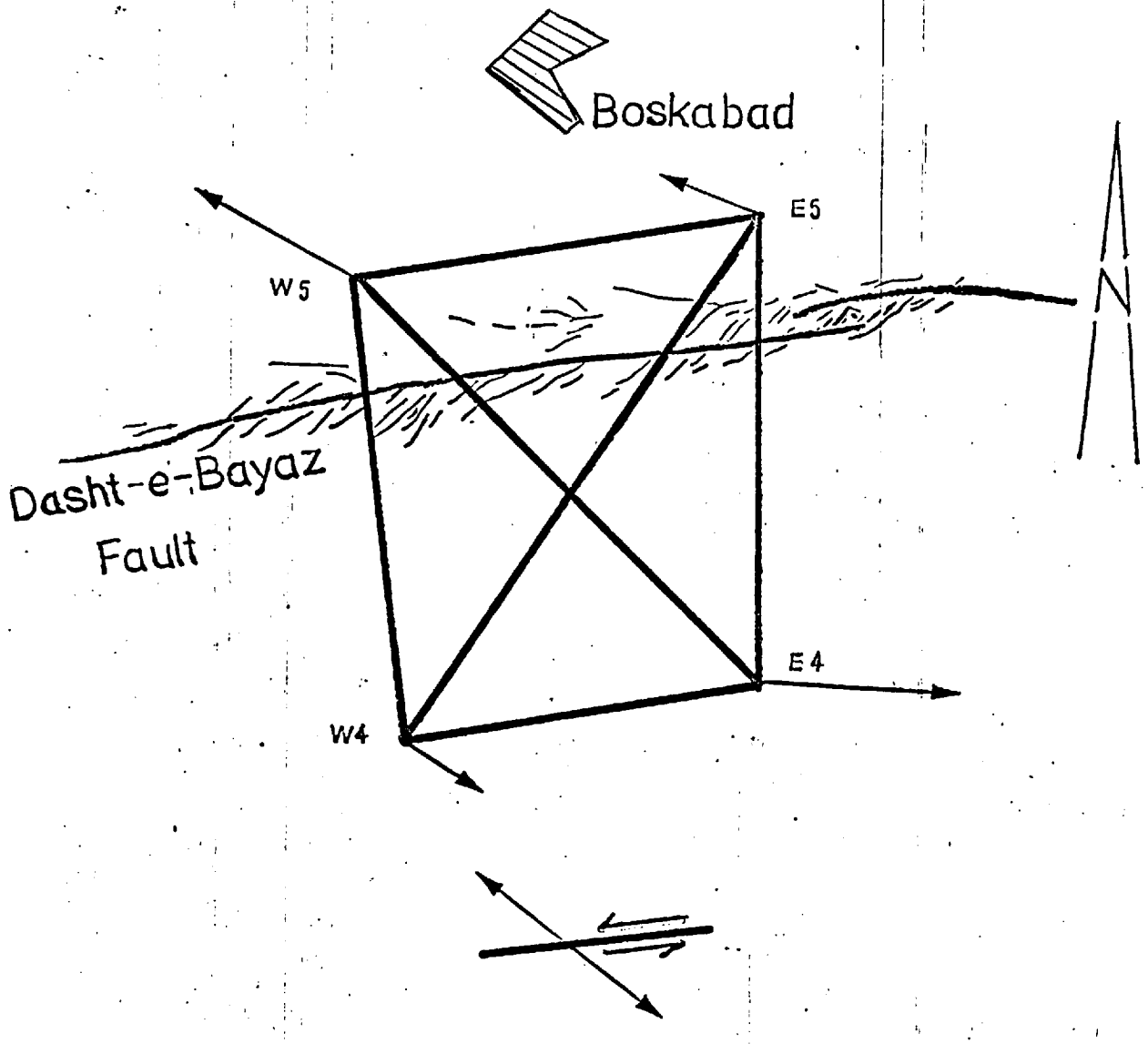



Fig. 3.5. Slip vector analysis of the 1971-72 mekometer results in a quadrilateral straddling the fault.

TABLE 3.1

SUMMARY OF RESULTS

HORIZONTAL DISTANCES AT DASHT-E-BAYAZ NETWORK

| Line | 1971 | 1972 | 1974 |
|---|---|---|---|
| | m. | m. | m. |
| W2-W1 | 652.3379 | 652.3467 | 652.3475 |
| E2-W2 | 975.8188 | 975.7967 | 975.8044 |
| E2-W1 | 1383.6594 | 1383.6470 | 1383.6499 |
| W2-W3 | 428.5599 | 428.5547 | 428.5647 |
| E3-W3 | 829.9383 | 829.9432 | 829.9426 |
| E2-E3 | 346.8200 | 346.8181 | 346.8281 |
| W2-E3 | 1223.2128 | 1223.1996 | 1223.2035 |
| E2-W3 | 652.0075 | 651.9884 | 651.9856 |
| W4-W3 | 887.1015 | 887.1006 | 887.0915 |
| E4-W4 | 601.0595 | 601.0648 | 601.0585 |
| E4-E3 | 934.5153 | 934.5188 | 934.5175 |
| E4-W3 | 1185.7049 | 1185.7099 | 1185.7067 |
| W4-E3 | 1117.1940 | 1117.1932 | 1117.1916 |
| W4-W5 | 803.2083 | 803.2044 | 803.1953 |
| W5-E5 | 676.1999 | 676.1937 | 676.1981 |
| E4-E5 | 800.5459 | 800.5485 | 800.5477 |
| W4-E5 | 1077.8578 | 1077.8551 | 1077.8555 |
| E4-W5 | 967.9758 | 917.9876 | 967.9841 |
| W6-W5 | 1014.5531 | 1014.5528 | 1014.5559 |
| E6-W6 | 399.0731 | 399.0614 | 399.0737 |
| E6-E5 | 764.4060 | 764.4190 | 764.4094 |
| E6-W5 | 1052.8363 | 1052.8431 | 1052.8358 |
| W6-E5 | 992.8071 | 992.8166 | 992.8069 |

TABLE 3.1 (cont'd)

| Line | 1971 | 1972 | 1974 |
|---|---|---|---|
| | m. | m. | m. |
| W6-W7 | 846.6489 | 846.6380 | 846.6332 |
| W7-E7 | 706.6880 | 706.6757 | 706.6790 |
| E6-E7 | 767.0476 | 767.0417 | 767.0393 |
| W6-E7 | 919.3351 | 919.3389 | 919.3361 |
| E6-W7 | 1010.5817 | 1010.5708 | 1010.5714 |
| W8-W7 | 669.5935 | 669.5962 | 669.6026 |
| W8-E8 | 524.8284 | 524.8147 | 524.8196 |
| E8-E7 | 707.2969 | 707.3123 | 707.2968 |
| E8-W7 | 651.6584 | 651.6700 | 651.6625 |
| W8-E7 | 1123.3569 | 1123.3672 | 1123.3679 |

TABLE 3.2

1971-72 Strain Analysis Summary

| Triangle | $\varphi^\circ$ | $\gamma$ | $\Delta$ | $e_1$ | $e_2$ |
|---|---|---|---|---|---|
| W1-W2-E2 | 357° | 36.7 | 9.0 | 45.7 | -27.7 |
| W2-W3-E2 | 47° | 20.1 | -41.5 | -20.6 | -61.6 |
| W3-E3-E2 | 91° | 127 | -114 | 13 | -241 |
| W2-W3-E3 | 111° | 67.8 | -85.9 | -18.1 | -153.7 |
| W2-E2-E3 | 61° | 92.5 | -95.4 | - 2.9 | -187.9 |
| W3-W4-E3 | 75° | 8.9 | 4.0 | 12.9 | - 4.9 |
| W3-W4-E4 | 74° | 11.7 | 5.6 | 17.3 | - 6.1 |
| W3-E4-E3 | 113° | 5.2 | 12.1 | 17.3 | 6.9 |
| E3-W4-E4 | 47° | 15.5 | 13.4 | 28.9 | - 2.1 |
| W4-W5-E5 | 107° | 13.7 | - 4.6 | 9.1 | - 18.3 |
| W4-W5-E4 | 104° | 28.7 | 4.0 | 32.7 | - 24.7 |
| E4-W5-E4 | 332° | 26.7 | - 0.4 | 26.3 | - 27.1 |
| W4-E5-E4 | 129° | 15.0 | 15.0 | 3.0 | 0 |
| W5-E6-E5 | 167° | 27.9 | 8.5 | 36.4 | - 19.4 |
| E5-W6-E6 | 21° | 58 | - 23.6 | 34.4 | - 81.6 |
| W5-W6-E6 | 42° | 44.9 | - 28.0 | 16.9 | - 42.9 |
| W5-W6-E5 | 322° | 21.2 | - 0.9 | 20.3 | - 22.1 |
| W6-W7-E7 | 64° | 28 | - 19.5 | 8.5 | - 47.5 |
| W6-W7-E6 | 89° | 24.1 | - 1.9 | 22.2 | - 26.0 |
| E6-W7-E7 | 28° | 10.0 | - 24.1 | - 14.1 | - 34.1 |
| W6-E7-E6 | 64° | 61.8 | - 51.9 | - 10.0 | -113.7 |
| W7-W8-E8 | 93° | 26.8 | 32 | 58.8 | 5.2 |

TABLE 3.2 (Cont'd)

| Triangle | $\varphi^\circ$ | $\gamma$ | $\Delta$ | $e_1$ | $e_2$ |
|---|---|---|---|---|---|
| W7-E8-E7 | $21^\circ$ | 50.8 | 19.6 | 70.4 | 31.2 |
| W7-W8-E7 | $342^\circ$ | 47.0 | - 19.7 | 27.3 | - 66.7 |
| E7-W8-E8 | $70^\circ$ | 144 | 161 | 305 | 17 |

$\varphi$ = Azimuth of the extension axis

$\gamma$ = Shear strain

$\Delta$ = Dilatation

$e_1$, $e_2$ = Principle longitudinal strains

TABLE 3.3

1971-74 Strain Analysis Summary

| Triangle | $\varphi^\circ$ | $\gamma$ | $\Delta$ | $e_1$ | $e_2$ |
|---|---|---|---|---|---|
| W1-W2-E2 | 3° | 35.4 | 5.5 | 40.9 | - 30 |
| W2-W3-E2 | 51° | 53.3 | - 28.5 | 24.8 | - 81.3 |
| W3-E3-E2 | 305° | 129 | - 82.4 | 46.6 | -211.4 |
| W2-E2-E3 | 168° | 117 | 102 | 219 | - 15 |
| W2-W3-E3 | 129° | 168.6 | 148 | 316.6 | - 20.8 |
| W3-W4-E3 | 98° | 16.9 | - 5.7 | 11.2 | - 22.6 |
| W3-W4-E4 | 56° | 29.4 | - 20.2 | 9.2 | - 49.6 |
| E3-W4-E4 | 33° | 9.1 | 1.1 | 10.2 | - 8.0 |
| W3-E4-E3 | 109° | 4.6 | 6.9 | 11.5 | - 2.3 |
| W4-W5-E4 | 106° | 42.1 | - 14.4 | 27.7 | - 56.5 |
| W4-E5-E4 | 23° | 5.4 | - 0.3 | 5.1 | - 5.7 |
| E4-W5-E5 | 324° | 9.2 | 8.0 | 17.2 | - 1.2 |
| W4-W5-E5 | 45° | 27.9 | - 13.8 | 14.1 | - 41.7 |
| E5-W6-E6 | 78° | 2.7 | 2.6 | 5.3 | 0 |
| W5-W6-E6 | 338° | 10.5 | 0 | 10.5 | - 10.5 |
| W5-E6-E5 | 138° | 8.6 | 7.3 | 15.9 | - 1.3 |
| W5-W6-E5 | 49° | 5.2 | - 3.4 | 1.8 | - 8.6 |
| W6-W7-E6 | 146° | 62.9 | - 37.0 | 25.9 | -100.0 |
| W6-W7-E7 | 76° | 25.0 | - 21.7 | 3.3 | 46.7 |
| W6-E7-E6 | 85° | 36 | - 19 | 17 | - 55 |
| E6-W7-E7 | 356° | 19.7 | - 19.3 | 0 | - 39 |
| W7-W8-E8 | 22° | 32.8 | - 2.8 | 30.0 | - 35.6 |
| W7-W8-E7 | 351° | 38.5 | - 3.0 | 35.5 | - 41.5 |
| W7-E8-E7 | 26° | 25.4 | 0 | 25.4 | - 25.4 |
| E7-W8-E8 | 338° | 31.4 | - 11.8 | 19.6 | - 43.2 |

Symbols as in Table 3.2

1971 to 1974 and 1972 to 1974 are very complicated and mostly in a reverse sense to that of 1971 to 1972 (as summarized in Tables 3.1 to 3.3), which might suggest development of an elastic rebound type of strain release through the observed time interval. Alternatively, relaxation of the dominant NE-SW compressive stresses might be the causative agent.

# CHAPTER IV

# MICROEARTHQUAKE STUDIES

## 4.1 Introduction

If there is a true correlation between earthquakes and faulting, then areas of high earthquake risk should be looked for around zones of extensive faulting. The same consideration applies to the selection of sites for constructing geodetic networks for investigating any gradual or episodic movements which might be related to earthquake occurrence. There are, however, several problems and comments related to this proposal, such as:

1. Geological faults might not be active at the present time, or their activity might be episodic, with long quiescent time intervals of the order of several tens or hundreds of years.

2. It is not necessary that all fault planes in the crust extend to the surface.

3. Substantial displacements may be accommodated by numerous small earthquakes in some sections without the occurrence of major shocks.

4. The frequency of occurrence of large magnitude earthquakes may be low in relation to the less than 50 years since seismographic stations were first established, and historical records are scattered and sometimes insufficiently complete to reveal narrow bands of earthquake activity.

5. Accuracy of NOAA instrumentally located earthquakes is in the order of $\pm$ 20 kilometers and the locations of historical shocks are vaguely defined. This is the main source of uncertainty in pinpointing the main active trace in a complex and close packed fault system.

The above-mentioned difficulties in delineating the active fault strips become quite important in the process of selecting sites for the precise measurements of the ground movements, as the author found when looking for sites for Mekometer networks among the complicated pattern of Quaternary faulting in Iran.

In eastern Iran, where the frequency of large earthquakes is not high and the historical record is short, zones of seismicity can only be vaguely delineated on the information given by past earthquakes. Thus, some other criterion is necessary for deciding where to concentrate the effort.

It has been suggested by many investigators that there must be a great deal of information on current tectonic activity in the form of seismic wave radiation from the very small earthquakes known as microearthquakes.

Asada (1957) showed that, in an active region, many small earthquakes could be detected by ultra-sensitive seismographs, and the following year (Asada, *et al.* 1958) suggested that observation of such activity might yield a quick measure of the general seismicity. Since then, microearthquakes have been recorded in the United States and elsewhere on very sensitive portable equipment in attempts to describe the areal distribution of seismicity with better resolution than that obtainable from fixed networks.

Although a single small shock obviously does not, in general, have the significance of a single large shock, microearthquakes are important because of their high rate of occurrence and their widespread distribution.

It is frequently asserted that there exists a logarithmic

relationship between the number of earthquakes and their seismic magnitudes. This situation is expressed as (recurrence curve)

$$\log N = a - bm$$

where N is the number of earthquakes occurring usually in one year, m the seismic magnitude, and a and b are constants established by observation. Evernden (1970) has studied all the available recurrence curves from all over the world and concluded that the relation between log N and m is linear down to magnitude 3 or below. An example of these recurrence curves is shown in Figures (4.1)

In theory, the logarithmic increase in the number of earthquakes with decreasing magnitude, if maintained, could allow a useful sample of the seismic activity to be recorded in a few days or weeks rather than the tens or hundreds of years required by conventional networks.

As pointed out in Chapter 1.2, microearthquakes have also been extensively used to delineate the traces of presently active belts in many areas (Allen 1968 and Healy et al., 1972). In addition, it is widely assumed that microshocks could represent the same source mechanism as the major shocks in an area and thus, a composite fault plane solution (CFPS) might serve as a quick substitute for a normal fault plane solution in the same region. Composite fault

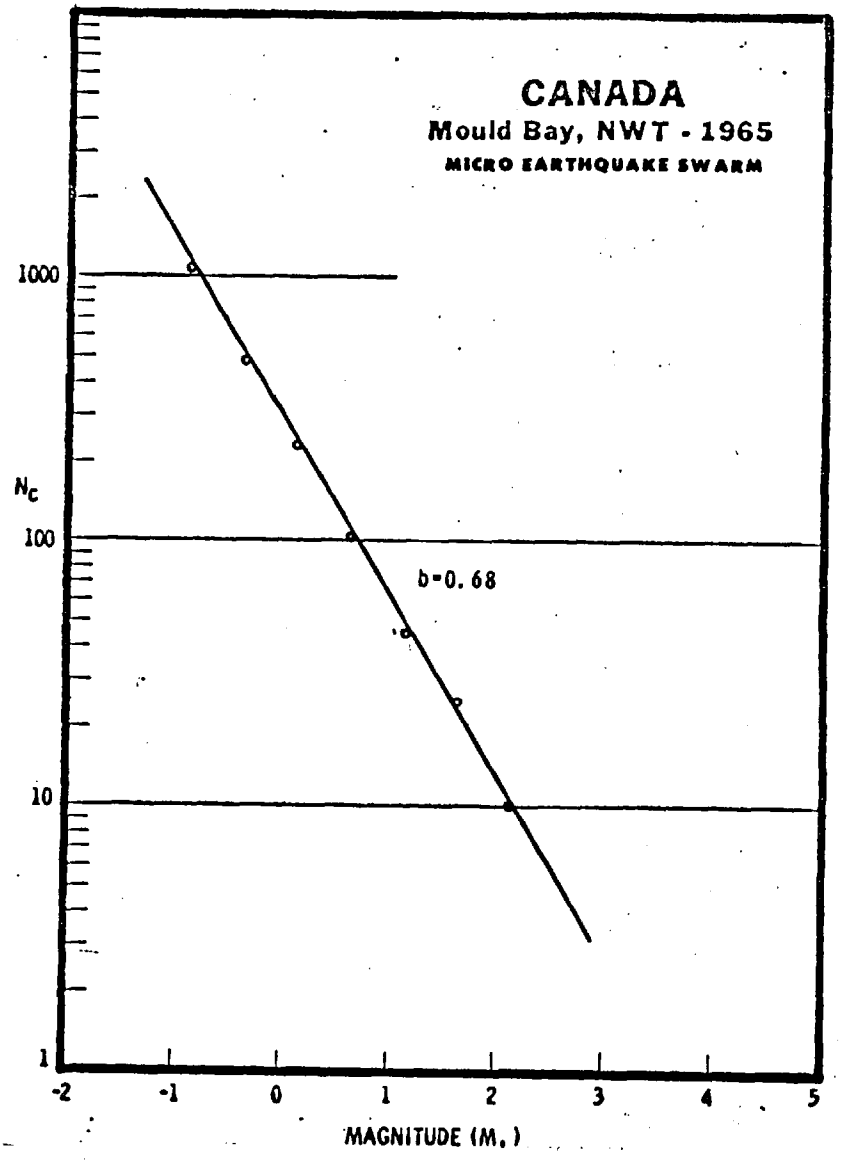



Fig. 4.1. An example of the regional seismicity curve extending to low and negative magnitude ranges. (After Evernden, 1970).

plane solutions have been successfully used by many authors (e.g. Gutenberg, 1941; Aki, 1966; Scholz et al., 1969; Seeber et al., 1970; and Crosson, 1972) to infer the details of slip patterns in complex areas. It might be feared that small shocks are the result of such localized stress patterns and zones of weakness that their focal mechanisms might correlate with each other only in a statistical way. However, Scholz et al., (1969) have shown that for a limited segment of the San Andreas fault the CFPS were nearly identical and a unique composite solution could be obtained.

As discussed in Chapter 1.2 microearthquakes are also capable of revealing the premonitory changes in seismic velocities which are thought to correlate with time of occurrence and size of large earthquakes (Aggarwal et al., 1973, Whitcomb et al., 1973 and Scholz et al., 1973).

Major shocks are the result of sudden energy release in an area subjected to considerable strain accumulation. Although a higher proportion of this strain is released by the main shock, the aftershock phase, with numerous microearthquakes,which might continue for several years, is responsible for a small but steady energy release within the zone. Thus, careful study of the aftershocks could lead to an estimate of the dimension of the strain relieved area; in other words it would define the extent of subsurface crack propagation associated with the seismic activity of the area.

An attempt has been made to summarize all the above ideas and hypotheses in the form of a flow chart (Figure 4.2) and this motivated the author to propose a systematic approach to the use of microearthquake observations in tackling problems of neotectonics, and in particular the question of the most suitable sites for constructing geodetic networks.

## 4.2 Programme of microearthquake studies in eastern Iran

In principle, the simplest way to study microearthquake activity is to count them, so we started by constructing during the winter of 1971/72 a batch of five seismic event counters in Imperial College. These were designed to make a continuous count of seismic events, defined as ground motion in excess of a certain pre-set level. The intention was to deploy them during 1972 along one or other of the faults, at separations of perhaps 10 km, and to move them progressively along the fault, moving one instrument each day, so that each instrument remained in the same place for five days. By this means, 10 km. of fault could be scanned each day and in the course of one month some 300 km. of fault might be examined. In order to provide a basis for deciding what the counters were in fact counting, I borrowed two Sprengnether portable smoked drum seismographs from the University of Mashad.

Unfortunately, the counters were not particularly successful because they tended to be unstable and to give spurious

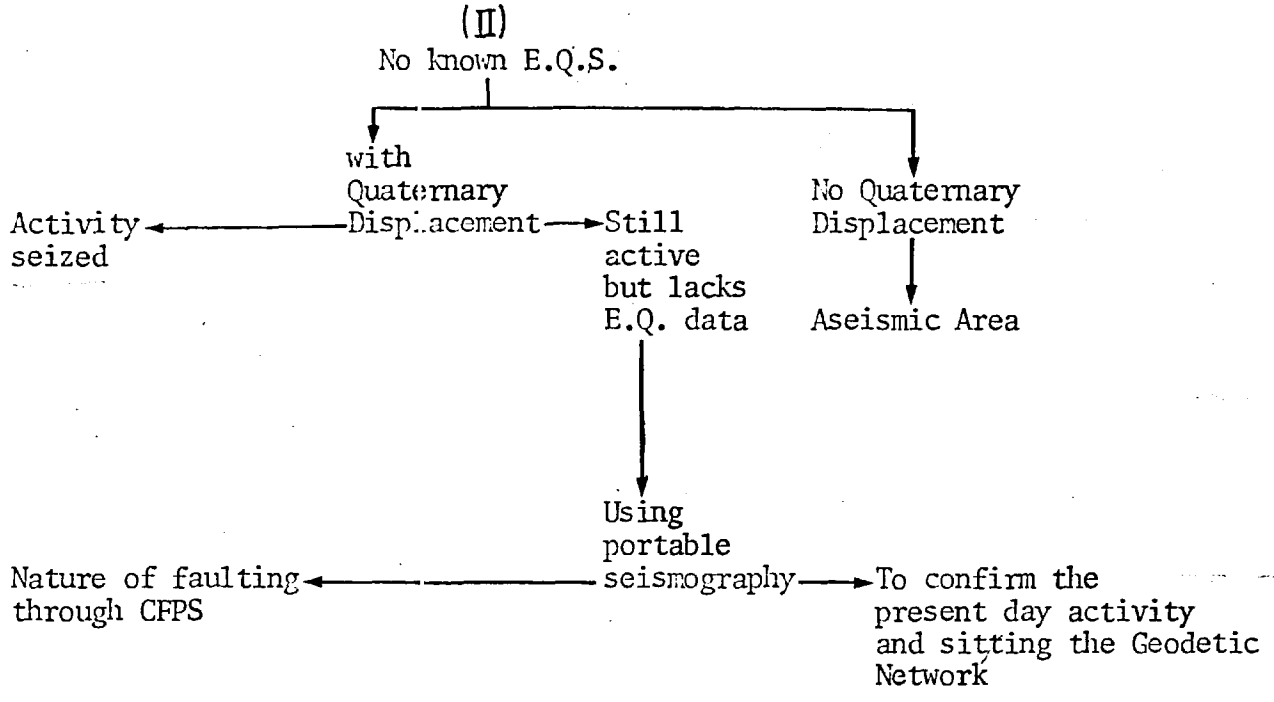
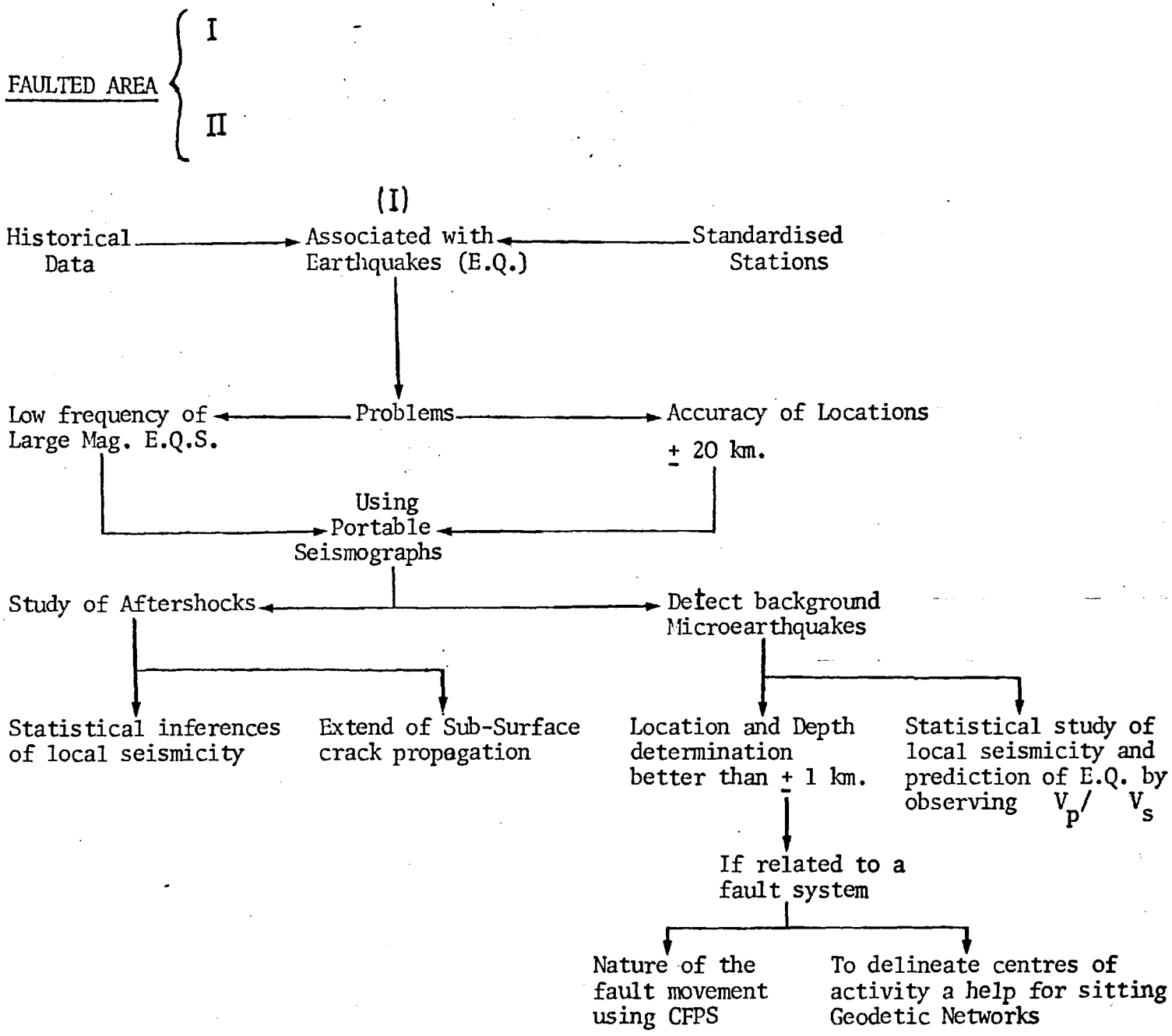



Figure 4.2. Flow chart of the application of microearthquakes in seismotectonics investigation of an area.


FAULTED AREA
I
II
(I)
Historical Data
Associated with Earthquakes (E.Q.)
Standardised Stations
Low frequency of Large Mag. E.Q.S.
Problems
Accuracy of Locations ± 20 km.
Using Portable Seismographs
Study of Aftershocks
Detect background Microearthquakes
Statistical inferences of local seismicity
Extend of Sub-Surface crack propagation
Location and Depth determination better than ± 1 km.
Statistical study of local seismicity and prediction of E.Q. by observing $V_p/V_s$
If related to a fault system
Nature of the fault movement using CFPS
To delineate centres of activity a help for sitting Geodetic Networks

readings. However, the seismographs proved very satisfactory, and with them I made a reconnaissance of the microearthquake activity on part of the Dasht-e-Bayaz fault. This gave useful information about the nature of the earthquakes and their frequency of occurrence, but with only two instruments it was not possible to make a point-to-point comparison or to cover as much ground as had been intended. One fact to emerge was that there were a surprising number of man-made and natural disturbances that an event counter would be unable to distinguish from an earthquake.

For the 1973 field season I looked into ways of using a cheap cassette-type of tape recorder so that it would run for more than 24 hours and record microearthquakes rather than count them. However, it was discovered that Oxford Instruments already made such an instrument and so the Geophysics Department borrowed one of these for field evaluation. I also borrowed, from the University of Mashad, two Sprengnether smoked drum microearthquake recorders which, with a similar instrument belonging to Imperial College, provided me with a tripartite array of seismographs. With this, I made microearthquake studies along the Dasht-e-Bayaz fault between Ferdows in the west and Kuli in the east and on the Great Kavir fault from Rushtkhar near the Iran-Afghan border at its eastern end and to Bardaskan in the west (Figure 4.6) in June and July 1973, which are reported in the following.

## 4.3 Instrumentation

Three short-period high-gain portable seismographs were used in this study. Two of them, Sprengnether MEQ600 microearthquake recorders, were kindly provided by the University of Mashad, and the third, a Sprengnether MEQ800, a new model, having higher magnification, high and low pass filters and more compact, belongs to the Geophysics Department of Imperial College.

The MEQ800 system is housed in an aluminium weatherproof case measuring 46 x 32 x 24 cm and weighs 32 lbs. (14.5 kg ). A Willmore fixed period (1 Hz) geophone drives the amplifier, whose output impedance is matched to a friction pen motor. The pen writes on a sheet of glazed paper 13'5" x 24" (343 x 600 mm ) that is smoked and mounted on a rotating drum.

Time marks are provided on thc records by a precision digital clock every minute and are calibrated daily with radio time (BBC London or Radio Moscow). The whole system draws about 16 ma, equivalent to 0.4 watts, in the quiescent state and about 150 ma at maximum signal level. System power is supplied by four internal 12 volt, 1.5 ampere hour sealed lead-acid batteries, connected in series/parallel, normally providing 200 hours of operation. However, under the high temperatures between 35°C and 45°C encountered in the desert area along the Great Kavir Fault, the batteries were

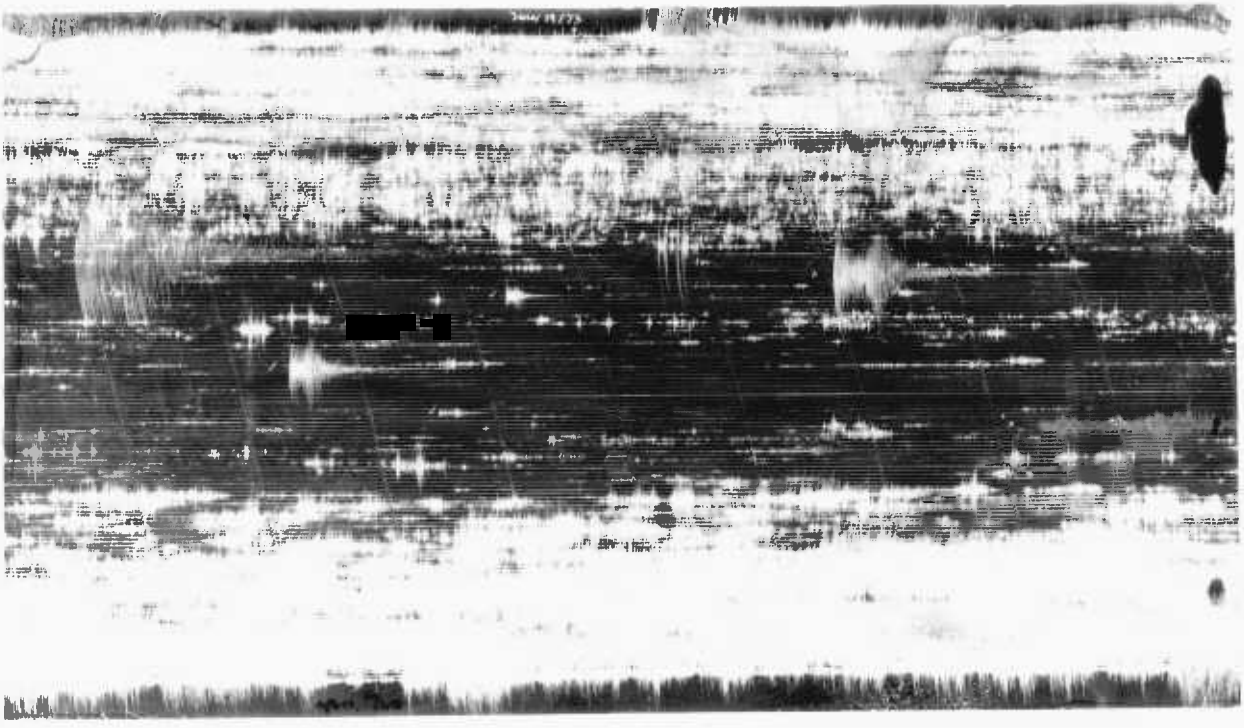
exhausted within 10 to 12 hours. The excessive heat was also found to have an undesirable effect on the regulated drive of the drum and the pen motors. Examples of records which suffered from this trouble are shown in Figure (4.3).

In this field work the amplifier gains were normally set in the range of 90 to 102 db., corresponding to an overall magnification of between 32,000 and 100,000, based on the background noise of the station. Figure (4.4) shows the absolute magnification as a function of frequency in the seismograph used.

The recorder was normally operated with a drum speed of either 30 or 60 mm/min., running unattended for two and one days respectively on the MEQ600 and MEQ800 models. A few records from the N. Kashmar area were run for 12 hours at a speed of 120 mm/min to obtain a greater time resolution.

With care, and using a magnifying lens, records could be read to 0.2 mm. or better, giving timing precisions of 0.4, 0.2 and 0.1 seconds for drum speeds of 30, 60 and 120 mm/min respectively. This time resolution is not adequate for distinguishing high frequencies and, therefore, introduces a problem for the Richter magnitude determination. There are other problems involved with the Richter scale when using this type of portable seismograph, which are discussed later (section 4.5), and alternative methods are presented there.

Fig. 4.3. Two examples of the smoked paper records which have suffered from excessive background noise in two windy periods (top figure) and from excessive air temperature which has affected drive of the pen motor and consequently caused sub-parallel kinks in the minute marks alignments (bottom figure). The lower record also exhibits some harmonic patterns which are thought to relate to cyclic noises generated in the amplifier.



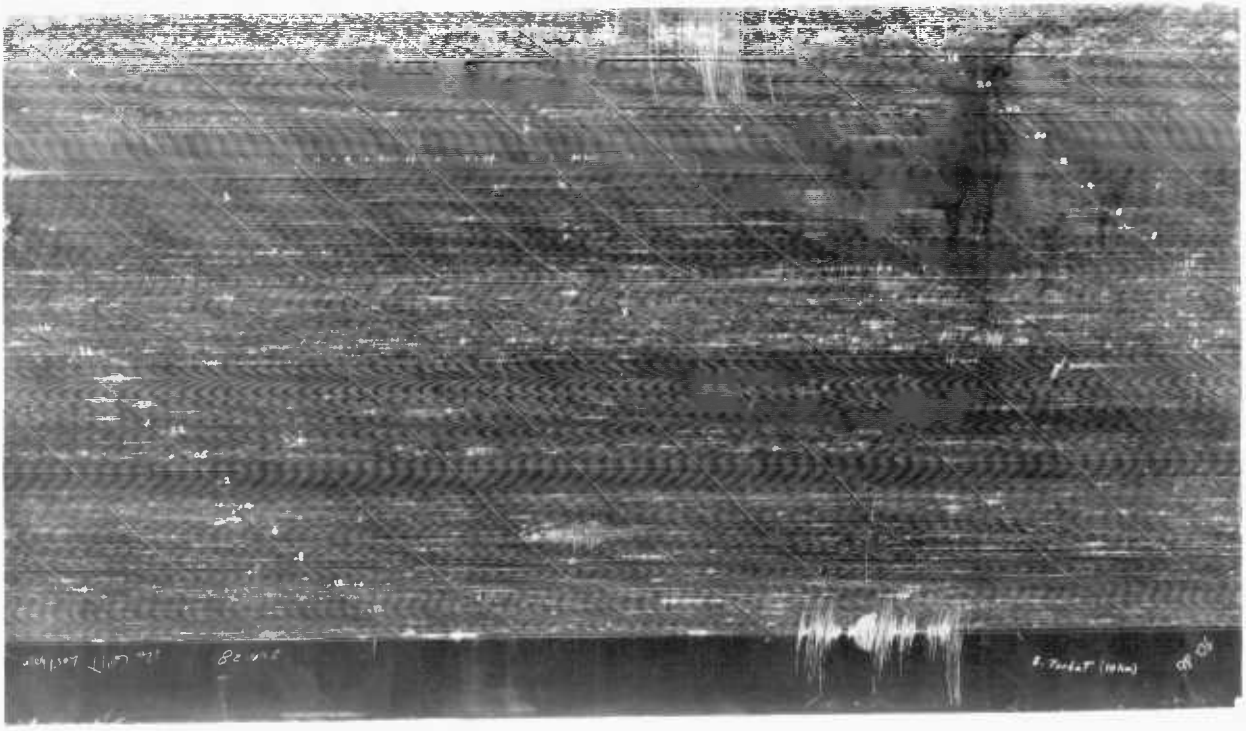


Fig. 4.4. Frequency response curve for MEQ 800 Sprengnether seismograph.

Curves

I, when High and Low frequency filters out

II, when low frequency filter = 5

III, when low frequency filter = 10

IV, when high frequency filter = 5

V, when high frequency filter = 10

VI, when high frequency filter = 30

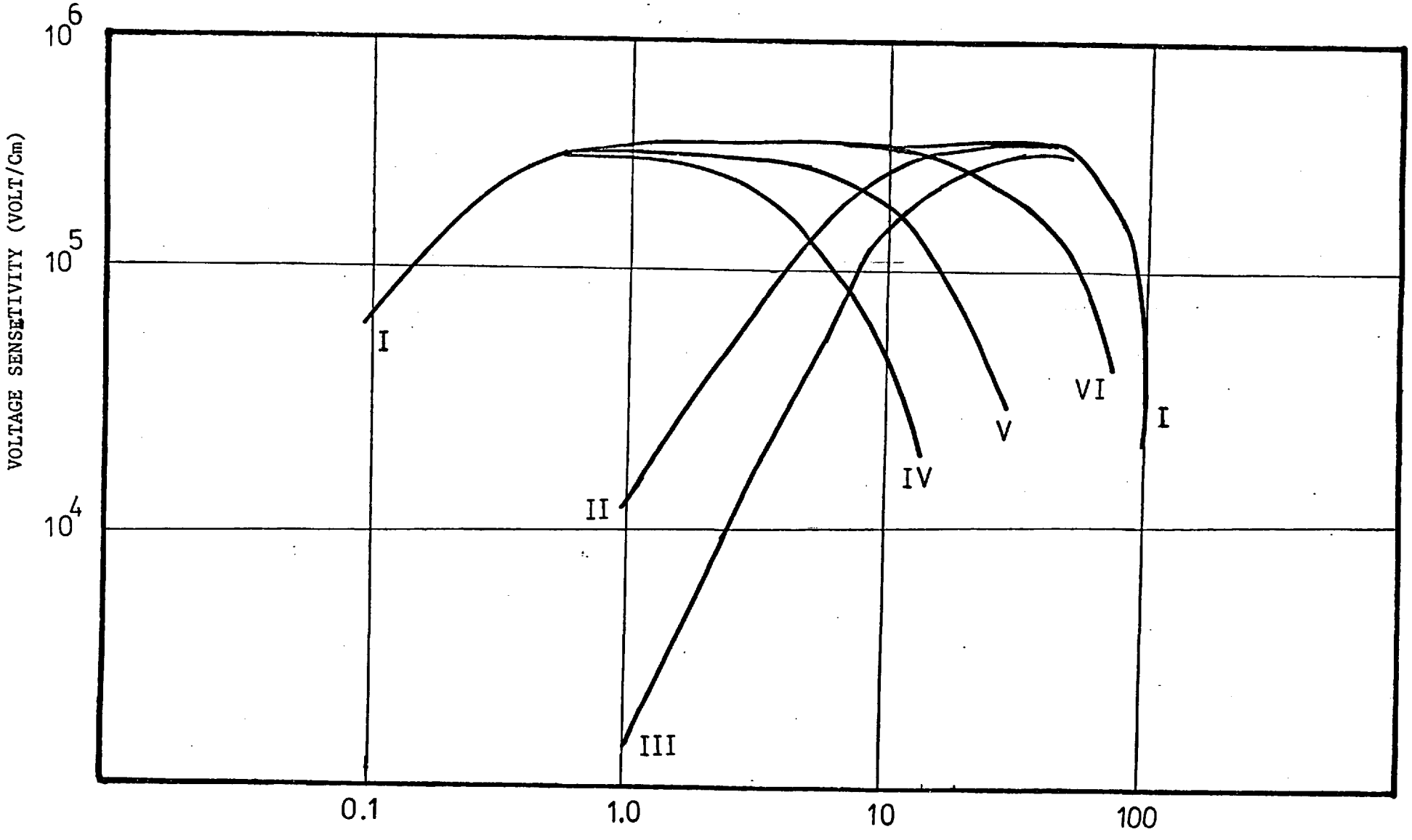

VOLTAGE SENSETIVITY (VOLT/Cm)
$10^6$
$10^5$
$10^4$
I
II
III
IV
V
VI
I
0.1
1.0
10
100
FREQUENCY (Hz)

Fig. 4.4

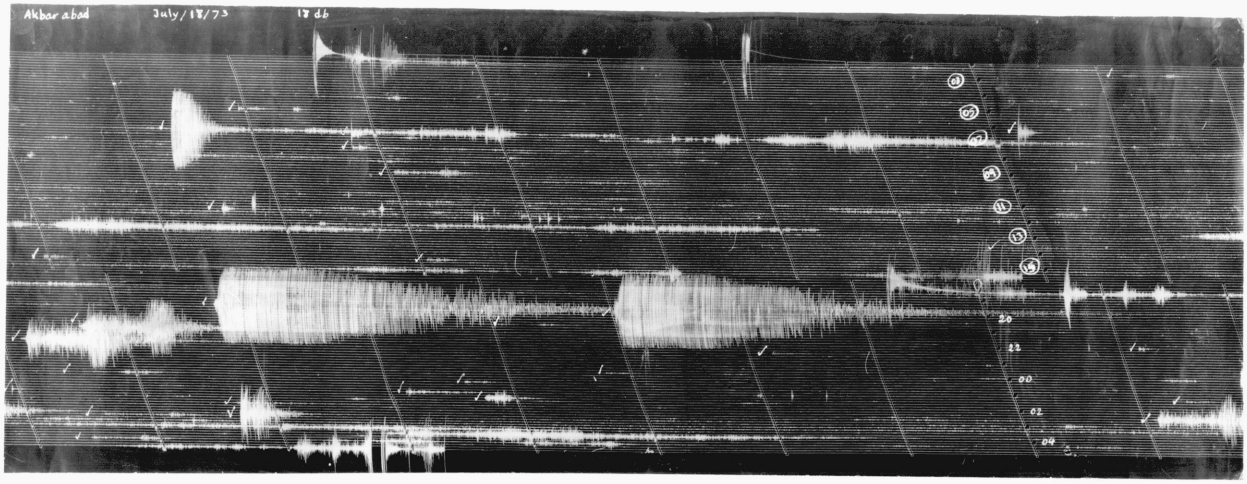
## 4.4 Data analysis

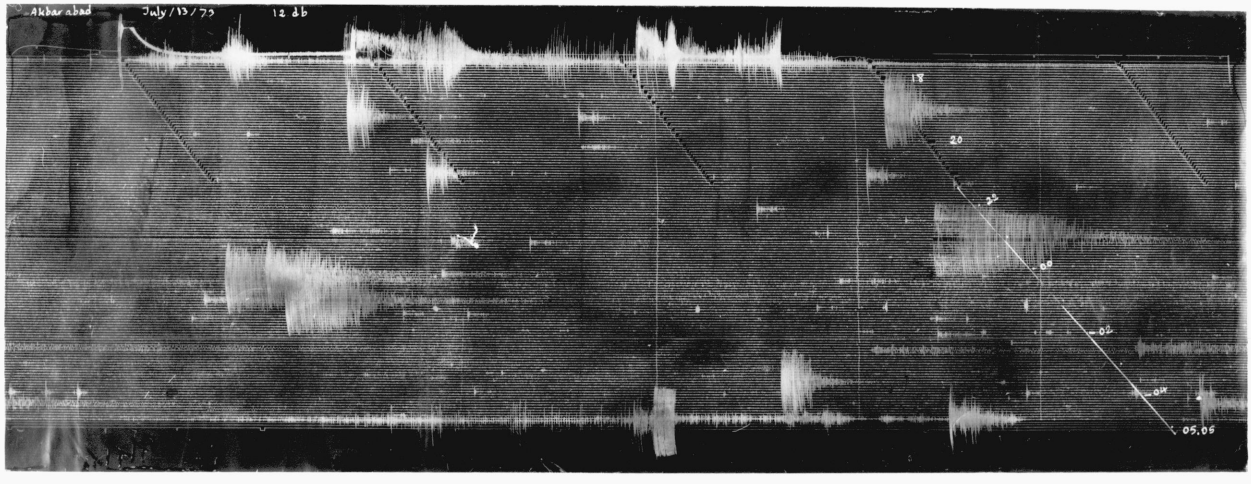
Earthquakes were identified by their abrupt beginnings, distinct P and S phases, frequency characteristics and a slowly-decaying coda. In smaller events, these properties are often difficult to distinguish and, therefore, to be on the safe side many doubtful events were eliminated from final consideration. Furthermore, each record was correlated with other stations whenever possible. Examples of microearthquakes identified on records obtained in the north Kashmar area are shown in Figure (4.5). Most of the shocks recorded there exhibited impulsive first arrivals and a fast decaying coda, which is thought to be related to their mechanism (see section 4.9) and their magnitude.

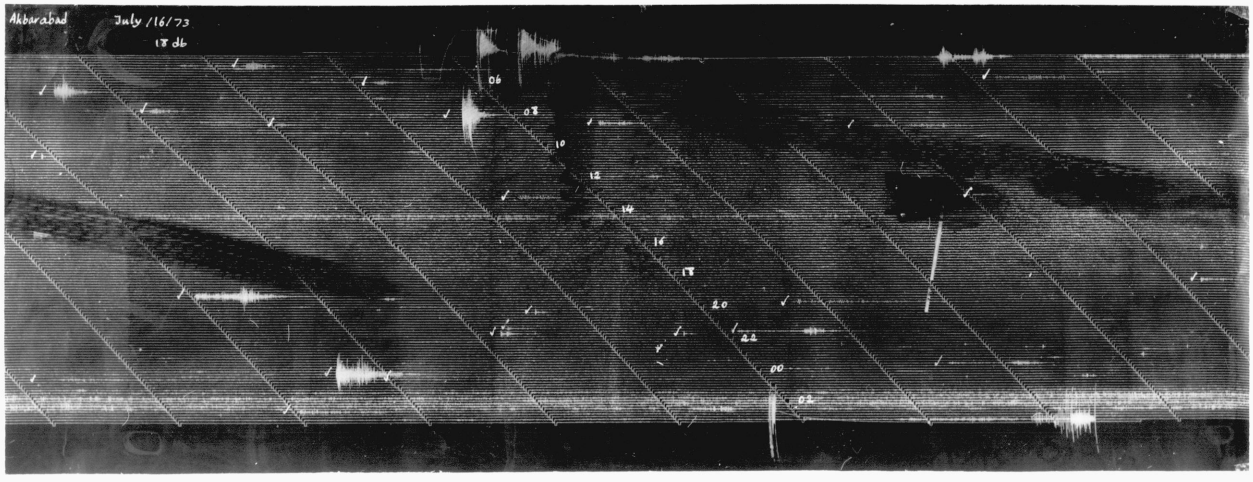
With the usual drum speed of 24 or 48 hours per record (corresponding to 60 mm/min. and 30 mm/min) it is difficult to determine the frequencies involved. However, the dominant frequency of the waves is mostly between 7 and 12 Hz, as measured on the few records run at the greatest drum speed (12 hours per record or 120 mm/min.).

A magnifying lens was always used to read P arrivals and S-P times, also to estimate the coda length of the events and their maximum amplitudes. Care was taken not to use any intervals of time with high noise levels. This simplified the analysis considerably,

Fig. 4.5. Three smoked paper records of N. Kashmas (Akbarabad) station showing typical impulsive character of most of the micro-earthquakes recorded in this station. However, there are two exceptions at the left-hand side of the top figure. Note how the limitation on the maximum deflection of the pen produced a rectangular wave signature for the larger magnitude shocks.


Akbar abad
July/12/73
12 db


Akbar abad
July/13/73
12 db
05.06


Akbar abad
July/16/73
12 db

and provided a more homogeneous set of data for comparison between stations. The low-noise recording time totalled 441 hours in the Dasht-e-Bayaz area in 1972 and 105 hours in the same area in 1973. There are also a total of 722.5 hours of noise-free records along the Great Kavir Fault in 1973, of which 333 hours belong to the N. Kashmar area.

## 4.5 Microearthquake occurrence rates

As explained earlier, one of the main purposes of microearthquake surveys along the Dasht-e-Bayaz and the Great Kavir Faults was to find the centres of present day activity and then to concentrate the subsequent geodetic and other detailed crustal studies in them.

This task was started in 1972 by deploying two short-period, high-gain seismographs in Kuli and Ghain, at the eastern end of, and south of, the Dasht-e-Bayaz faults respectively. A similar seismograph was operated simultaneously by the University of Mashad as a permanent station in Kakhk, 30 km. to the north, and its records were made available to the author by kind permission of Professor Niazi. This survey in 1972 was carried out for one week only, subsidiary to other field programmes, and was intended to enable experience to be obtained with the equipment and an estimate to be made of the level of background seismicity. In the following year, in June and July 1973, an extensive survey along these two faults was carried out

TABLE 4.1

Summary of the Microearthquake Survey Data in 1972 and 1973

| Station | Latitude N Deg. | Min. | Longitude E Deg. | Min. | Dates of Recording From | To | Noise Free and Usable Hours of Records | Number of Local Events S-P < 5 sec. | Standardized Daily Activity (Shock/Day) | Standardized Recurrence (Period Min/Shock) |
|---|---|---|---|---|---|---|---|---|---|---|
| 1. Kuli | 34 | 00.0 | 59 | 18.5 | 09 06 - | 15 06 72 | 130 | 105 | 19.3 | 74 |
| 2. Kakhk | 34 | 05.5 | 58 | 38.5 | 08 06 - | 15 06 72 | 145 | 39 | 6.9 | 202 |
| 3. Gain | 33 | 50.2 | 59 | 05.8 | 08 06 - | 15 06 72 | 166 | 26 | 3.6 | 382 |
| 4. Dasht-e-Bayaz | 34 | 01.0 | 58 | 45.0 | 18 06 - | 22 06 73 | 40 | 10 | 4.8 | 159 |
| 5. Kuli | 34 | 01.1 | 59 | 21.0 | 21 06 - | 22 06 73 | 33 | 14 | 10.0 | 141 |
| 6. N. Ferdows | 34 | 08.0 | 58 | 13.0 | 24 06 - | 25 06 73 | 12 | 5 | 6.0 | 140 |
| 7. E. Ferdows | 34 | 00.0 | 58 | 13.1 | 24 06 - | 25 06 73 | 20 | 8 | 9.6 | 150 |
| 8. Torbat-e-Heidarieh | 35 | 13.0 | 59 | 18.0 | 26 06 - | 30 06 73 | 53 | 8 | 0.6 | 529 |
| 9. Zaveh | 35 | 19.1 | 59 | 20.3 | 27 06 - | 04 07 73 | 101 | 10 | 1.6 | 378 |
| 10. Malek-Abad | 35 | 11.2 | 59 | 25.0 | 02 07 - | 04 07 73 | 48.5 | 2 | 0.9 | 1455 |
| 11. N. Rushtkhar | 35 | 06.0 | 59 | 43.1 | 01 07 - | 03 07 73 | 10 | 4 | 9.6 | 150 |
| 12. Nai | 35 | 15.7 | 58 | 43.6 | 06 07 - | 14 07 73 | 177 | 11 | 1.4 | 965 |
| 13. N. Kashmar | 35 | 35.9 | 58 | 33.6 | 06 07 - | 19 07 73 | 266 | 252 | 9.8 | 145 |
| 14. Bardaskan | 35 | 18.0 | 58 | 00.2 | 07 07 - | 09 07 73 | 25 | 11 | 5.7 | 249 |
| 15. Kahriz | 35 | 28.2 | 58 | 23.5 | 13 07 - | 15 07 73 | 30 | 9 | 7.2 | 199 |
| 16. Rivash | 35 | 29.0 | 58 | 26.0 | 15 07 - | 16 07 73 | 12 | 10 | 19.9 | 72 |

using three portable seismographs, and a total of 13 new sites were occupied. Locations of these seismographic stations and occurrence rates are shown in Figure (4.6), and other details such as exact dates of recording, total time of noise-free records, together with the number of shocks recorded in that time, is summarized in Table(4.1).

An attempt has also been made to calculate the rate of occurrence of earthquakes in units of earthquakes per day for each recording station. These rates, of course, become more reliable as the recording time increases. In determining these rates, only events with an S-P time of 5 seconds or less were counted. This corresponds to an epicentral distance of less than 35 km. In the Dasht-e-Bayaz area, where the average station spacing is about 40 kilometers, only events with an S-P time of about 4 seconds or less were considered, in order to minimize the overlap between stations while still including most of the recorded events. Histograms of frequency of occurrence against S-P time Figures (4.7), (4.8) and (4.9) suggest that there is little or no overlap between stations.

Another important point to consider here is the consequence of using different instrumental magnifications. This is responsible for many low - magnitude events to be undetectable at low - magnification stations. Therefore, standardized rates of occurrence were calculated for a possibly more meaningful comparison of relative activity, as shown in Table(4.1). These rates are the expected rates of occurrence

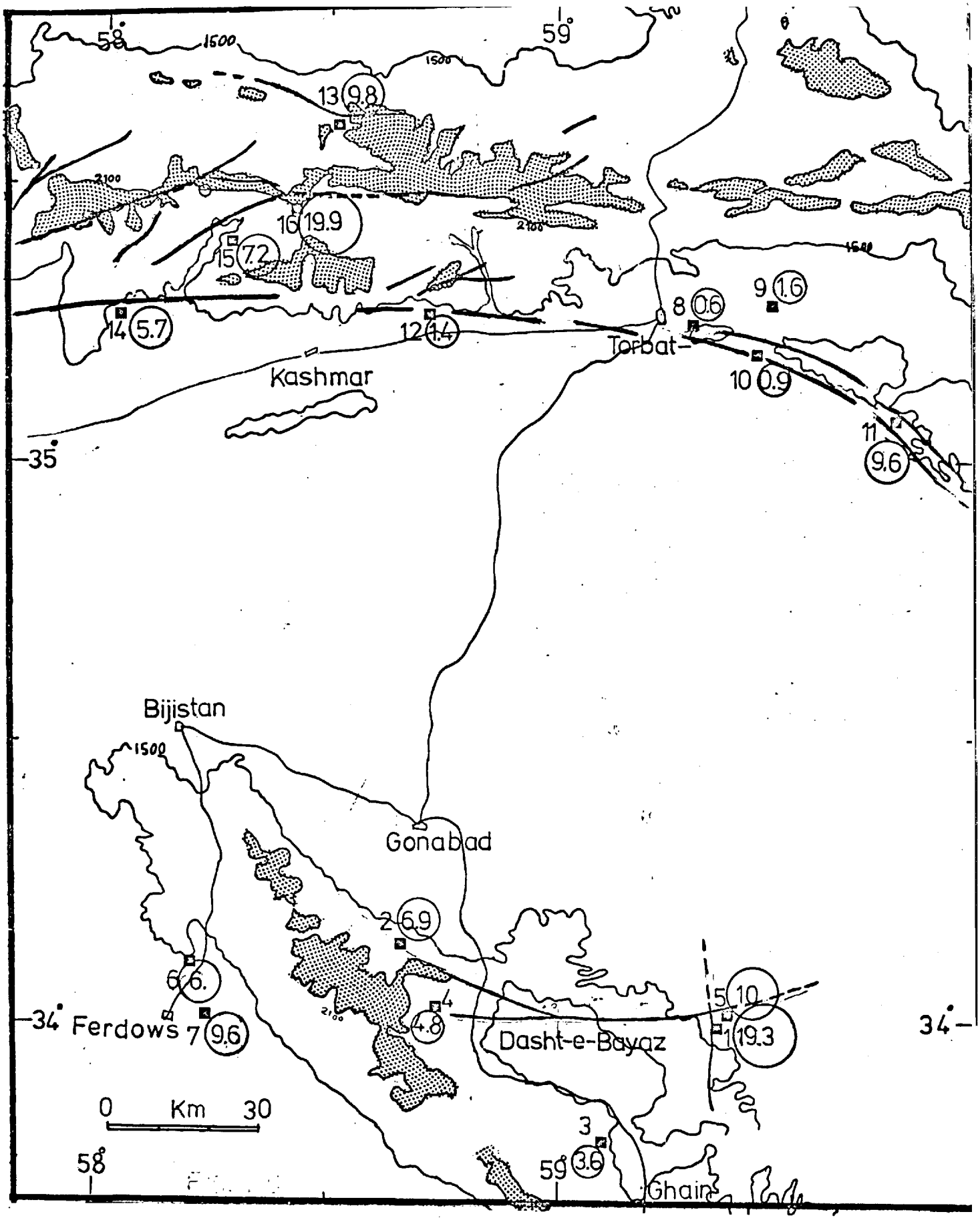



Fig. 4.6. Location of 16 stations occupied to carry out a microearthquake survey along the Dasht-e-Bayaz and the Great Kavir faults in 1972 and 1973. Stations are numbered as in Table 4.1. Numbers inside circles signify the normalized rate of occurance of microearthquakes per day. Topography higher than 2100 m are shown by dotted contour.

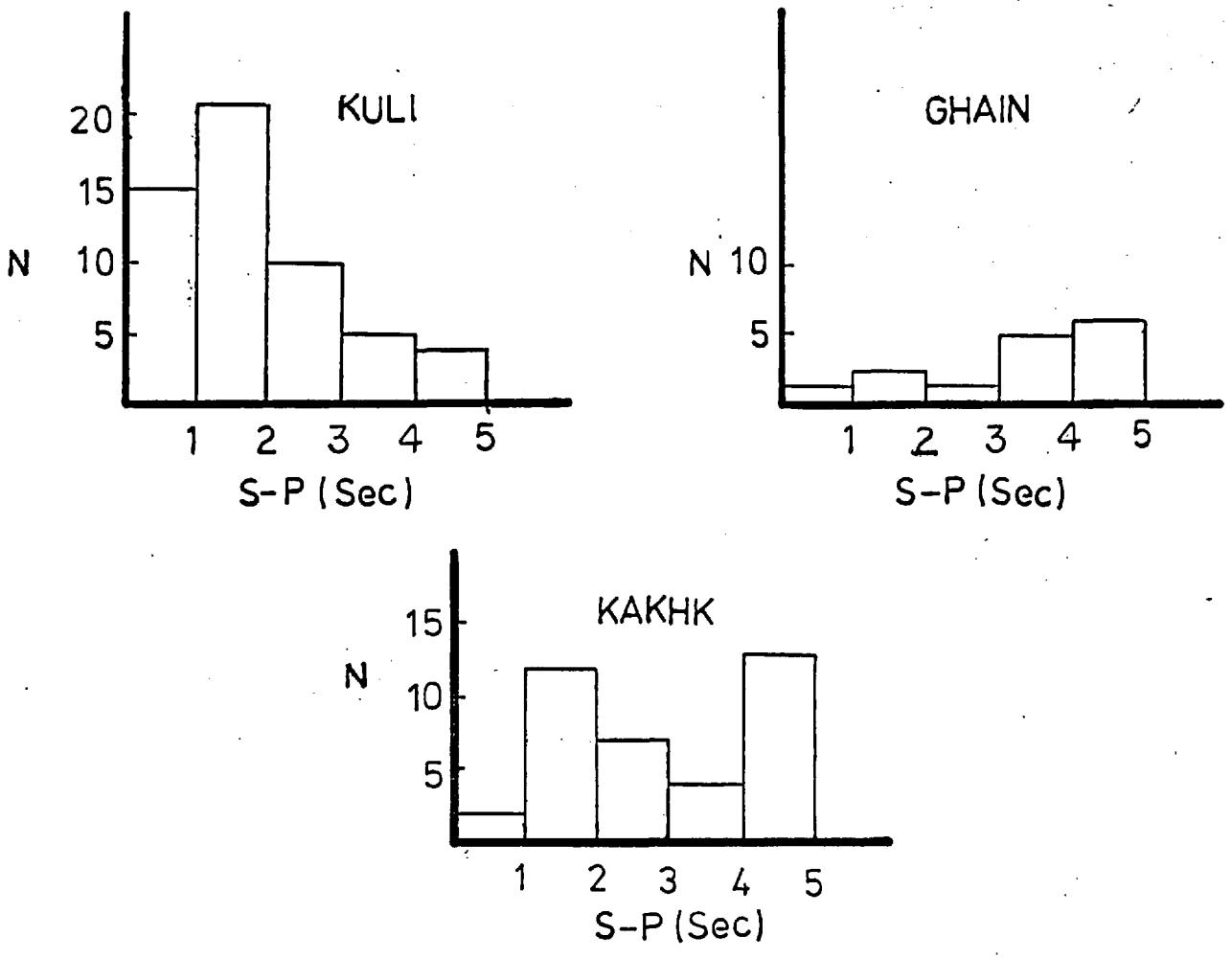
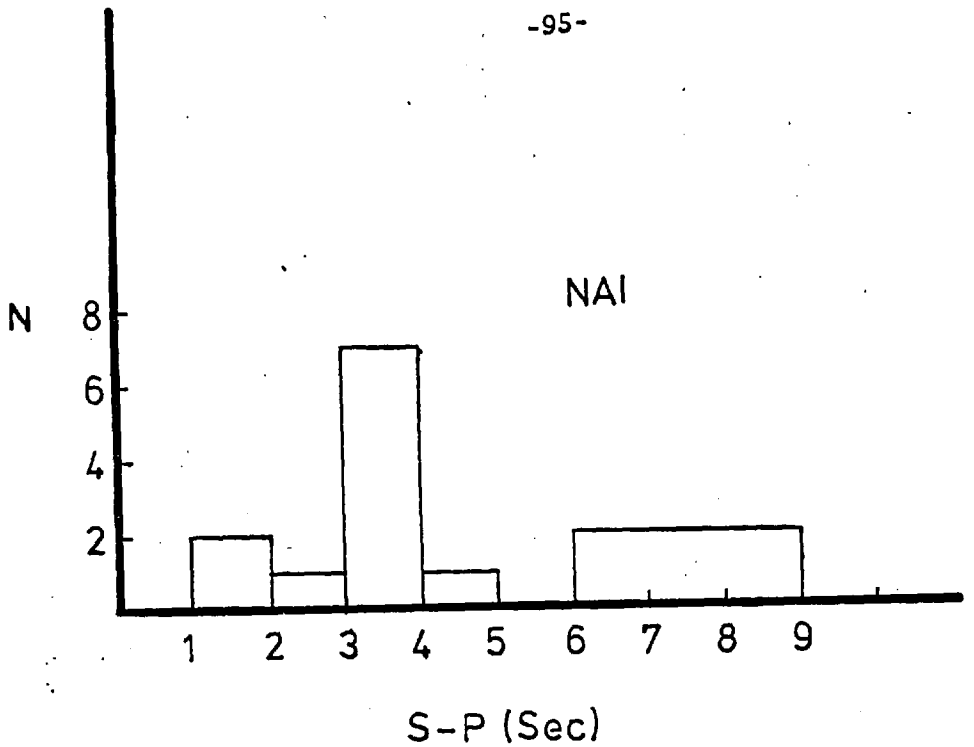



Fig. 4.7 Frequency of microearthquakes versus distance from the recording station. Distances are in terms of the difference between P wave and S wave arrival times( S-P intervals ).



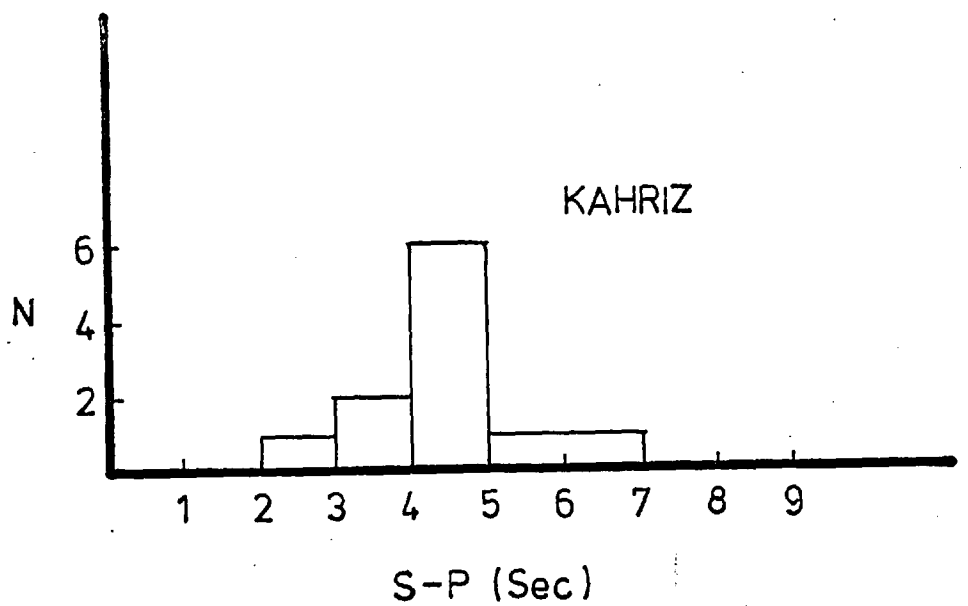




Fig. 4.8 Caption as in Fig. 4.7.

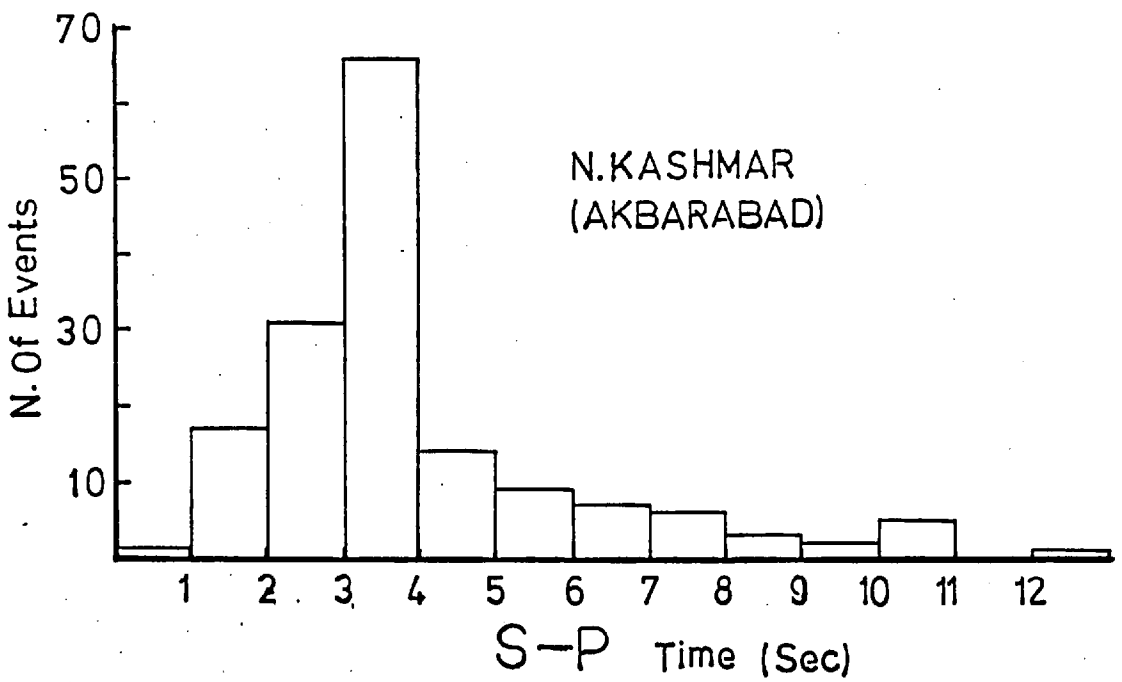



Fig.4.9 Caption as in Fig. 4.7.

at a magnification of 30,620 the lowest used at any of the stations. To normalize all the recorded events to this base magnification, their maximum amplitudes were reduced proportionally to the ratio of their recorded magnifications to the base magnification. This was done using the relation

$$Ndb = 20 \cdot \log \frac{v_2}{v_1}$$

in which Ndb signifies the number of attenuation decibels registered on the MEQ600 equipment (or a representation of magnification on the MEQ800 Sprengnether seismograph) and $v_2/v_1$ is the ratio of the amplitudes of the magnified signal. In these instruments, magnification can be changed in steps of 6db and, therefore, for each step, the magnification and the amplitude are approximately doubled. Thus, the magnification of the instrument is normally set up to obtain the maximum reasonable background noise level. The records are then normalized to reject any microearthquake whose amplitude was such that it would not have been recorded if the standard gain of 30 db (attenuation) had been used.

The normalized frequency of the shocks per day at each site is shown on the map in Figure (4.6). The geographical distribution of the frequencies of the shocks is characterized by the fact that the frequencies are very low (about 1 to 4 shocks per day) in the central part of the Dasht-e-Bayaz fault. These low rates of occurrence

are also observed for the central part of the Great Kavir Fault, the area between Zaveh (40 km. east of Torbat-e-Heidarieh) in the east and Nai in the west, whereas, microearthquakes occur at higher rates at Kuli, Kakhk and Ferdows. This figure tentatively suggest that microearthquakes are presently occurring at higher rates at both ends of the Dasht-e-Bayaz fault and particularly at the eastern end (Kuli area). McEvily and Niazi (in press) also observed similar high levels of activity in these localities and show that they may represent the continued aftershock phase of the 1968 earthquake.

Application of dislocation theories in explaining the nature of fault movements (Chinnery, 1961, 1963 and 1966) has revealed the pattern of stress concentration along a major active fault. As has been shown in Chapter (VI) these stresses tend to concentrate towards the ends of the fault and are responsible for its growth in the form of splay faulting. If this interpretation of stress distribution is correct, then a concentration of microearthquakes is expected in the zone where active faults terminate.

Other areas with higher rates of microearthquake occurrence observable on Figure (4.6) are Rushtkhar, near the eastern end of the Great Kavir Fault (station 11), and the Rivash (N. Kashmar) area, along the northeast extension of the Great Kavir Fault (stations 13, 15 and 16).

A more detailed picture of the seismicity in the area under study may be obtained by observing the frequency distribution of S-P time at several sites. These distributions are given as sample histograms in Figures (4.7), (4.8) and (4.9). The histogram for Kuli shows that about 65 per cent of the well-recorded shocks originated within 2 seconds of S-P time interval. This normally corresponds to a hypocentral distance of less than 15 km., and the fact that most of these events show impulsive arrivals and short duration suggests focal depths of over 10 km, which reduces the epicentral distances to within 10 km. or less. No significant peak was observed at Ghain, whereas the Kakhk station shows two identifiable source areas with S-P times between 1 and 2, and 4 and 5 seconds, respectively.

In the N. Kashmar area, the frequency distribution peak occurs at 3 to 4 seconds at both Nai and Akbarabad (sites 12 and 13), Figures (4.8) and (4.9). At Kariz (site 15) the dominent S-P times are between 4 and 5 seconds.

Though these S-P values are used primarily in this analysis of occurrence rates, it is also possible to make use of them in obtaining approximate locations when the same event has been recorded by two stations. (If the same event has been recorded at three stations then it is possible to use computerised location techniques, as is shown more fully in a later section.)

This S-P location (for events recorded at two stations) has been applied to twenty-seven events, twelve of which were recorded at N. Kashmar and Kariz stations, and fifteen at N. Kashmar and Nai. Eight of the N. Kashmar and Nai events group very closely together in the area A of Figure (4.10). Seven of the N. Kashmar and Kariz events also lie very closely together in area B of Figure (4.10). Areas A and B can be seen from Figure (4.10) to share common maximum and minimum S-P times at N. Kashmar, which suggests that the fifteen earthquakes occurring in the combined area A + B come from the same source region. The limits of the source region are shown as the shaded area on Figure (4.17), which is obtained from the overlap of the maximum and minimum S-P times from the three stations.

This shaded area, representing an area of about 2 by 10 km, lies on the eastern end of the newly found ENE-WSW trending (see Chapter IV of this thesis) Kariz fault, on whose western end the magnitude 5.5(1971) earthquake probably occurred.

## 4.6 Estimation of magnitudes and regional seismicity curves

It is customary to determine the magnitude of local shocks using the standard Richter (1935) scale. This method is based on measurement of the largest amplitude of the longest period wave on each record, and comparing the response with what would be expected from a Wood-Anderson seismograph, taking into account (where necessary), the different response characteristics of this instrument.

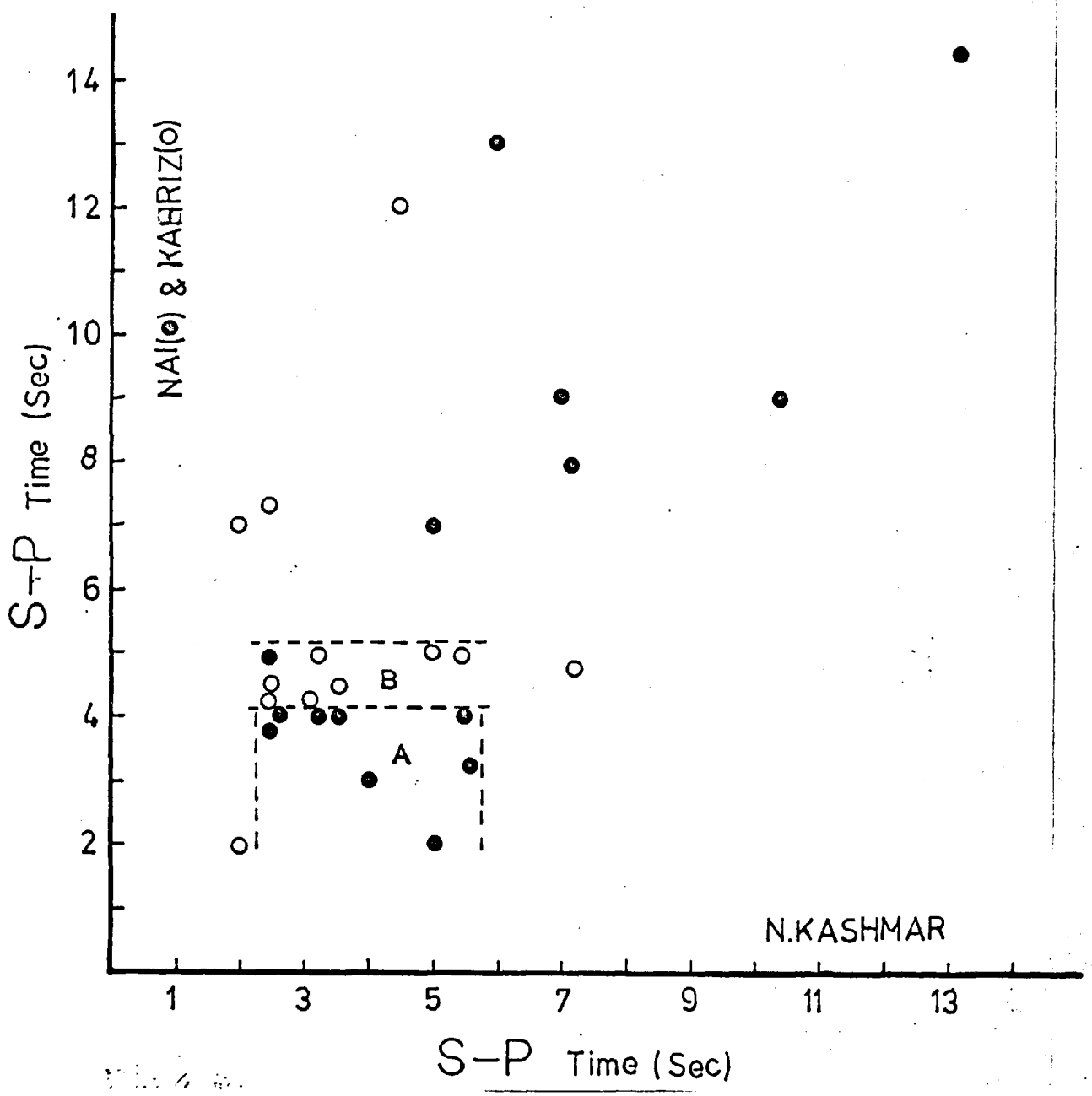



Fig. 4.10. Graphical representation of the common areas( A , B ) with certain distance( in terms of S-P ) from the N.Kashmar and Nai or Kariz stations to be used for graphical location of micro-earthquakes which have been recorded in two stations.

Nevertheless, in attempting to use the commonly applied amplitude measurements to determine magnitudes, one is faced with difficulties such as the following:

1. As pointed out in section 4.3, the time resolution in portable seismograph records is not adequate for distinguishing different wave components in the high-frequency coda of small earthquakes.

2. Maximum deflection of the pen on the seismogram is limited to 25 mm. each side of the centre zero. This introduces a constraint on measuring the maximum amplitude of many of the larger microearthquakes.

3. There are differences in response characteristics between the Wood-Anderson seismometer and the modern high-sensitivity short-period vertical instruments, such as used in this study.

4. Lateral variations in attenuation and elastic properties of the crust may produce significantly different response at different stations in the array.

Most of the above difficulties can be avoided by the use of a new technique which has recently become popular. This is based on the measurement of the duration of the seismic signal. Signal duration as a measure of magnitude has previously been used by Biszricsony (1958), Tsumura (1967), Lee et al.(1972): Crosson 1972, Real and Teng (1974). Justification for the application of this technique to local earthquakes has been given by Aki (1969), who showed that the duration is virtually independent of epicentral distance up to 100 km and suggested that the energy in the coda of signals from local shocks comes from back-scattered waves. Hence, magnitudes can be estimated for events only approximately located; also, the technique can deal with earthquakes over a wide range of magnitudes because signal clipping is not a factor. Thus, the main advantages of the method are:

1. Coverage of a wide range of magnitudes with a single seismograph, without such troubles as "saturation" or under-exposure in the case of the maximum amplitudes, and

2. The simplicity of the treatment, especially for earthquakes at short epicentral distances.

In practice, the relationship between magnitude and coda length is of the form:

$$m = A + B \log (F-P) \qquad \text{(after Tsumura, 1967)}$$

where F-P is the coda length in seconds and A and B are constants. Tsumura (1967) has determined these constants for the Hanshu region in Japan as

$$M = -2.23 + 2.85 \log (F-D), \text{ or}$$

$$m = -2.53 + 2.85 \log (F-P) + 0.0014$$

for larger epicentral distances. Crosson (1972); Lee et al. (1972); Real and Teng (1974) also adopted this method to estimate the magnitudes of local shocks in the states of Washington and California.

TABLE 4.2

Existing Empirical Formulas Relating Earthquake Magnitude and Signal Duration

| Investigator | Region Studied | A | B |
|---|---|---|---|
| Bisztrisony (1958) | Eastern Europe | -2.92 | 2.25 |
| Tsumura (1967) | Hunshu, Japan | -2.53<br>2.23 | 2.85 |
| Crosson (1972) | Puget sound, Washington | -1.72 | 2.42 |
| Lee et al. (1972) | Central California | -0.87 | 2.00 |
| Real & Teng (1974) | Southern California | -1.01<br>0.08 | 1.89<br>1.63 |
| A. Mohajer-Ashjai (this thesis) | Eastern Iran | $m_b$ -0.80<br>$M_L$ -3.53 | 2.45<br>3.32 |

A and B values obtained from the above studies are summarized in Table 4.2. Similarly, an attempt has been made to determine the constants of this empirical relationship between duration and magnitude of East-Iranian shocks. The data used is based on sixteen shocks well recorded on the smoked drum seismograph operated by the University of Mashad at Kakhk in 1971. During field preparations in Mashad, the author took advantage of the availability of these records to measure the coda length of shocks for which NOAA had already assigned a magnitude (Table 4.3). These standardized magnitudes were plotted against the natural Log of their respective durations Figure (4.11). The total duration of an earthquake in this study, was taken to be the time interval (in seconds) between the onset of the first arrival and the point at which the earthquake signal falls and remains below the background noise level. A least squares regression of these points revealed an empirical linear relationship such as the following, for this area:

$$m_b = -0.804 + 2.45 \text{ Log } (F-P)$$

Although the number of observations is limited in this study, the values obtained are quite comparable with those in other parts of the world, with minor differences which are thought to be due to differences in local geology and the different magnitude scale used.

As noted in section 4.1, the linear relationship between the number of shocks and their magnitudes expresses the facts of seismicity,

TABLE 4.3

List of Earthquakes used to infer the relation between Magnitude and Duration in Iran

| DATE | TIME | STANDARDIZED MAGNITUDE | | SIGNAL DURATION |
|---|---|---|---|---|
| | h m s | mb | $M_L$ | sec. |
| 18 04 71 | 07 24 14.3 | 4.5 | 3.7 | 180 |
| 24 07 71 | 00 49 21.5 | 5.0 | 4.4 | 222 |
| 09 08 71 | 02 54 36.7 | 5.2 | 4.6 | 300 |
| 22 08 71 | 17 54 14.6 | 5.1 | 4.5 | 230 |
| 28 08 71 | 16 34 44.4 | 4.8 | 4.1 | 200 |
| 08 09 71 | 12 53 34.0 | 5.4 | 4.9 | 360 |
| 15 10 71 | 14 19 31.6 | 4.7 | 3.9 | 197 |
| 15 10 71 | 16 22 37.0 | 4.9 | 4.2 | 219 |
| 16 10 71 | 06 11 39.1 | 4.8 | 4.1 | 190 |
| 28 10 71 | 13 30 57.1 | 5.5 | 5.1 | 320 |
| 06 11 71 | 19 43 46.0 | 5.0 | 4.4 | 210 |
| 08 11 71 | 03 06 36.4 | 5.6 | 5.2 | 375 |
| 19 11 71 | 01 00 01.0 | 4.9 | 4.2 | 195 |
| 24 11 71 | 18 23 24.6 | 5.1 | 4.5 | 330 |
| 03 11 71 | 09 42 50.4 | 4.7 | 3.9 | 185 |
| 18 11 71 | 07 31 32.8 | 5.3 | 4.8 | 350 |
| 09 12 71 | 01 42 30.7 | 5.3 | 4.8 | 345 |
| 15 12 71 | 15 24 57.4 | 4.9 | 4.2 | 230 |
| 20 12 71 | 23 27 38.5 | 4.9 | 4.2 | 200 |

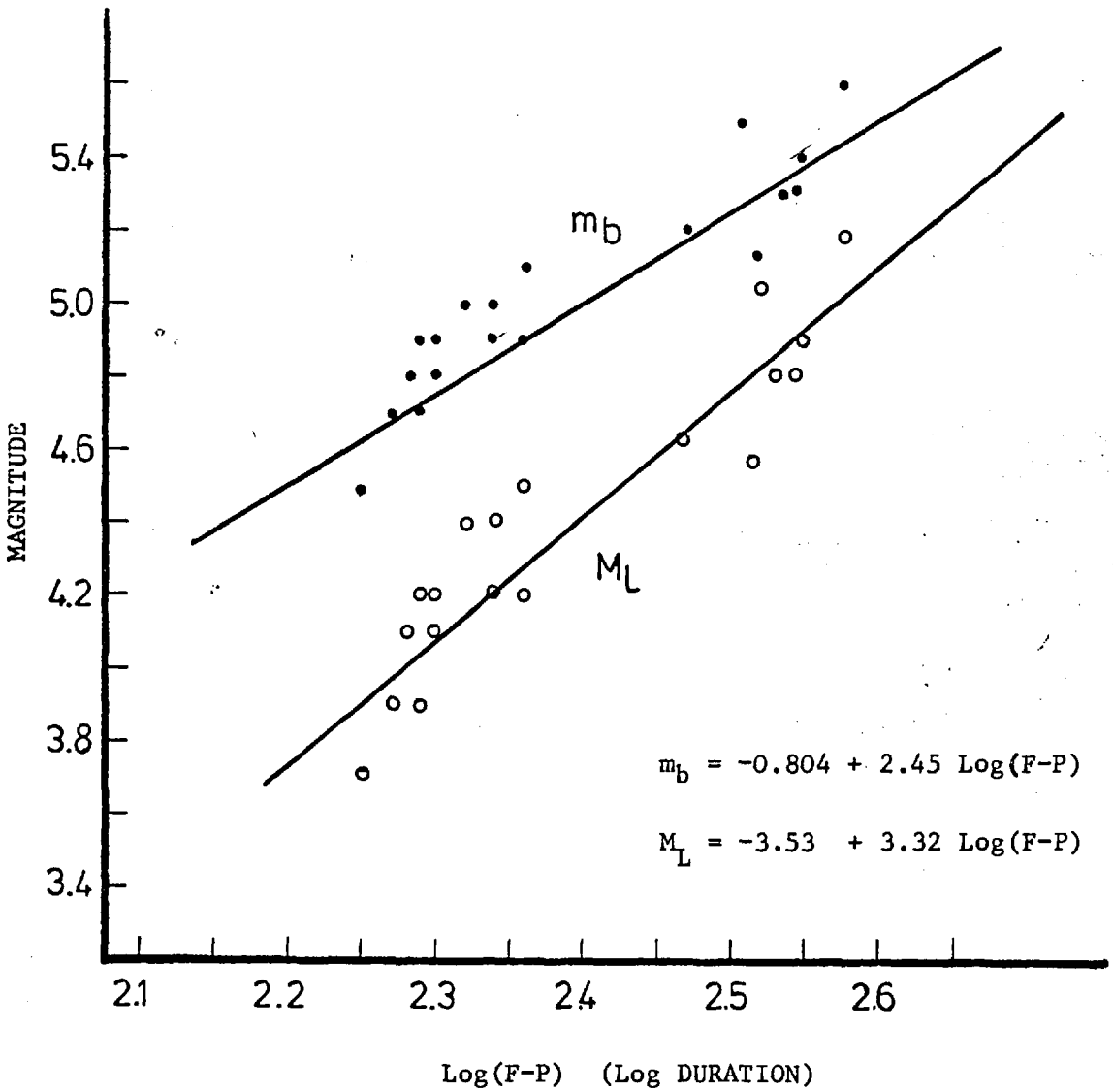



Fig. 4.11. NOAA determined magnitudes versus Log. of duration of the same earthquakes recorded on the smoked paper seismograph in the Kakhk station.

both for limited regions of the world and for the total world-wide seismicity. It is also implied that this relationship holds independently of the magnitude range under consideration (e.g. see Evernden 1970). To test this implication as well, the standardized bodywave magnitudes taken from the catalogue of Preliminary Determination of Earthquakes (PDE)* was converted to local magnitudes ($M_L$) using the Richter and Gutenberg (1956) formula:

$$m_b = 1.7 + 0.8\, M_L - 0.01\, M_L^2$$

Similarly, a linear relationship was found between the duration of the shock and calculated local magnitudes, in the form:

$$M_L = -3.53 + 3.32 \text{ Log } (F-P)$$

The above relations were used to construct two sets of recurrence curves for different recording stations and also for combinations of stations. As demonstrated in Figures (4.12 to 4.15), nearly similar slopes of these curves for different magnitude scales justifies the use of either scale in the study of regional seismicity through recurrence curves. However, there is a small difference between the two b values, in the order of 0.2 or less, which does not affect the conclusions derived from the observed low b values appreciably.

---

* The PDE is list of the earthquakes recorded on the WWSSN (world wide standardized seismographic network), which are located and published, monthly, by the NOAA (national oceanic and atmospheric administration, formerly known as the U. S. coast and geodetic survey).

Fig. 4.12 Magnitude versus $Log_{10}$ of cumulative number of events above specified magnitude in half a unit increments for the N. Kashmar region (combination of Akbarabad, Nai and Kariz stations). Solid and open circles signify the local and body wave magnitude scales respectively which are derived from measurement of the total signal duration. Solid lines are the least-square fit of LogN = a-bM to linear segment of data.

Fig. 4.13 Recurrence curves for Kuli station (at eastern end of the Dasht-e-Bayaz fault). Symbols as in Figure 4.12.

Fig. 4.14 Magnitude versus $Log_{10}$ of cumulative number of events above specified magnitude in half a unit increments for the Dasht-e-Bayaz region (combination of Kuli, Kakhk and Ghain stations). Symbols as in Figure 4.12.

Fig. 4.15 Magnitude versus $Log_{10}$ of cumulative number of events for eastern Iran (combination of N. Kashmar and Dasht-e-Bayaz regions). Symbols as in Figure 4.12.

Fig. 4.16 Duration of shocks (in sec.) versus cumulative number of events for the N. Kashmar region.

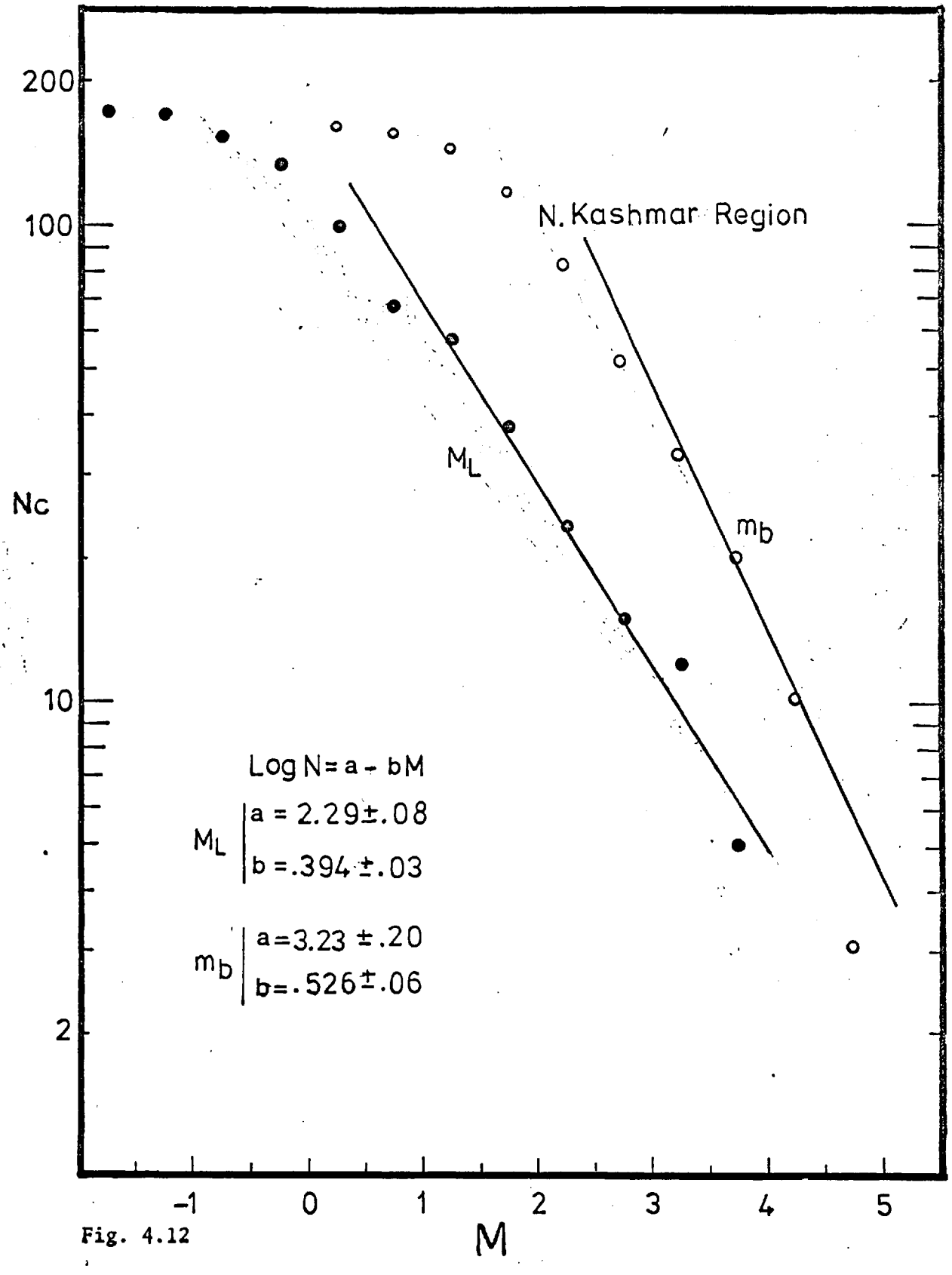

200
100
10
2
Nc
N. Kashmar Region
$M_L$
$m_b$
Log N = a - bM
$M_L$ a = 2.29±.08
b = .394±.03
$m_b$ a = 3.23 ±.20
b = .526±.06
-1
0
1
2
3
4
5
M

Fig. 4.12

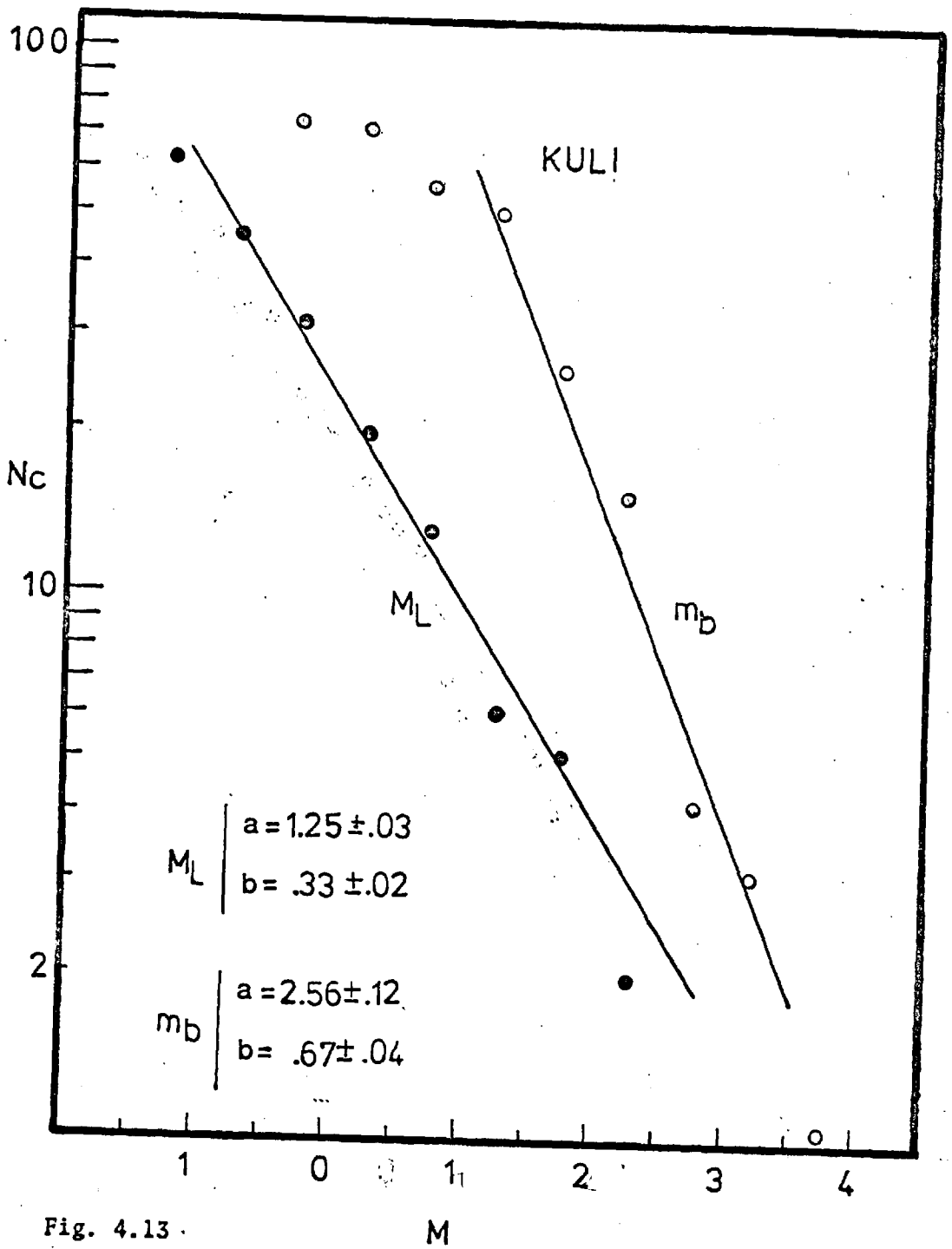



Fig. 4.13

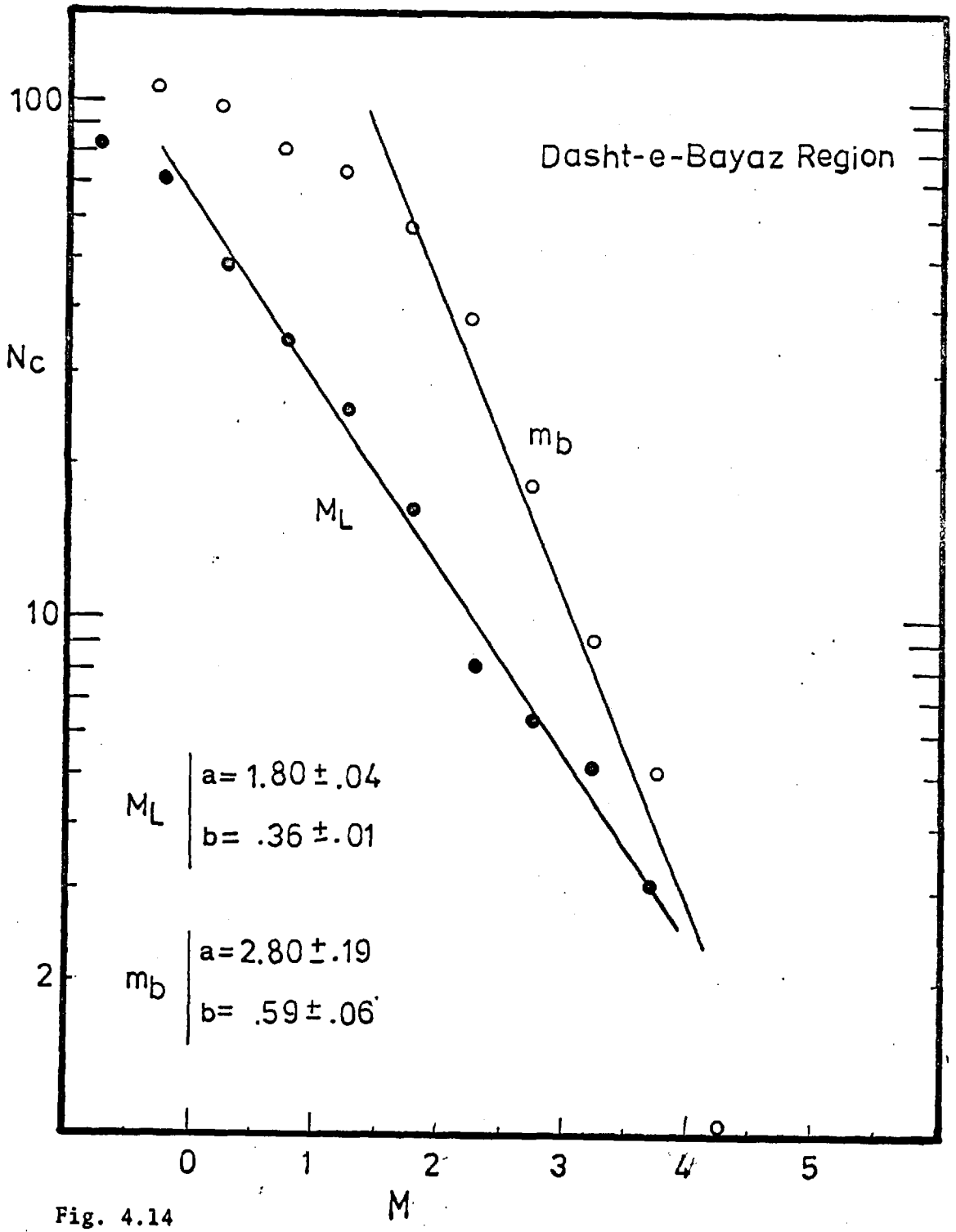

Dasht-e-Bayaz Region
100
10
2
Nc
$m_b$
$M_L$
$M_L$ a= 1.80 ± .04
b= .36 ± .01
$m_b$ a=2.80 ± .19
b= .59 ± .06
0
1
2
3
4
5
M

Fig. 4.14

Similar recurrence curves resulted from plots of the number of shocks against coda lengths directly, Figure (4.16), which lends additional strength at least to the statistical validity of the coda-length magnitude estimation for eastern Iran. Figures (4.12 to 4.15) show plots of magnitude versus the cumulative number of events above a given magnitude, based on the duration of shocks and the corresponding relationship between standardized $M_L$ and $m_b$ magnitudes for the area. As demonstrated in Figures (4.12 to 4.15), the relation is linear to about magnitude 0 in the $M_L$ scale and to about magnitude2 in the $m_b$ scale. There appears to be very little variation in the slope of the recurrence curves throughout this region.

The b values obtained for different recording stations from a least square regression to the linear segment of the data show a remarkable internal consistency for different localities, in particular between the Dasht-e-Bayaz and N. Kashmar areas, which attests to the similarity of seismic characteristics of these two areas. Careful compilation of all the data on these recurrence curves provides b values of 0.45 and 0.57 based on $M_L$ and $m_b$ magnitudes respectively, which could represent the short-term seismicity of east-central Iran. As mentioned earlier, Evernden (1970) compiled a standardized set of curves for a variety of regions of the world which are mostly normalized to 1000 $km^2$ per year. In order to compare the recurrence curves of other parts of the world with those obtained in the present study, the $\text{Log } N = 2.51 - .45M_L$ formula obtained for eastern

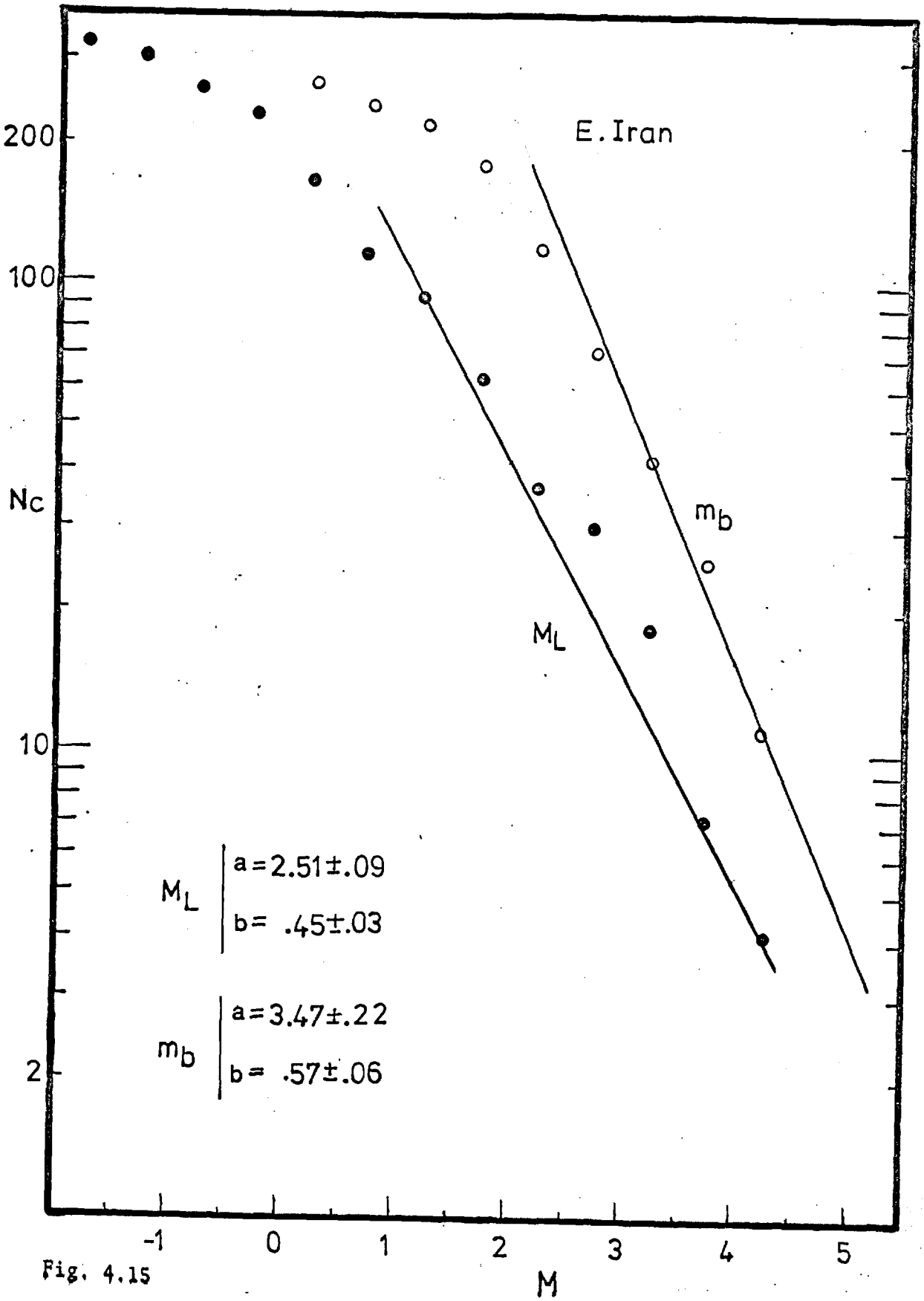

E. Iran
200
100
Nc
10
2
$m_b$
$M_L$
$M_L$ a=2.51±.09
b= .45±.03
$m_b$ a=3.47±.22
b= .57±.06
-1
0
1
2
3
4
5
M

Fig. 4.15

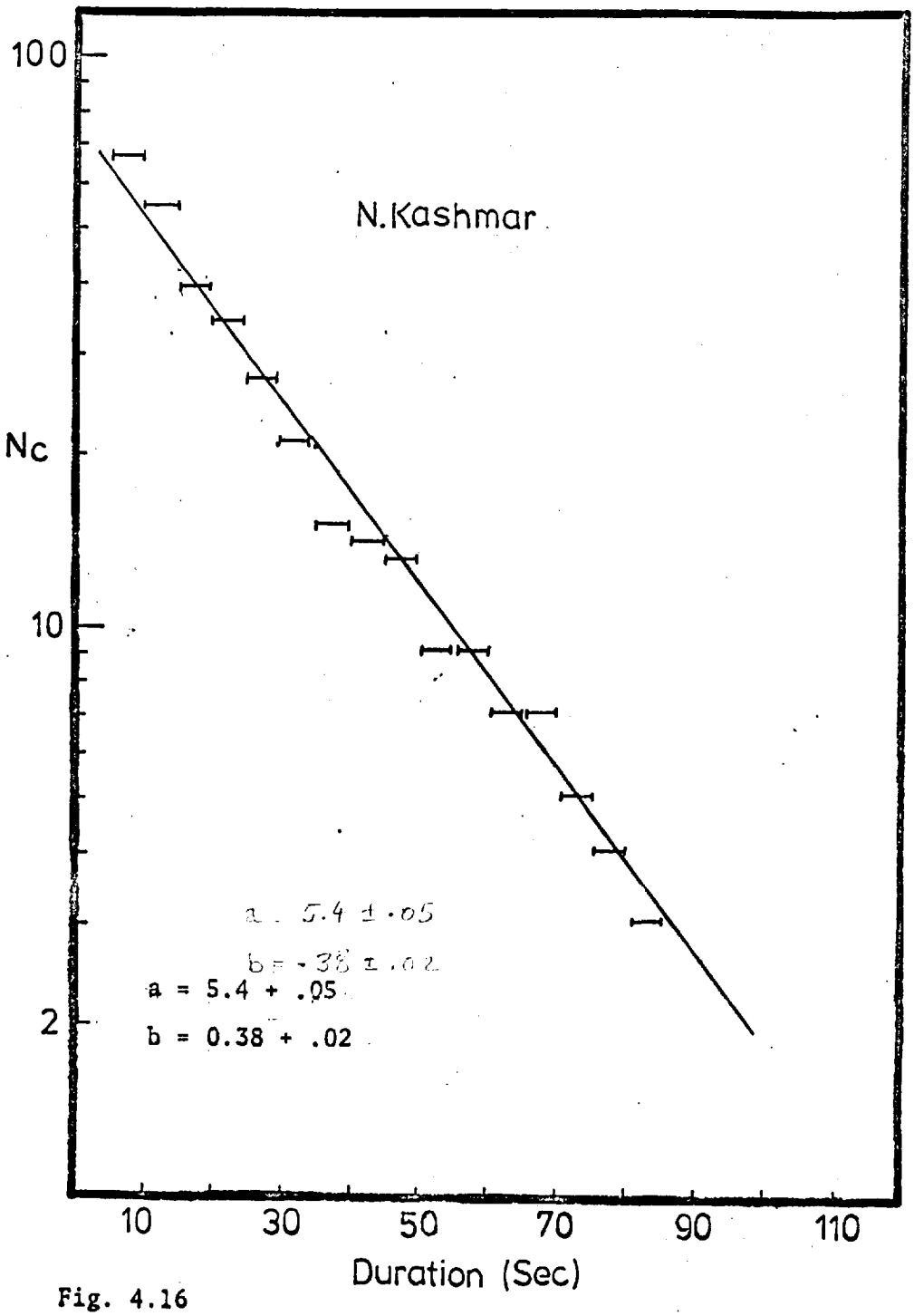

100
10
2
Nc
N.Kashmar
a = 5.4 ± .05
b = .38 ± .02
10
30
50
70
90
110
Duration (Sec)

Fig. 4.16

central Iran (area 210km by 160km, recording period one month) was normalized to 1000km$^2$ and one year, respectively, using the following relation:-

$$N_o = \frac{N}{s \cdot t}$$

where $N_o$ is the normalized cumulative number of events, s is the total area under observation, in units of 1000km$^2$, and t the period of recording in units of one year. Thus, we have

$$\text{Log } N_o = \text{Log } N - \text{Log } (s \cdot t)$$

Since $s = 33.6$ and $t = 1/12$

$$\text{Log } N_o = 2.51 - 0.45M_L - \text{Log } (33.6 / 12)$$

i.e. $$\text{Log } N_o = 2.08 - 0.45M_L$$

Similarly, for the mb scale:

$$\text{Log } N_o = 3.47 - 0.57m_b - \text{Log } (33.6 / 12)$$

i.e. $$\text{Log } N_o = 3.04 - 0.57m_b$$

The b values, obtained from this study are relatively low, considering the normal range of 0.5 to 1.5 found in other parts of the world, and it is compared with other areas in terms of the recurrence rate for magnitude 4

earthquakes which is 1.01 and 1.53 events/year/1000 $km^2$ for the area covered in this study. The corresponding rates of 0.2 for the San Andreas Fault (north), 0.15 for the Mendocino Escarpment and 0.8 for the Imperial Valley, California were reported by Crosson (1972). The following formulation was used in this comparison:-

$$\text{Log } Nc = a - bm_b$$
$$\text{Log } NI = a - 1 + \text{Log } b - bm_b$$

where Nc is the cumulative number of shocks for a given magnitude and above, NI is number of earthquakes in 1/10 of magnitude increments.

If this relatively short-term but statistically acceptable data represents the seismicity of these areas in a general sense, then it might be suggested that the region is characterized as being subjected to high stresses which are normally released through less frequent but relatively large scale shocks.

Scholz (1968) found that the frequency-magnitude relation for microfractures in a given rock is characterized by a b value which decreases when the stress level is raised. If a similar phenomenon prevails in the earth's crust, and if the observed low b value has any significance in this area, one might say that stresses in eastern Iran are higher than in the major plate boundaries, where the b values are typically higher than the values found for the Dasht-e-Bayaz and the N. Kashmar region. This would be consistent

with the concept of continuum deformation as opposed to the micro-plate tectonics proposal for eastern Iran, which will be considered later (see Chapter VI).

## 4.7 Location methods for microearthquakes

Various techniques have been proposed for locating near earthquakes using data from local networks. Among analytical methods, many hypocentre location programs have been developed for locating events by a least-squares iterative process from a net of local stations. (Flinn 1960; Nordquist 1962; James et al. 1969.)

The iterative least squares procedure, whereby origin time (To), Latitude (Ø), Longitude ($\lambda$) and depth (Z) are computed as independent parameters is found to yield solutions that depends upon the number and configuration of the observing stations and also upon the initial trial hypocentre location. This instability in solutions is demonstrated by the fact that different station sub-sets of the observational network produce different solutions for the same earthquake.

James et al. (1969) discovered that the instability in the least squares method is due to the following:

a) Variation in structure underneath the different station sub-sets of a particular station network.

b) The interdependence between the origin time To, as computed, and the depth Z.

A symptom of the effect of structure is that when many stations are used in the location, local stations may exhibit large time residuals, indicating errors in the computed hypocentre locations.

However, James et al. (1969) pointed out that the instability in solutions cannot be attributed to data errors and must arise from the least squares procedure. They developed a variation of the least squares procedure by calculating $T_o$ independently to correct for the mathematical instability in the procedure, since the mathematics demand that all variables be strictly independent. The independent variables $\lambda$, $\phi$, and Z are then calculated by least squares using P wave travel times only. S waves are used to provide a means of calculating $T_o$ from the formula

$$T_o = T_p - \frac{(V_k) \cdot (T_{s-p})}{V_p}$$

where $T_p$ = arrival time of P wave

$T_{s-p}$ = S-P travel time

$V_k$ = S-P velocity = $\frac{(T_s - T_p)}{\Delta}$ model

$\Delta$ = distance between station and epicentre

$V_p$ = P wave velocity

Unfortunately, S wave onsets cannot always be reliably determined, so this variation cannot be used for accurate work.

Other workers, including Bolt (1960) and Cisternas (1964), have studied the problems inherent in the location technique by the least squares method, and have specified conditions to be fulfilled for reliable solutions to be achieved. One is a large number of stations having good azimuthal coverage and range distribution relative to the epicentre.

In many parts of the world, however, it has been necessary to seek another more stable method of location such as follows:

Crampin (1970) has developed a method for locating local events within small network. Here the travel time equations are derived from the geometric ray paths in a known structure, modified by the time term at each point. Time terms may be used to provide for local variation in structure, which has not been considered by most workers. The program FAMG (Crampin and Willmore, 1973), using this method has been employed by the present author to locate and study the microtremors in Central Scotland (Mohajer-Ashjai and Neilson, in press). FAMG determines epicentres, depths of focus and magnitudes of events recorded by large-aperture low-density seismic networks. The small number of direct ray-paths to events within such networks removes much of the control over depth from the solution and inhibits

depth being solved as a free variable of the solution, as is possible in programs designed to locate within denser networks (Eaton 1969). FAMG maximises the depth control by holding the depth fixed (at intervals throughout a three-layered crust) and calculates adjustments to location by a least-squares iterative technique. The iterations at each depth are continued until the root mean square ( RMS ) of the residual has converged, or until an iterative limit has been reached. The program converges sufficiently fast for the location and arrival time at the station nearest to an event to be used as the initial location in the search for epicentres. The program is based on P-arrival reading and four or more station recordings are required for satisfactory location, but S readings, when clearly readable, could be used to improve epicentral determinations for smaller shocks and those recorded at only three stations.

## 4.8 Hypocentre determination in eastern Iran

Although, the main purpose of the present study was a survey of microearthauakes along some of the faults in eastern central Iran (see section 4.5), a few well recorded shocks were accurately located using both P and S arrival times. The FAMG program (Crampin et al. 1973) (see also section 4.7), was modified to take the velocity structures of eastern Iran into account. Since the crustal model in Iran is not accurately known, an attempt has been made to investigate the most suitable model through searching for the minimum residuals.

Several reasonable models with three crustal layers were tested to evaluate the effect of crustal structure on both the locations and composite fault plane solutions. The two most suitable models (models I and II, Table 4.4) were selected based on the minimum root mean square of residuals. The uppermost layer in model I and the crustal thickness and velocities, are adopted from Niazi (personal communication).

Locations were obtained for eight well recorded shocks in N. Kashmar and seven similar shocks in the Dasht-e-Bayaz areas. Tables 4.5 to 4.8 summarise the results in terms of Latitude and Longitude of epicentres, depth, root mean square (RMS) of residuals and magnitudes based on signal duration. The epicentral distribution for models I and II are shown in Figure (4.17), for comparison. From Figure (4.17) it is concluded that, for short epicentral distances, accuracy in location is less sensitive to the crustal model chosen than to accurate readings of P and S arrivals (lower RMS). p-arrivals on a fast play-back from a multichannel magnetic tape recorder are usually accurate to within 0.01 seconds, while S readings are often less reliable. Figure (4.18) shows an example of high quality records of the Lownet radio link seismographic network in Scotland which were used by the author to study microearthquakes in Stirlingshire (central Scotland). The three traces at the top of the record relate to the vertical, N-S and E-W component of Edinburgh (EDI) station which enable one to recognise the S arrivals precisely.

TABLE 4.4

CRUSTAL MODELS USED FOR
EPICENTRAL DETERMINATION

| Depth (km) | P wave velocity (km/sec) | S wave velocity (km/sec) | |
|---|---|---|---|
| 1.3 | 3.5 | 2.0 | Niazi's crustal |
| 31.3 | 5.75 | 3.3 | model for |
| mantle | 8.0 | 4.6 | northern part |
| | | | of eastern Iran |
| 1.3 | 3.5 | 2.0 | Model I |
| 15.00 | 5.75 | 3.30 | (a combined three |
| 31.3 | 6.70 | 3.90 | layered crust used |
| mantle | 8.00 | 4.70 | in this study) |
| 3.00 | 5.00 | 2.89 | Model II |
| 15.00 | 6.00 | 3.50 | (the second best |
| 27.00 | 6.70 | 3.90 | model used here |
| mantle | 8.00 | 4.70 | |

TABLE 4.5

Location of Microearthquakes in Dasht-e-Bayaz area using Crustal Model I

| DATE | | | ORIGIN TIME | | | LAT. | | | LONG. | | | DEPTH | RMS | MAG MLD |
|---|---|---|---|---|---|---|---|---|---|---|---|---|---|---|
| d | mon | yr | hr | min | sec | deg | min | sec | deg | min | sec | km | | |
| 09 | 06 | 72 | 21 | 02 | 37.37 | 34 | 20 | 33.81 | 59 | 08 | 44.79 | 17 | 0.452 | 1.5 |
| 10 | 06 | 72 | 11 | 47 | 31.19 | 34 | 14 | 29.35 | 59 | 08 | 19.73 | 16 | 1.474 | 0.7 |
| 12 | 06 | 72 | 06 | 19 | 30.55 | 34 | 01 | 34.67 | 59 | 09 | 10.71 | 09 | 0.030 | 1.6 |
| 13 | 06 | 72 | 01 | 20 | 58.56 | 34 | 01 | 44.15 | 58 | 54 | 57.98 | 05 | 0.026 | 1.2 |
| 14 | 06 | 72 | 03 | 11 | 38.43 | 34 | 01 | 36.26 | 59 | 02 | 41.75 | 16 | 0.336 | 2.0 |
| 14 | 06 | 72 | 18 | 12 | 38.19 | 34 | 33 | 09.64 | 59 | 06 | 48.31 | 4 | 2.239 | 0.3 |
| 15 | 06 | 72 | 07 | 31 | 41.98 | 34 | 02 | 22.34 | 59 | 21 | 32.23 | 0.0 | 0.078 | 0.5 |

TABLE 4.6

Location of Microearthquakes in Dasht-e-Bayaz area using Crustal Model II

| DATE | | | ORIGIN TIME | | | LAT. | | | LONG. | | | DEPTH | RMS | MAG MLD |
|---|---|---|---|---|---|---|---|---|---|---|---|---|---|---|
| d | mon | yr | hr | min | sec | deg | min | sec | deg | min | sec | km | | |
| 09 | 06 | 72 | 21 | 02 | 38.16 | 34 | 22 | 47.85 | 59 | 10 | 5.20 | 19 | 0.437 | 1.5 |
| 10 | 06 | 72 | 11 | 47 | 31.36 | 34 | 17 | 39.11 | 59 | 09 | 16.79 | 17 | 0.870 | 0.7 |
| 12 | 06 | 72 | 06 | 19 | 31.10 | 34 | 01 | 41.37 | 59 | 09 | 14.00 | 5 | 0.013 | 1.6 |
| 13 | 06 | 72 | 01 | 20 | 58.66 | 34 | 01 | 39.97 | 58 | 54 | 42.89 | 0 | 0.047 | 1.2 |
| 14 | 06 | 72 | 03 | 11 | 38.88 | 34 | 01 | 49.90 | 59 | 03 | 20.03 | 17 | 0.202 | 2.0 |
| 10 | 06 | 72 | 18 | 12 | 35.92 | 34 | 40 | 05.37 | 59 | 18 | 26.14 | 3 | 2.187 | 0.3 |
| 15 | 06 | 72 | 07 | 31 | 41.76 | 34 | 02 | 18.09 | 59 | 23 | 55.85 | 0.0 | 0.309 | 0.5 |

TABLE 4.7

Location of Microearthquakes in N. Kashmar area using Crustal Model I

| DATE | | | ORIGIN TIME | | | LAT. | | | LONG. | | | DEPTH | RMS | MAG MLD |
|---|---|---|---|---|---|---|---|---|---|---|---|---|---|---|
| d | mon | yr. | hr | min | sec | deg | min | sec | deg | min | sec | km | | |
| 13 | 07 | 73 | 18 | 59 | 45.38 | 35 | 31 | 19.83 | 58 | 49 | 17.14 | 17.0 | 0.336 | .78 |
| 13 | 07 | 73 | 19 | 17 | 38.58 | 35 | 31 | 22.25 | 58 | 47 | 52.64 | 10.0 | 0.053 | .80 |
| 13 | 07 | 73 | 23 | 04 | 37.40 | 35 | 43 | 09.23 | 58 | 45 | 54.77 | 16.0 | 0.598 | 2.3 |
| 14 | 07 | 73 | 04 | 15 | 09.97 | 35 | 31 | 13.36 | 58 | 35 | 52.61 | 00.0 | 0.265 | 2.2 |
| 14 | 07 | 73 | 01 | 01 | 34.69 | 35 | 24 | 45.45 | 58 | 47 | 05.45 | 17.0 | 0.164 | 1.7 |
| 14 | 07 | 73 | 00 | 21 | 37.29 | 35 | 24 | 39.37 | 58 | 10 | 36.89 | 02.0 | 0.660 | 1.9 |
| 14 | 07 | 73 | 00 | 11 | 46.56 | 35 | 46 | 47.67 | 58 | 29 | 22.24 | 17.0 | 0.509 | 1.3 |
| 14 | 07 | 73 | 06 | 16 | 30.84 | 35 | 16 | 37.88 | 58 | 31 | 55.14 | 0.0 | 0.547 | 0.0 |

TABLE 4.8

Location of Microearthquakes in N. Kashmar area using Crustal Model II

| DATE | | | ORIGIN TIME | | | LAT. | | | LONG. | | | DEPTH | RMS | MAG MLD |
|---|---|---|---|---|---|---|---|---|---|---|---|---|---|---|
| d | mon | yr. | hr | min | sec | deg | min | sec | deg | min | sec | km | | |
| 13 | 07 | 73 | 18 | 59 | 46.29 | 35 | 32 | 2.77 | 58 | 47 | 37.29 | 18 | 0.310 | .98 |
| 13 | 07 | 73 | 19 | 17 | 38.85 | 35 | 31 | 52.5 | 58 | 49 | 10.00 | 07 | 0.021 | .20 |
| 13 | 07 | 73 | 23 | 04 | 37.21 | 35 | 45 | 23.29 | 58 | 47 | 13.14 | 17 | 0.580 | 2.3 |
| 14 | 07 | 73 | 04 | 15 | 10.31 | 35 | 31 | 44.06 | 58 | 36 | 2.28 | 0.0 | 0.422 | 2.2 |
| 14 | 07 | 73 | 01 | 01 | 35.63 | 35 | 24 | 40.53 | 58 | 48 | 36.33 | 18 | 0.109 | 1.7 |
| 14 | 07 | 73 | 00 | 21 | 36.83 | 35 | 24 | 34.36 | 58 | 06 | 52.27 | 03 | 0.744 | 1.9 |
| 14 | 07 | 73 | 00 | 11 | 47.20 | 35 | 48 | 39.61 | 58 | 28 | 11.77 | 18 | 0.703 | 1.3 |
| 14 | 07 | 73 | 06 | 16 | 30.59 | 35 | 14 | 24.14 | 18 | 30 | 26.20 | 0.0 | 0.568 | 0.0 |

Fig. 4.17. Epicenters of local earthquakes in the N.Kashmar and Dasht-e-Bayaz regions. Solid and open circles signify computations based on crustal models I and II respectively. Sixteen graphically located shocks (corresponding to A, B areas in figure 4.10) cluster in the dotted area north of Kashmar. Triangles show cites of the portable seismographs used for the above locations.

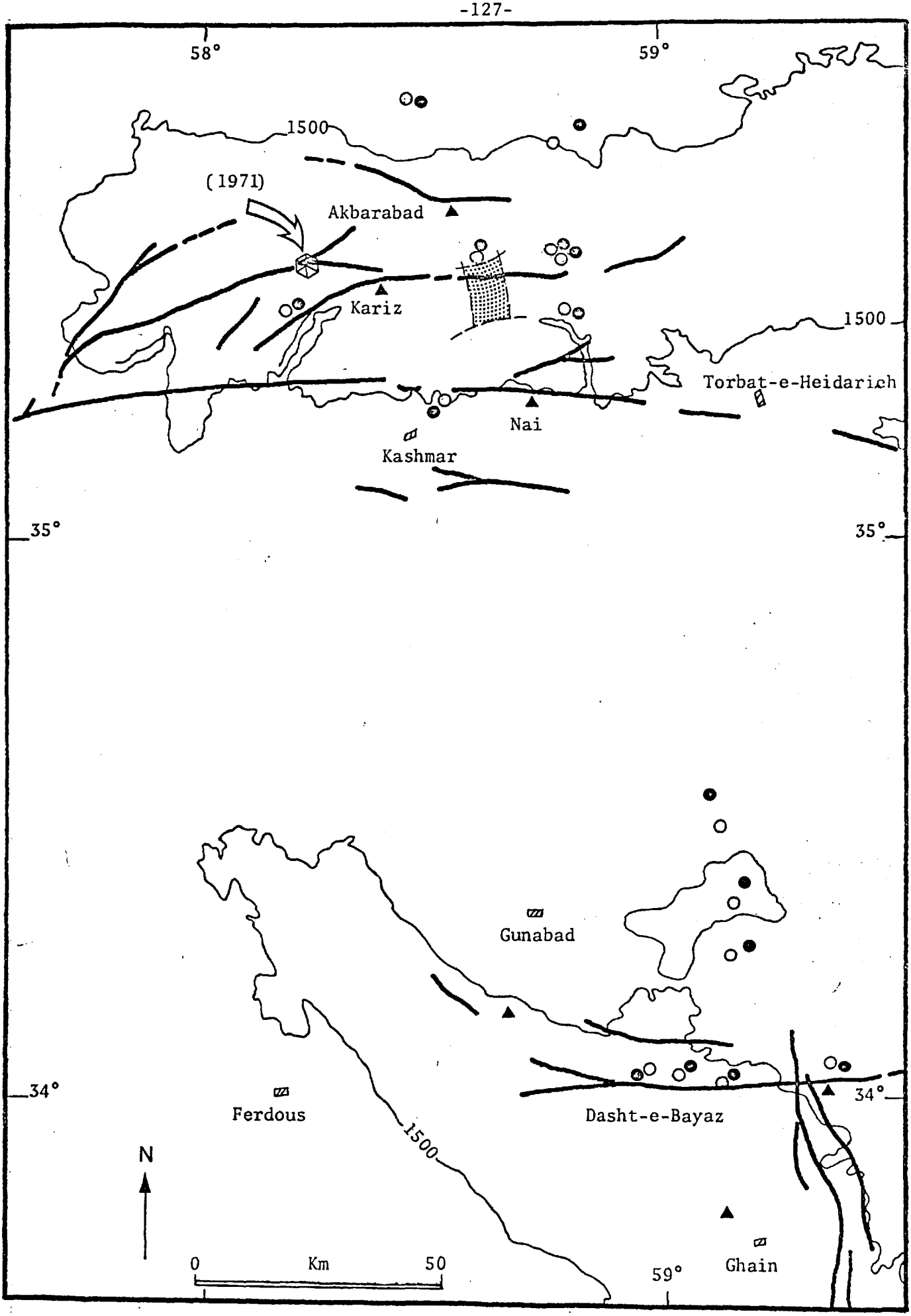
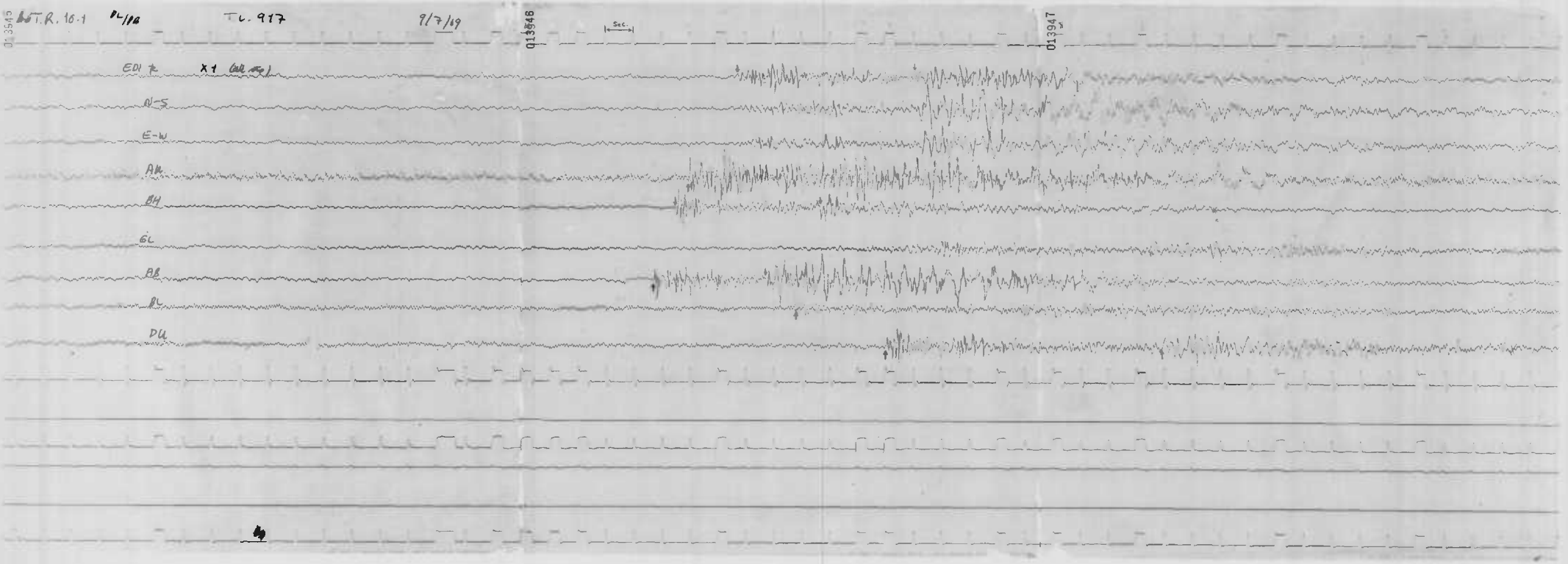

58°
59°
1500
(1971)
Akbarabad
Kariz
1500
Torbat-e-Heidarich
Nai
Kashmar
35°
35°
Gunabad
34°
34°
Ferdous
Dasht-e-Bayaz
1500
N
0
Km
50
59°
Ghain

Fig. 4.18. An example of high quality fast play back of a microearthquake recorded on the multichannel magnetic tape recorder of the LOWNET radio link seismographic network in Central Scotland. The first three traces(at the top) are the three components of the Edinburgh station, and the other six represent the vertical component of six out stations across Scotland.



High precision of arrival readings, coupled with an accurate crustal model and formulation of the FAMG program, which makes use of travel times along the ray path, could reveal hypocentral locations better than $\pm$ 200 m, provided residuals remain below 0.3 seconds

As explained in section 4.3, P and S wave arrivals on the smoked paper records in eastern Iran can be picked ~~to better than~~ to within 0.1 second, and considering the relatively low residual convergence obtained for the data used, the precision in the hypocentral locations is thought to vary between less than 1 km and 3 km , depending on the related RMS's.

As discussed in section 4.5, a less accurate graphical method was also used to locate many other shocks which were only recorded at two stations (shaded area on Figure 4.17).

Three of the above accurately-located shocks from the N. Kashmar region occurred in the same general area as the fifteen earthquakes located by the S-P times. This supports the conclusion presented earlier that the eastern end of the Kariz Fault is currently a focus of high seismic activity in the northern part of east Iran.

## 4.9 Composite fault plane solutions in eastern Iran

As mentioned in section 4.1 microearthquakes could be utilized

to reveal the mechanism of faulting in an area where the major shocks are lacking, or are not frequent enough to give meaningful solutions of the focal mechanism problem.

To investigate the mechanisms of the microearthquake activity and the related fault movements in eastern Iran based on the data presented in this study, an attempt has been made to use the composite fault plane solutions (CFPS) technique (Gutenberg 1941; Aki 1966 and Seeber et al. 1970), where the first motion from many microearthquakes is compiled in one focal sphere using only a few seismograph stations.

At first sight, the three fixed seismograph stations used to determine the CFPS in this study seem to reveal specific azimuths from the source to each of these stations that would naturally put a limitation on the distributions of data points and subsequently make it difficult to draw reliable nodal planes. The same difficulties were experienced by the author with Stirling (Central Scotland) microearthquakes, which were recorded at only a few fixed stations. Thus, it seemed to be necessary to move the small number of portable seismographs around and occupy new sites in the same region in order to get a better distribution of azimuths and take-off angles. However, owing to the short epicentral distances and relatively larger dimensions of the source area, there are reasonably good azimuthal coverages in the Dasht-e-Bayaz and N. Kashmar CFPSs.

The success of the technique entails the proper projection of the ray path back to the focal sphere. Hamilton (1971) and Crosson (1972) have argued against the calculation of the take-off angles based on the layered model and favoured a continuous model consisting of a linear increase in velocity with depth. The best average approximation to the layered models used in the hypocenter determinations in this study is taken as V = 5.45 + 0.06 h for crustal model I and as V = 3.64 + 0.11 h for the model II. However, in this particular case ,where epicentral distances are short, distribution of take-off angles and azimuths were not sensitive to details of crustal model,and also deviations of best linear relationship. Therefore, the first velocity model is used in a simple equation, suggested by Crosson (1972), which relates the take-off angle from the horizontal at the focus with the epicentral distance and the focal depth.

$$\theta = \tan^{-1} \frac{D^2 - 2hV/a - h^2}{2D\,(h + V/a)}$$

where $\theta$ is the take-off angle, h the focal depth, D the epicentral distance, and V and a the coeffcients of the linear velocity model.

The polarity of 18 first motions from seven well recorded microearthauakes in the eastern Dasht-e-Bayaz region are plotted on an equal-angle projection of the lower hemisphere Figure (4.19).

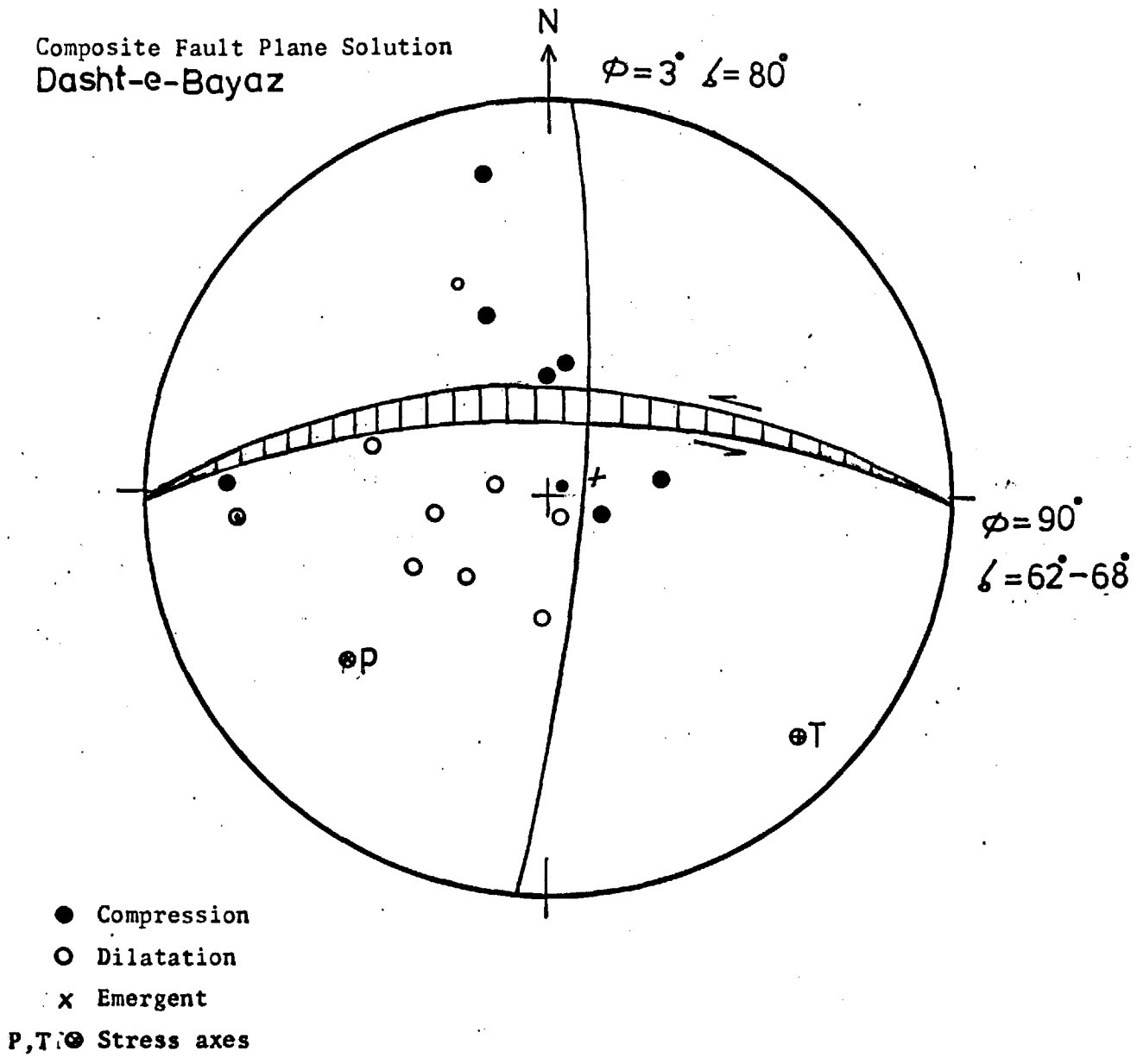

Composite Fault Plane Solution
Dasht-e-Bayaz
N
φ=3° δ=80°
φ=90°
δ=62°-68°
P
T
Compression
Dilatation
Emergent
P,T Stress axes

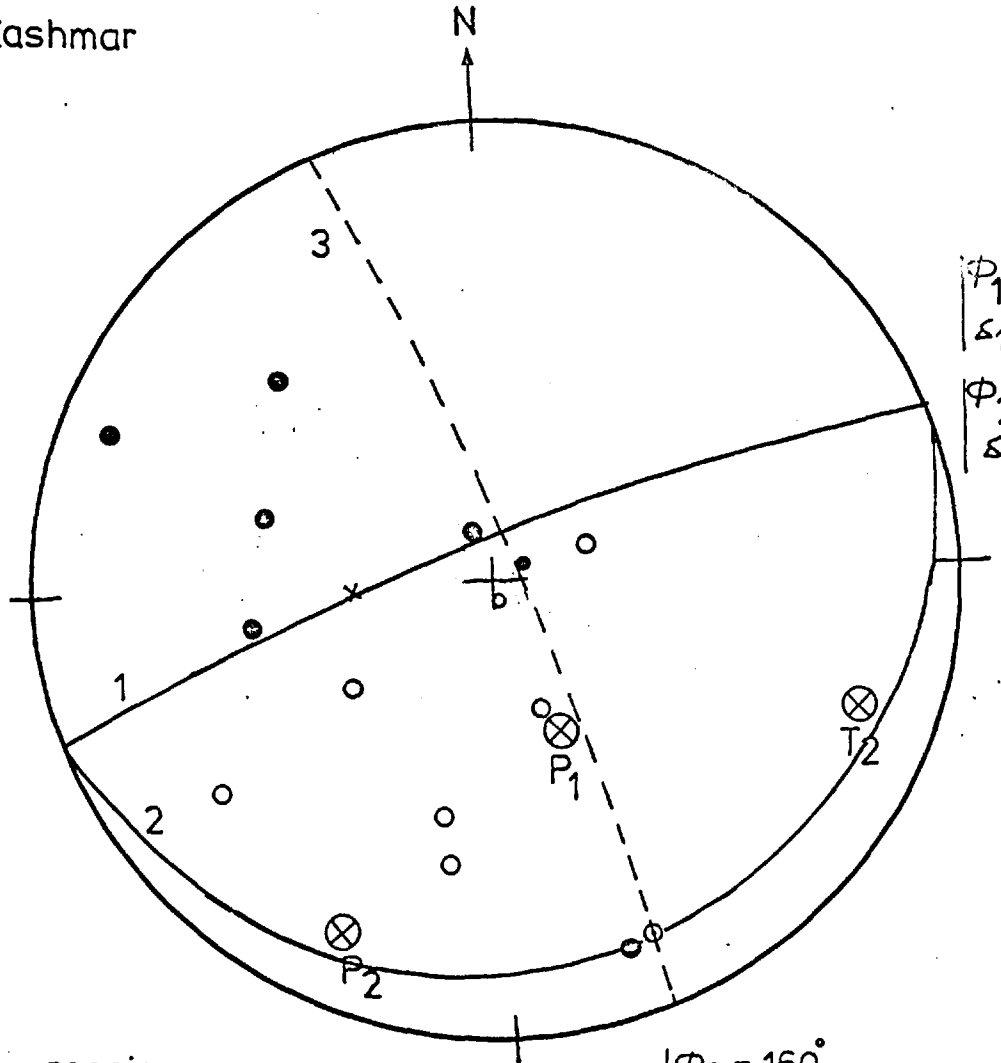
Fig. 4.19

There are fifteen first motions from five shocks located in the N. Kashmar region which are similarly plotted on Figure (4.20). Estimates were made of the quality of the observations, and more reliable ones are shown with larger symbols. Where first arrivals were emergent, they were assumed to represent rays close to a nodal plane and were plotted with a cross symbol. Ignoring three inconsistent data points, the resulting CFPS indicate a predominantly sinistral faulting in the Dasht-e-Bayaz region with two nodal planes striking N3°E and N90°E with dips of 80°E for the first plane and a possible range of 62° to 68°N for the second one. The strike of the N90°E plane is in close agreement with the Dasht-e-Bayaz fault, which produced a maximum of 4.5 m sinistral displacement horizontally and 1.5 m vertically during the 1968 earthquake (Ambraseys and Tchalenko 1969). The fault plane solution of the main 1968 earthquake, presented by Niazi (1969), suggests a fault plane striking N95°E and dipping 80°N, which is in accord with a later CFPS (McEvilly and Niazi, in press), having two nodal planes striking N-S and N90°E, with dips of 90° and 70°N respectively, and both are in agreement with the CFPS determined in this study. Axes of compression and tension are at N44°E and N136°E and plunging 24°SW and 8°SE respectively. These stress directions are comparable with a 124°E axis of tension deduced from the Mekometer measurement in the same region (see Chapter III).

The CFPS determined from five shocks for the N. Kashmar region, Figure (4.20), is not a good one and does not give a unique

Composite Fault Plane Solution

N.Kashmar




- ● Compression
- ○ Dilatation
- × Emergent
- ⊗P, T Stress Axes
- ⊙ Normal to $\varphi_1$ Plane

solution. However, one of the nodal planes, striking at N70 $\pm$ 6E and dipping at 72$^{o}$NW, can be very confidently drawn. The strike of this plane is in quite good agreement with the segment of the proposed Kariz Fault (N85$^{o}$E) on which several of the earthquakes occurring in the N. Kashmar have been located (by both computational and S-P time graphical techniques), which strongly suggests that this plane is indeed the fault plane.

Unfortunately though, the auxiliary plane, which in this case defines the mechanism of the CFPS, is very ill-defined, and two choices exist. Considering the necessary and sufficient condition that the two nodal planes are at right angles, which implies each of them to pass through the other's normal, the first auxiliary plane is almost parallel in strike (plane 2, Figure 4.20) and of perpendicular dip and implies a high angle reverse faulting mechanism. The second is perpendicular in strike, implying sinistral strike slip mechanism (plane 3, Figure 4.20).

The compression axis indicated by the first of these mechanisms is N164$^{o}$E and by the second N26$^{o}$E, of which the second is undoubtedly more in agreement with compression direction inferred from other observation in adjacent areas (i.e. the CFPS from Dasht-e-Bayaz N44$^{o}$E, the Mekometer results in Chapter III, N34$^{o}$E, and the geological observations in Chapter V, NE to NNE, also fault plane solutions from major earthquakes published by Nowroozi, 1972, and McKenzie, 1972).

McKenzie (personal communication) gives a fault plane solution for the magnitude 5.5 event which occurred on the western end of the Kariz fault in 1971 (Figure 4.21). This solution has one nodal plane striking at N57°E while the other is at N129°E. The former direction, which implies sinistral movement, compares well with the local strike of the fault and indicates a compressional axis at N10°E, quite in agreement with other values for these parameters from this area (see above).

Thus, despite its vagueness, one perfectly acceptable interpretation of the CFPS from the N. Kashmar region is in excellent agreement both with regional tectonics and with other observations from the same fault. It does therefore seem that some conclusion can be reached regarding the motion on the Kariz Fault both during the 1971 earthquake and during the subsequent aftershock activity, and that this motion is probably sinistral with some degree of thrusting under the influence of a compression directed at about N20°E.

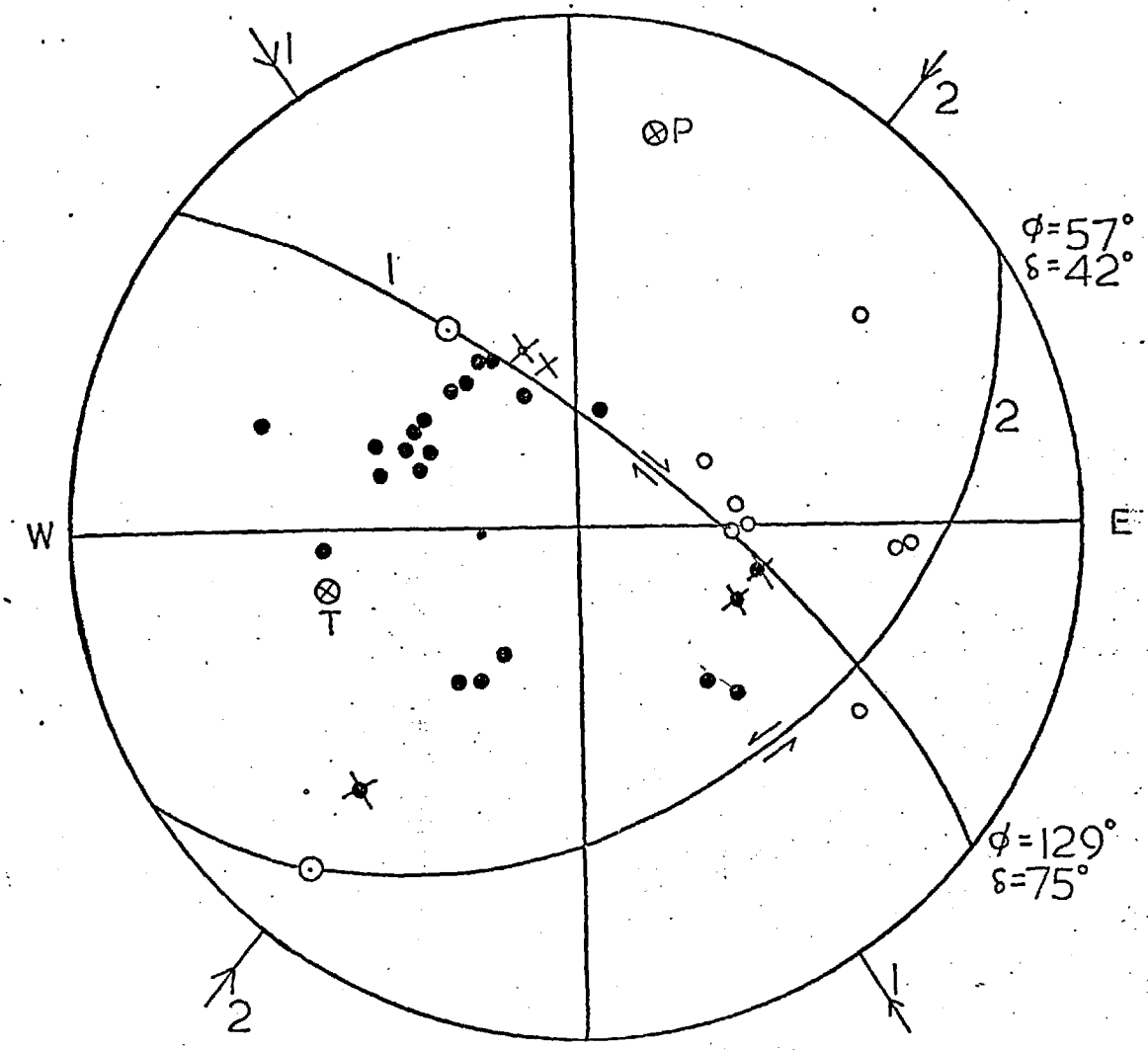



Fig.4.21 Fault Plane Solution of the Kariz earthquake ( 26, 5, 1971 ).
Lat. 35.5, Long. 58.2 , . Depth 26 Km and $V_p$=6.8 Km Sec
(After McKenzie, personal comunication)

# CHAPTER V

# GEOMORPHIC STUDIES

## New Evidence on the Extent and the Nature of Movement of the Great Kavir Fault

### 5.1 Introduction

The Great Kavir (Doruneh) Fault, which extends for about 700 km from the eastern frontiers of Iran to the central Dasht-e-Kavir desert (Figure 2.1), was previously considered by many authors (Wellman 1965, Nowroozi 1972, Tchalenko et al. 1973, Tectonic Map of Iran, G.S.I. 1971) to be the major structural feature of eastern and central Iran. The fault was thought to trend broadly east-west, being concave toward the south.

The relatively smaller Dasht-e-Bayaz Fault, on which the magnitude 7.3 earthquake in 1968 occurred, lies 130 km to the south, and the possible connection of this fault with the Great Kavir Fault is not understood as yet. The very length of the Great Kavir Fault and its clear trace on the recent alluvial deposits has attracted many investigators interested in the study of active faults. Interpreting a number of offset drainage channels on aerial photographs, Wellman (1966) concluded that the whole length of the fault should be moving left-laterally, and in a proposed plate tectonic model of the Middle East, Nowroozi (1972) makes use of this interpretation

to delineate an active left lateral plate boundary at the northern edge of the Lut-Block Figure (1.2). Wellman's inference was contested by Tchalenko et al. (1973), who, on the basis of field observation on a 60 km segment between Torbat-e-Heidarieh and Kashmar, proposed that movement on the fault was mainly vertical.

The investigations reported here do not agree with either of these generalized conclusions, although both vertical and left-lateral movements, combined or separately, have been observed in different segments of the fault. It is also postulated here, that the Great Kavir fault system does not show a unified system of faulting and should be divided into separate sections distinguished by differences in dominant patterns of faulting, senses of recent movement,and other criteria which will be discussed later.

More than six lines of evidence are presented in support of this proposed model of the northern Lut faulting. What was previously known as the Great Kavir (Doruneh) fault system can conveniently be divided into two segments, one extending from the eastern Iranian frontier westward through Rusht-Khar and Torbat-e-Heidarieh to Kashmar, the other running north-eastward from the central Dasht-e-Kavir desert through the village of Doruneh and straight up to Kariz village and probably to Asadabad. The justification for this comes from the following observations, and its usefulness will be discussed in section 5.4.

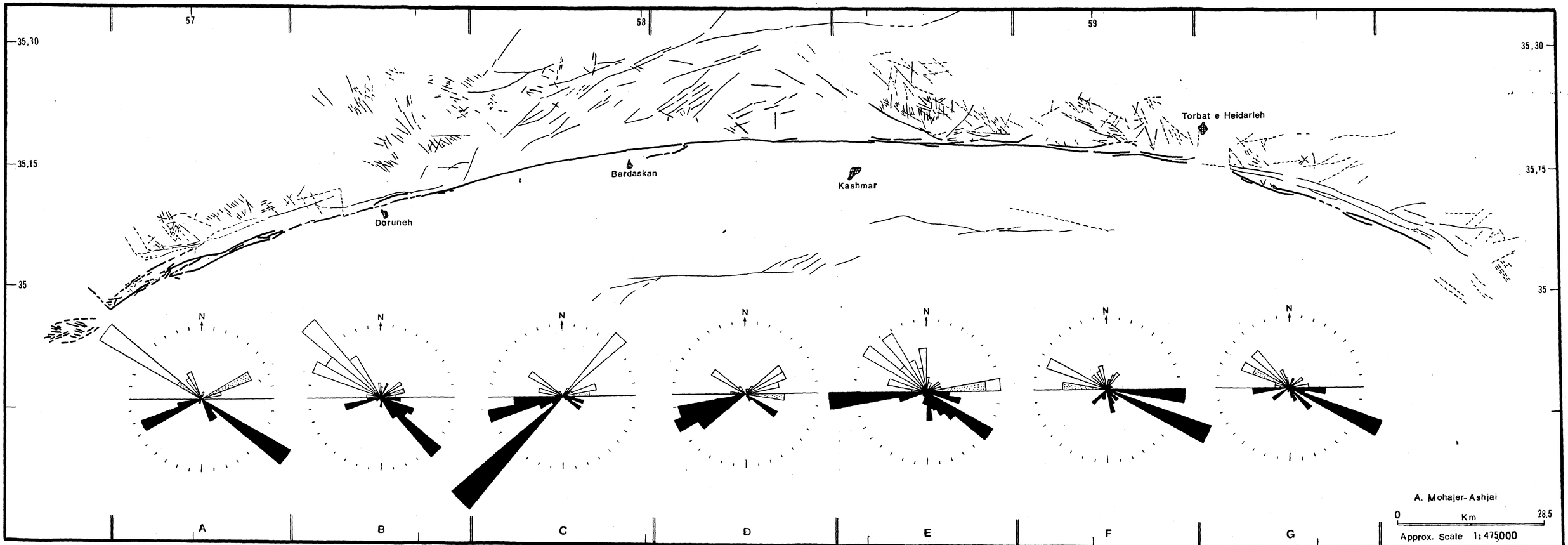
## 5.2 The pattern of faulting of the Great Kavir Fault System

From a detailed study of the 1:55,000 aerial photographs, maps have been prepared of the fault traces that make up the Great Kavir Fault system zone. Marked changes can be seen in both the azimuths and lengths of the lineaments between one end of the system and the other (Figure 5.1). In an attempt to express the nature of these changes quantitatively, the fault zone has been divided arbitrarily into seven sectors, for each of which the number of lineaments and their total length have been determined as a function of azimuth. The results are presented on Figure 5.1 in the form of rose diagrams.

These frequency and length diagrams are not an attempt to deduce the actual structure of the area, for they are based on trend lines that are two-dimensional. Rather, they are an attempt to show where structural differences may exist. For each sub-division the upper half of the rose diagrams indicates the number of lineaments versus azimuth, and the lower half represents total length of the lineament versus azimuth. This may facilitate the comparison of distribution of the larger fault lines with that of the smaller ones. The practice was conducted for two generations of faults separately; the recent faults (cutting through Quaternary deposits) are shown in dotted rosettes and the older faults in open and solid rosettes (Figure 5.1). It should be noted that the mapping is limited to the immediate vicinity of the main continuous fault trace, up to about 10 km on each side,

Figure 5.1

Surface fracture patterns and fault trends along the Great Kavir (Doruneh) Fault system, eastern Iran. The most recent fault traces are indicated by a heavy line and less clear lineations are shown by dash lines. Rose diagrams of seven equal zones (A to G) are illustrated for comparison. The upper half of each rose diagram uses the number of lineations versus azimuth, whereas the lower half (solid rays) illustrates lineations weighted by their length. The dotted trends signify the recent faultings. (The map is based on air-photo and field observations made by A. Mohajer-Ashjai.)


57
58
59
35,30
35,15
35
Torbat e Heidarieh
Bardaskan
Kashmar
Doruneh
N
A
B
C
D
E
F
G
A. Mohajer-Ashjai
0 Km 28.5
Approx. Scale 1: 475000

Map 2

and that there are many areas close to the fault zone which are obscured by alluvial fans or desert sands which, therefore, have been left blank on Figure 5.1.

Statistical observation of the fault traces in the western section of the Great Kavir fault system is represented by the three rose diagrams in the zones A, B and C. In zone A, the prevailing direction for the recent faulting is N 60°E, with less frequent trends at N 50°W. The dominant direction of the older faults lies somewhere between NW-SE and WNW-ESE in this zone. The pattern of faulting in zone B is very similar to that of zone A, but the dominant trend shifts to a NE-SW direction in zone C. Combining the rose diagrams from these three zones (Figure 5.2) and considering the sense of movement of the dominant directions, a conjugate shear system results which suggests a regional N-S to NNE-SSW compression with continued activity through time. The angular relationship between the shear faulting and their causative compressional axes is shown in Figure (5.3), and discussed by Badgely (1965) in detail.

In the central region around Kashmar and some distance to the west (zones E, D) the pattern becomes complicated both for recent and older geological times. This feature has been interpreted either as the transition between two different tectonic regimes or alternatively as the area where two different fault systems meet. The characteristic of these particular zones is block faulting, which sometimes combines with a small component of left-lateral motion (section 5.5). The dominant azimuth of the trend lines in zone E

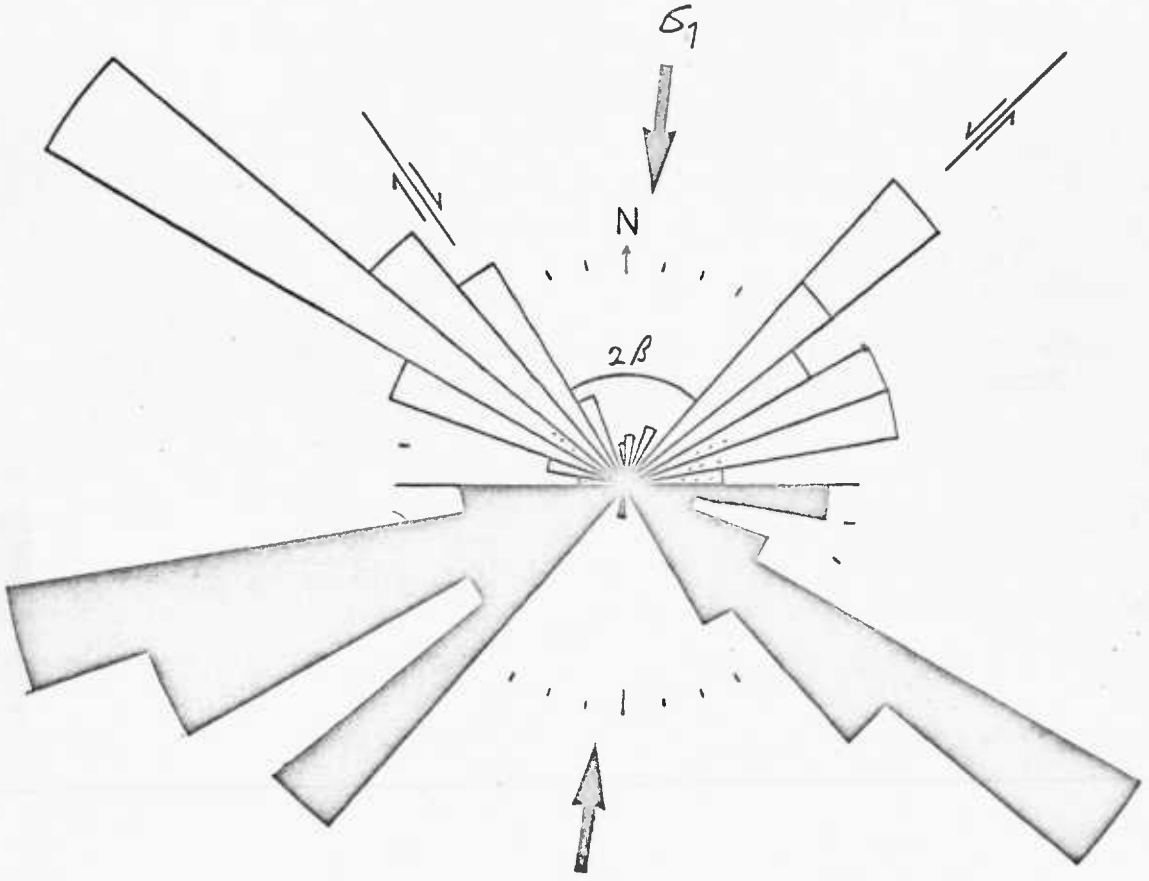



Fig. 5.2. Combined rose diagrams of zones A B, and C. Sense of movements in dominant azimuths were also considered when inferring the the compressive directions.

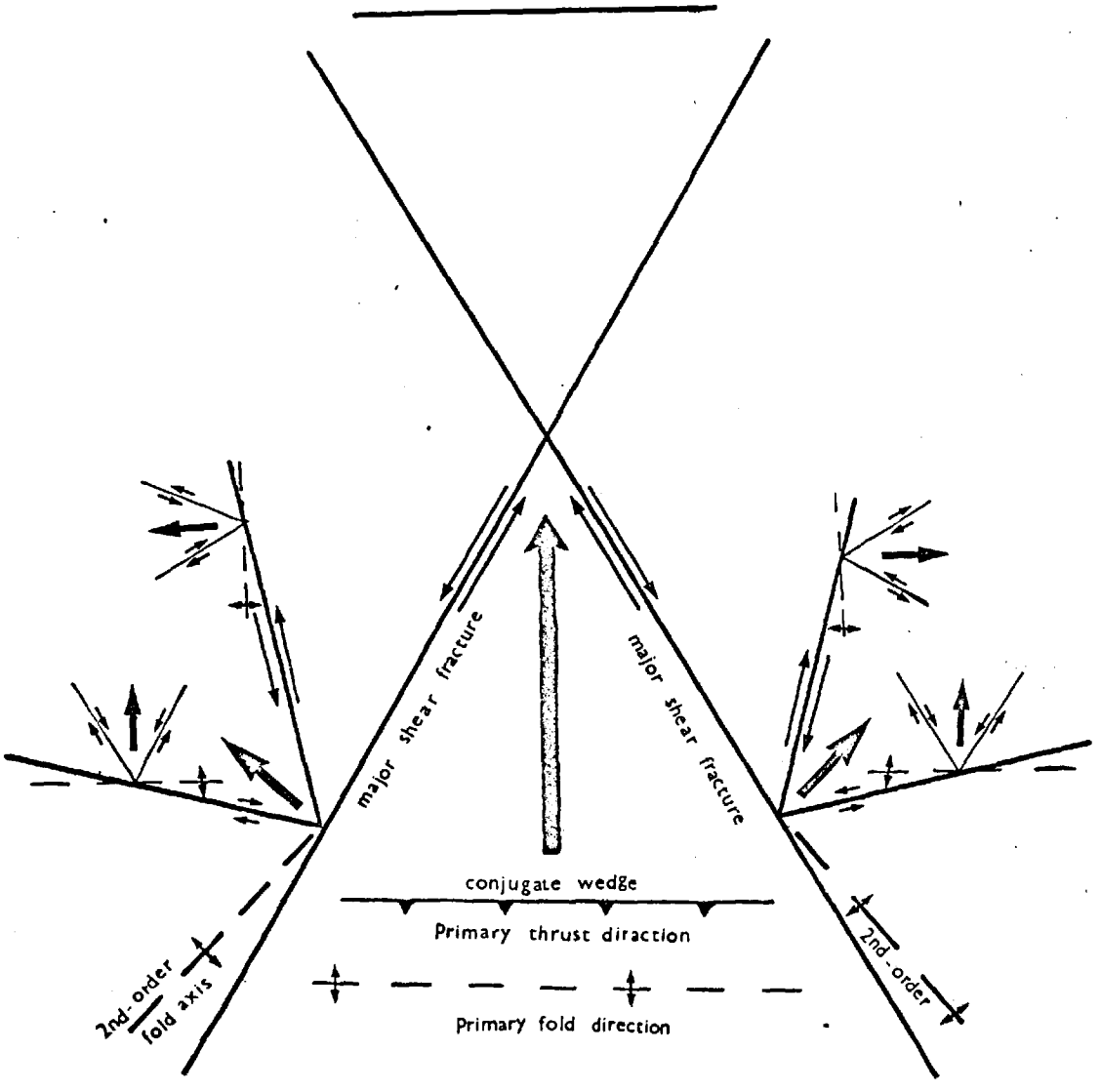



Fig. 5.3. Wrench-Fault system of Moody and Hill (1956), revised by Badgley (1965) to show all second and third order shear fractures.

is N 90°E, which is quite different from the areas to the east and the west.

The two pairs of diagrams for the eastern section covering the two zones around and east of Torbat-e-Heidarieh (zones F and G) are fairly similar and show predominantly NW-SE and E-W strikes, with minor deviations. Quaternary faulting clearly follows the older fault trends which are usually parallel to the fold axes of the area (Figure 5.5). This fact, plus the observation of high angle reverse faulting in the field, attest to a major NNE to NE compression active in this area.

An attempt has been made to cross correlate the directional frequency of the fractures in the different zones (A to G) along the Great Kavir Fault. The results are shown in Figure 5.4, which summarizes the common dominant azimuths throughout the region. There seems to be very little correlation of the azimuths of fractures in this area, although, a N 45°W direction of fracturing occurs in zones A to G. There are other vague correlation of fracturing in zones A to E pointing to N 55°W and N 75 E, and to N 65 E in zones A to G.

Other points which pertain to the statistical study of the fracture pattern in this area are:

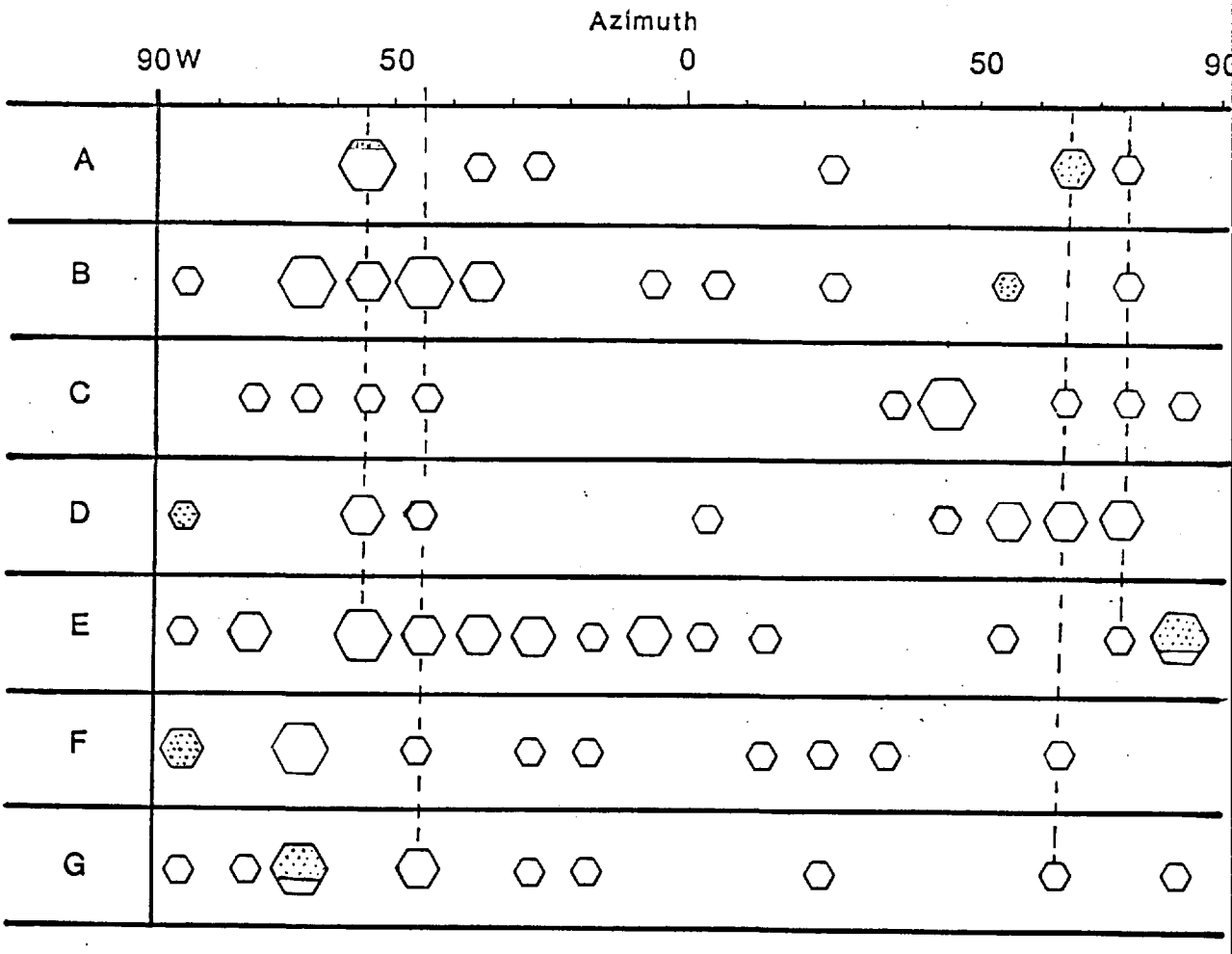



Figure 5.4

Summary of preferred trends from lineations in different zones along the Great Kavir Fault. The large polygons signify the trends with over fifty percent of the total number of fractures. Medium and small size polygons refer to population between 50% to 25% and less than 25% respectively. The vertical bars indicate possible correlation of the common dominant trends in these structural units (zones A to G).

a) The similar proportion of the number of lineaments and the total length of fractures at any dominant azimuth. This might signify that the fractures originate from tectonic activity and are extended deeply into the crust.

b) The distinct difference between the patterns of the recent and older faulting along the Great Kavir Fault system. This might indicate changes of the direction of principal stress through geological time, or rotation of some structural features.

## 5.3 Variations in the relative sense of movement along the Great Kavir Fault

The author has made several field investigations along parts of the fault system which are mapped and presented here (Figure 5.5 a, b, c). Three distinct sections along this fault were chosen and discussed separately.

### 5.3.1 Sense of movement in the western section (zones A, B and C)

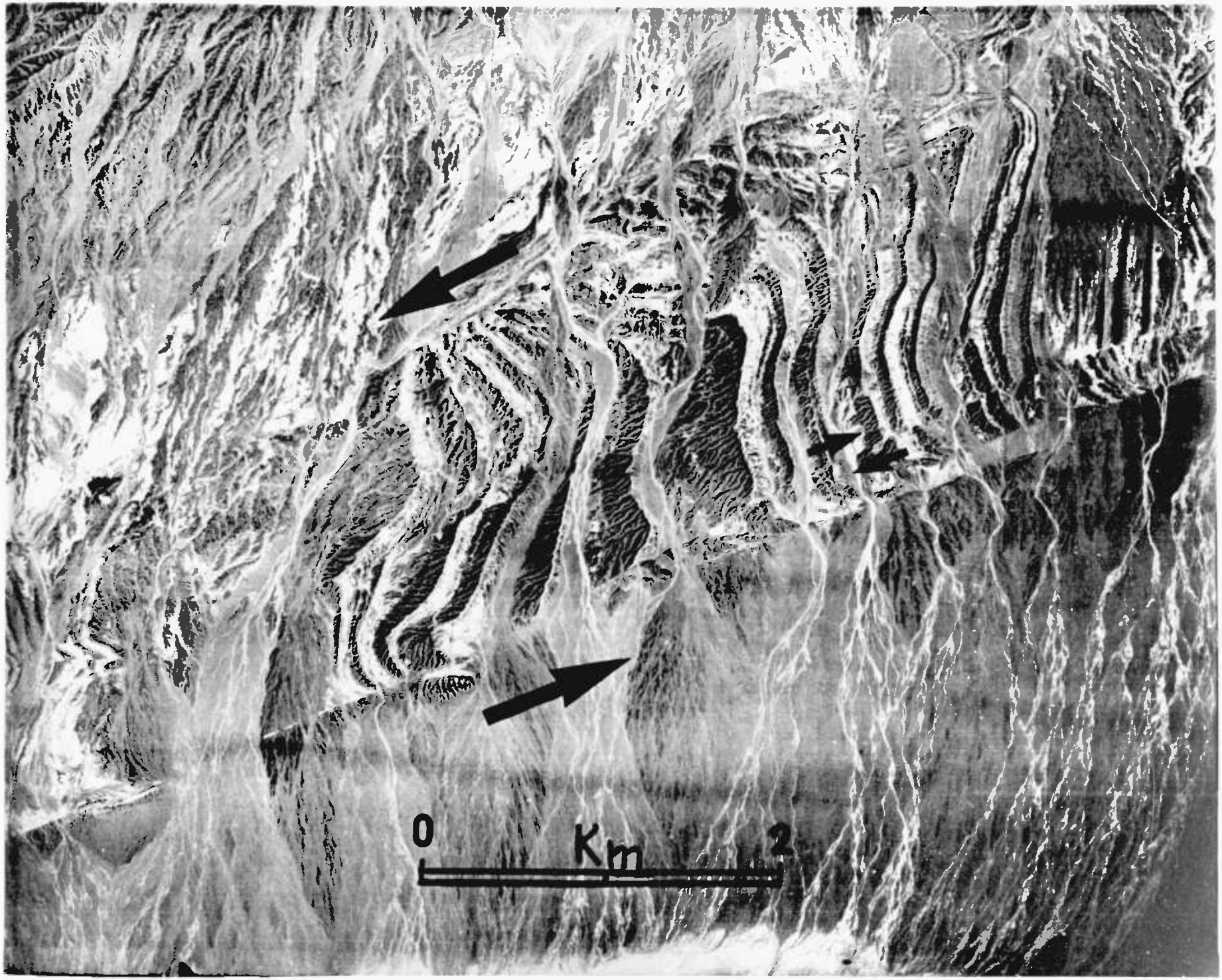
A detailed mapping of the fault traces based on 1:55,000 aerial photographs (Figure 5.5a) revealed unmistakable signs of wrench faulting both in Quaternary and earlier times. In Figure (5.5b) many

vivid conjugate shear systems are marked which represent a N-S horizontal axis of compression for pre-Quaternary times. There are also fault traces cutting clearly through the Quaternary and recent alluvial fans and sometimes even through the youngest gravel and sand deposits of Dasht-e-Kavir desert. This younger generation of faults is shown by heavier lines in Figure 5.5a and is interpreted as being part of a main sinistral shear system with minor dextral movements within the system. An example of Quaternary alluvial ridges displaced by the activity of these wrench faults is illustrated in plate 5.1. A consistent dextral offset of the alluvial ridges equivalent to 82 metres of displacement on the ground, is measurable in this locality. Also on a larger scale, the dragging effect of a sinistral shear system has been well preserved on these ridges. An attempt has been made here to determine the value of the finite strain accumulated in this area since these sub-recent sedimentary ridges were deposited. The method is described in the next section.

### 5.3.2 Longitudinal and shear strain components in the Quaternary alluvial deposits west of Doruneh

Various techniques have been developed for determining the component of linear strain in rocks (see for example Ramsay 1967). An attempt has been made to apply these techniques to the distortion of linear ridges revealed on the aerial photographs of the Great Kavir Fault (west of Doruneh).

Plate 5.1. Sinistral dragging of sub-recent alluvial ridges along the Great Kavir Fault (70 km west of Doruneh Village).


0
Km
2

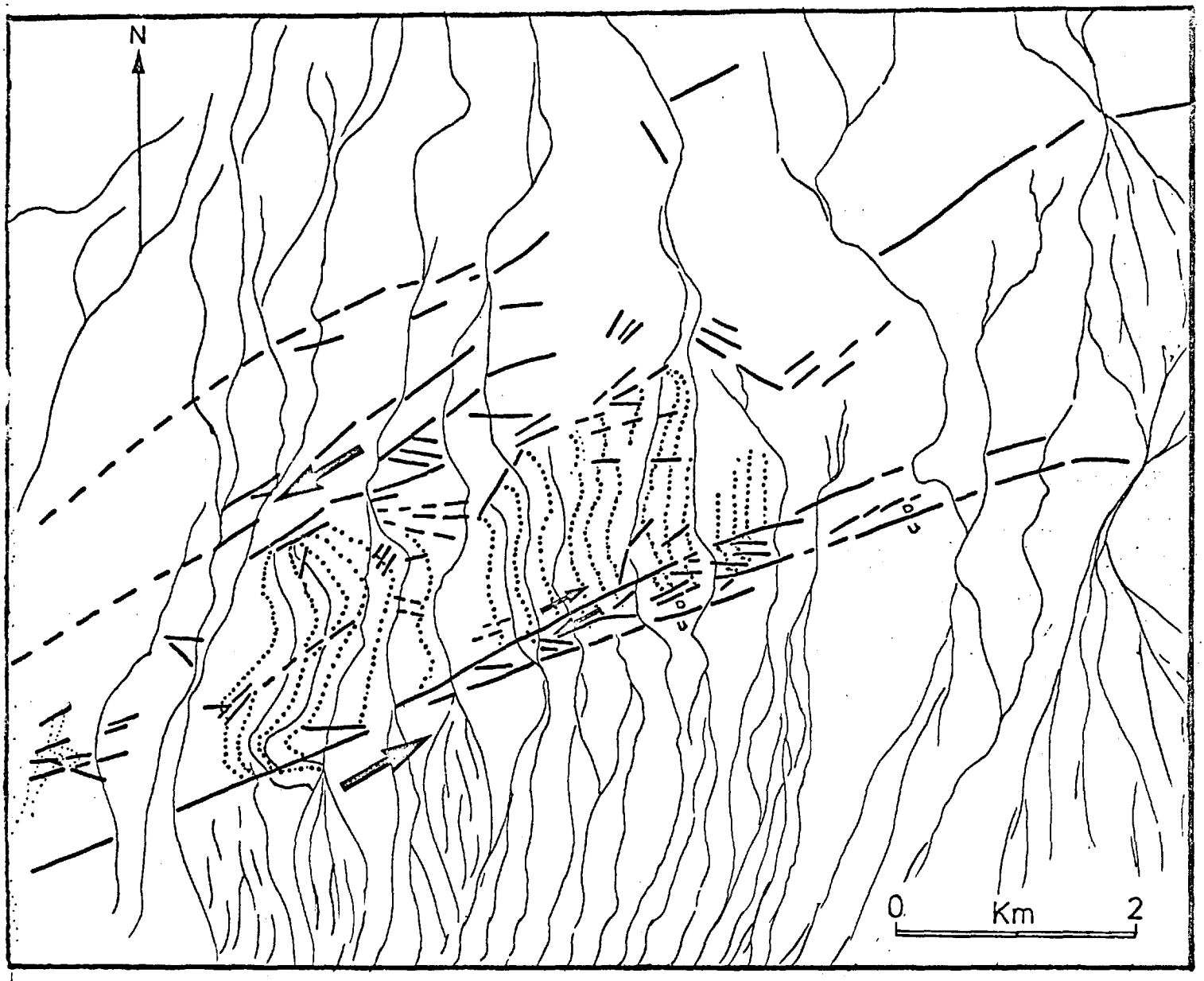



Fig. 5.5a. Structural map of a section of the Great Kavir Fault( 70 Km west of Doruneh Village ), based on the 1:55,000 aerial photographs.

. . . . . Crest line of Quaternary alluvial ridges.

Faults

Drainage

Sense of horizontal movements

U/D Sense of vertical movements

This is the only feature along the whole length of this major fault which could possibly be used as a strain marker. In addition to that, the dragging effect on these well bedded and compacted young sedimentary ridges indicates hitherto unknown major left-lateral shear movement.

Thus, it is assumed that the folded sedimentary ridges shown in Plate 5.1 (Figure 5.5a) were initially straight and have been deformed in a horizontal plane without much thickening or vertical folding. This assumption has been checked and verified to a certain extent, by studying stereo-pairs. Unfortunately, the area is situated a fair distance inside the Dasht-e-Kavir desert and, therefore, is not readily accessible. That is why it has not been possible to confirm the matter in the field.

It is, therefore, possible to estimate the component of the longitudinal strain in the azimuth of the ridge by comparing the distance between the ends of the ridge with the original length in the undistorted state. If the initial length of the crest line of the Quaternary alluvial deposits in this area (Figure 5 5a) is lo, and the length of the contracted crest line $l_1$, then the extension e, which should bear a negative sign in this particular case, is:

$$e = \frac{l_1 - l_o}{l_o} = \frac{\Delta l}{l_o}$$

By applying this relationship to several of the ridges shown in Plate 5.1, values of longitudinal strain have been obtained as a function of azimuth: the results are plotted in Figure 5.6 together with standard deviations based on at least five independent readings.

Even though the number of measurements and their azimuth range is limited, Figure 5.6, contains sufficient information to enable a crude estimate to be made of the parameters of the strain ellipse. This requires a knowledge of the strain in three independent directions, which in this case may be taken to be -0.15, -0.11 and -0.05 in azimuth N6$^{o}$E, N1$^{o}$E and N350$^{o}$E respectively. The necessary formulation can be derived as follows:

It is customary, in geological computation, to present such changes of length in terms of the quadratic elongation ($\lambda$), which is defined as the square of the length of a line of originally unit length.

$$\lambda = \left(\frac{l_1}{l_o}\right)^2 = (1 + e)^2$$

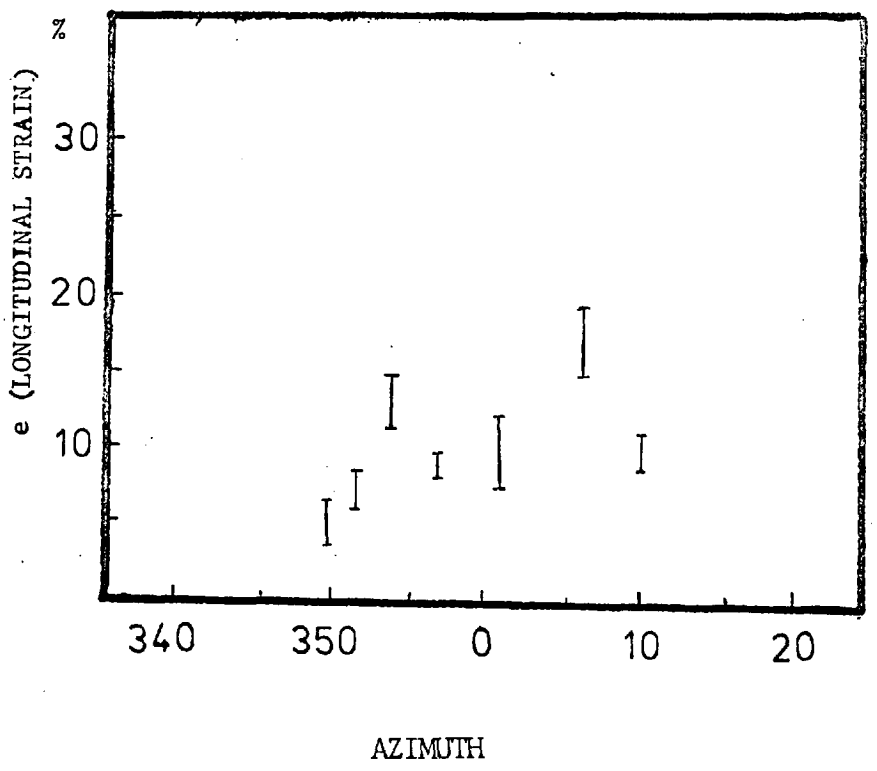



Figure 5.6

Variations of the contraction of the alluvial ridges in different directions expressed as a percentage. The vertical bars represent the standard deviation of a set of independent estimates.

Quadratic elongation for the three dominant directions of the contracted alluvial ridges are, $\lambda_i = 0.722$, $\lambda_j = 0.792$ and $\lambda_k = 0.902$ corresponding to azimuths $\alpha = 6°, \beta = 1°$ and $\gamma = 350°$ respectively. To derive the appropriate formulation for determining $\lambda_1$ and $\lambda_2$, squares of the principal axes of the strain ellipse, with their corresponding azimuths and values of the shear strain based on known values of longitudinal strain in three general directions, we proceed as follows:

As a result of deformation there are changes in the lengths of lines and consequently a circle with unit radius (1) normally alters to an ellipse of the form (2)

$$x^2 + y^2 = 1 \qquad (1)$$

$$\frac{x'^2}{(1+e_1)^2} + \frac{y'^2}{(1+e_2)^2} = 1 \qquad (2)$$

having principal axes $1 + e_1$ and $1 + e_2$. $e_1$ and $e_2$ are defined as the longitudinal strain or extension along the two principal axes (Figure 5.7).

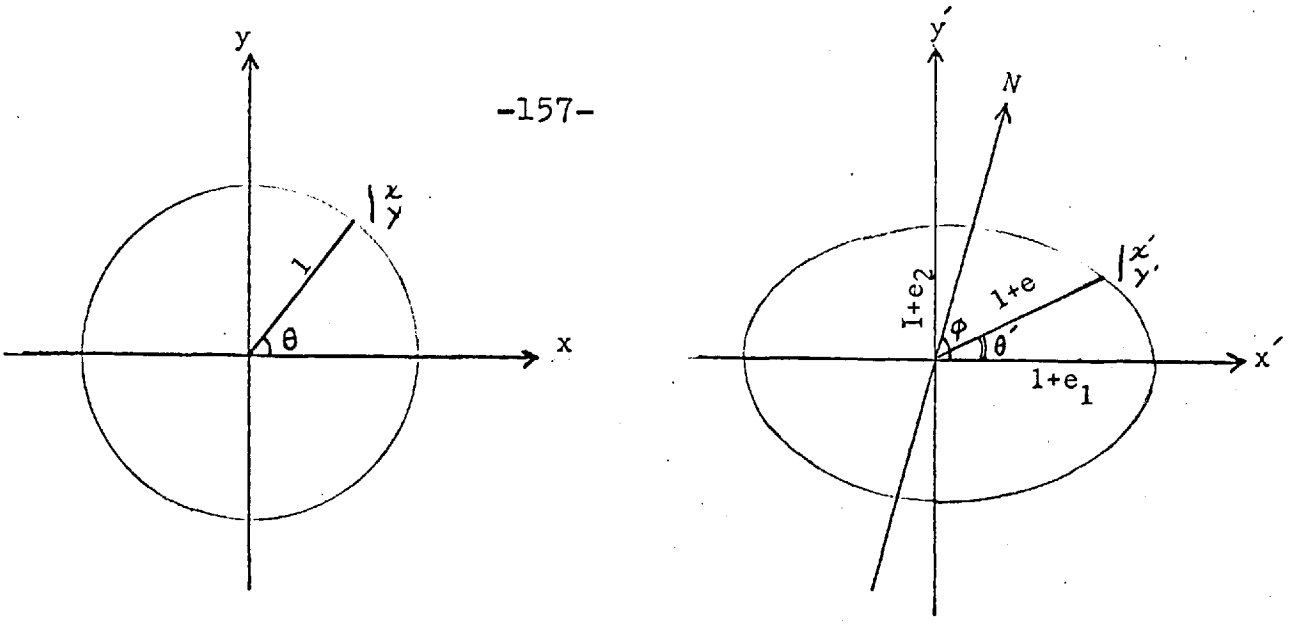



Figure 5.7. The unit circle is altered to an elipse as a result of a homogeneous strain.

---

But as

$$x' = (1 + e)\,\mathrm{Cos}\,\theta'$$
$$y' = (1 + e)\,\mathrm{Sin}\,\theta'$$

by putting these values in (2) we obtain

$$\frac{(1+e)^2\,\mathrm{Cos}^2\theta'}{(1+e_1)^2} + \frac{(1+e)^2\,\mathrm{Sin}^2\theta'}{(1+e_2)^2} = 1 \qquad (3)$$

as mentioned earlier
$(1+e)^2$ is called the quadratic elongation ($\lambda$).

By substitution in equation 3, we obtain:

$$\frac{\lambda \cos^2 \theta'}{\lambda_1} + \frac{\lambda \sin^2 \theta'}{\lambda_2} = 1 \qquad (4)$$

or $$\frac{\cos^2 \theta'}{\lambda_1} + \frac{\sin^2 \theta'}{\lambda_2} = \frac{1}{\lambda}$$

Defining the reciprocal value of the quadratic extension in a general direction as $\lambda'$, by substitution we obtain a simple equation for the lengths of deformed lines with reference to the angle they make with the x coordinate axis in the strained state (see also Ramsay 1967, p.65).

$$\lambda' = \lambda_1' \cos^2 \theta' + \lambda_2' \sin^2 \theta' \qquad (5)$$

Three well measured values for $\lambda'$ namely $\lambda_i'$, $\lambda_j'$ and $\lambda_k'$ making unknown angles of $\theta_i$, $\theta_j$ and $\theta_k$ with the principal axis of strain ellipse, will produce three equations which can be solved simultaneously by appropriate manipulation. These equations are:

$$\lambda_i' = \lambda_1' \cos^2 \theta_i + \lambda_2' \sin^2 \theta_i$$

$$\lambda_j' = \lambda_1' \cos^2 \theta_j + \lambda_2' \sin^2 \theta_j$$

$$\lambda_k' = \lambda_1' \cos^2 \theta_k + \lambda_2' \sin^2 \theta_k$$

First, we solve these equations in their general form, then we put in the respective values. The solution has been derived in a simple form as in the Appendix I.

This formulation requires the assumption that homogeneous finite strain, without significant change of volume, has accumulated through geological and recent times in the area under observation.

A similar assumption of homogeneous strain distribution in an area covering a few square km is made by Frank (1966) and by Savage and Burford (1970) in order to interprete the results of successive measurements of triangulation networks.

Nevertheless, many research workers have also considered the assumption of homogeneous strain in even larger areas, in the order of a few hundred square km. when calculating different components of strain based on their long range direct distance measuring devices such as the Mekometer or the Geodimeter.

As discussed earlier, three well measured initial and contracted lengths of alluvial ridges in a relatively small area ( 2 x 5 kilometers , Figure(5.5a), 70 kilometers west of Doruneh village revealed the following negative extension:

| Extensions | Corresponding Azimuth | Quadratic Elongation |
|---|---|---|
| $e_i = -.15$ | $\alpha = 6^o$ | $\lambda_i = .722$ |
| $e_j = -.11$ | $\beta = 1$ | $\lambda_j = .792$ |
| $e_k = -.05$ | $\gamma = 350^o$ | $\lambda_k = .902$ |

Using equation (16)(Appendix 1) and calculating values of K, L and M we have

$$-.00463 \tan^2\phi + 2\ (.00373) \tan\phi + .00463 = 0$$

for which there are two solutions for $\phi$, $-25.5^\circ$ and $+64.4^\circ$

Having found the azimuth of the principal axes of the strain ellipse we proceed to calculate $\theta_i$, $\theta_j$ and $\theta_k$ and subsequently values of $\lambda_1$ and $\lambda_2$, using equations (12) or (13) and equation (9)(Appendix).

The consequent values of the principal axis of the strain ellipse in the west Doruneh area are found from:

$$\lambda_1 = .971$$

$$\lambda_2 = .429$$

and the maximum value of the finite shear strain is (Ramsay 1967).

$$\gamma = \pm \frac{\lambda_1 - \lambda_2}{2(\lambda_1 \lambda_2)^{\frac{1}{2}}} = \pm 0.419$$

Typically strains of the order of $10^{-4}$ normally build up in competent rock before failure and the subsequent earthquake occure (Chinnery 1963 and Rikitake 1974). The large accumulated strain values calculated here, that are based on the bent alluvial ridges, suggest rather ductile (plastic) behaviour of the rocks in this area over a fairly short, geological time span (Quaternary to recent). If we suppose an upper limit of 1,000,000 years for the observed deformation in the young alluvial deposits, the strain rate in this area would be in the order of $4.10^{-7}$ per year. This is in good accord with the average strain rate observed in other areas, presently active in Iran (see Chapter III) and California (Chinnery 1963, and Savage 1973). However, the average rate of homogeneous strain in the Iranian plateau is about $4 \times 10^{-8}$ ppm/yr , almost one order of magnitude less than the above estimation for west of Doruneh. This average rate has been derived from the rate of sea floor spreading deduced from the marine magnetic anomalies (McKenzie 1972).

This fact leads to a tentative suggestion that the apparent concentration of large values of strain in places such as the western Doruneh could not be explained by the general low rates of homogeneous strain over the Iranian plateau and, therefore, it is sensible to look for other places in the area where higher rates of activity are prevailing, and try to find the mechanisms by which this concentration of strain might occur.

Unfortunately, there are not many other regions in Iran with known values of the strain rates to make this task possible at the present time. But as an example, the rate of strain measured by the Mekometer and Creepmeter on the Dasht-e-Bayaz Fault are in the order of $10^{-6}$, high compared with the average values. This high rate is thought to be related to the afterslip phase of the major 1968 earthquake in this area.

Other possible mechanisms for localized stress concentration might be related to the end effects of wrench faults, where higher stresses are predicted from theoretical considerations (Chinnery 1966) and high levels of microearthquake activity have been observed by the author (Chapter IV).

### 5.3.3 Sense of movement in the central section of the Great Kavir Fault

Much field evidence has been found by the author to suggest that in the central section (zones D and E) vertical movements predominate and that the south side of the fault has often gone up relative to the north side in the younger generation of the faults. Typical localities where this movement was clearly observed are the areas around Nai and Azgand. In Azgand village (30 kilometers east of Kashmar) a linear low elevated ridge consisting of recent colluvial sediments cemented by deposition of travertine, marks the uplifted hanging wall of the young fault in this region. The striations on

the south dipping fault mirror have a rake angle of about 65° toward the west, which signifies dominantly reverse faulting with a minor left-lateral component (Figure 5.8). A few hundred meters west of Azgand, in a river valley, a cross section through the young silt deposits clearly shows a marker green bed which has been offset about 1.5 meter by a high angle reverse fault dipping 60° to the south.

Around Nai village (20 kilometers east of Kashmar) there is another small ridge along the main young fault where the southern block thrusts over the northern side at an angle of 65°. There are several other parallel scarplets toward the piedmont of the Kuh-e-sorkh mountains (on the northern side of the Great Kavir Fault).

These successive scarplets are also clearly detectable under the stereopairs and are a common feature in the area between Bardaskan and Torbat-e-Heidarieh. These fault traces are specially vivid on the aerial photographs, because there is a colour contrast caused by light colour (yellowish) sandy clay, varying from 50 to 200 meters in width, along their path.

A schematic cross-section illustrating the dominant vertical and reverse faulting in this area is presented in Figure (5.9). Tchalenko et al. (1973) also found other evidence which support the sub-vertical movement in this region.



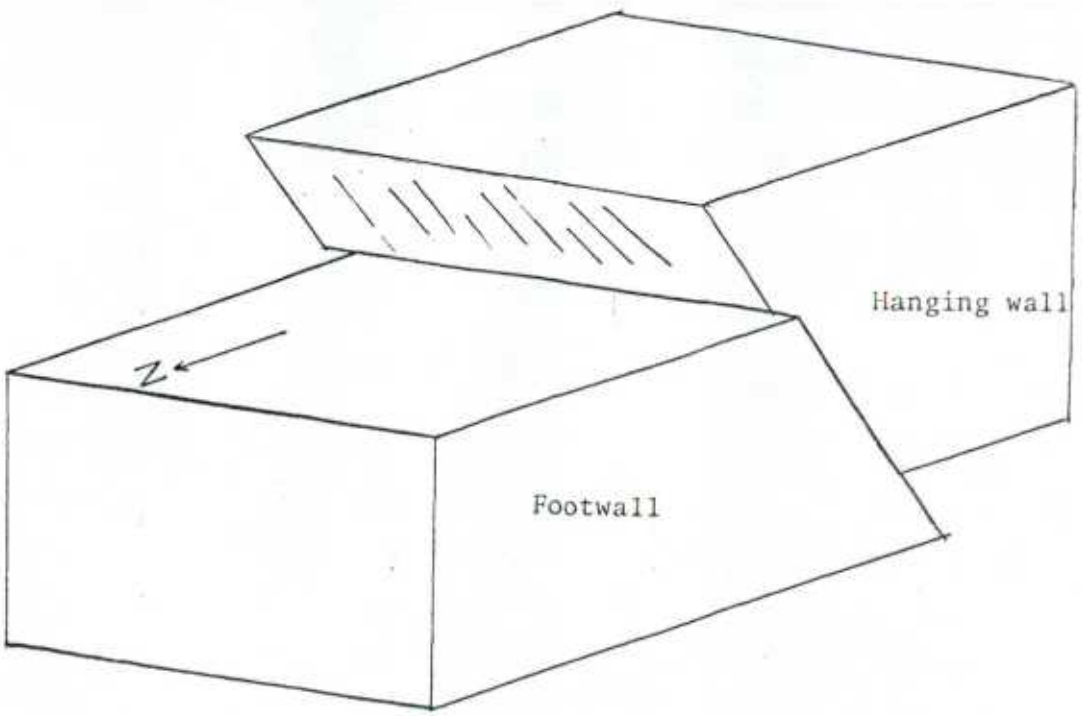



Fig. 5.8. A view and the block diagram of the high angle reverse fault with a small sinistral component, observed in the Quaternary deposites in Azgand( 30 Km east of Kashmar ).

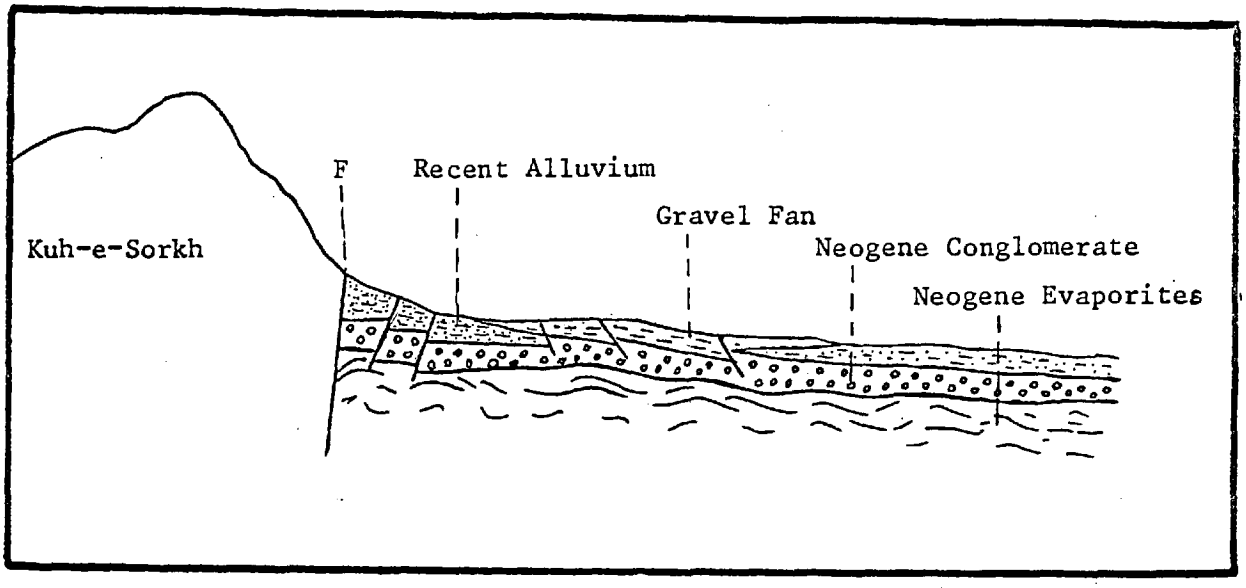



Fig. 5.9. A schematic and typical cross section of the recent high angle reverse faulting along the Great Kavir Fault, east of Kashmar.

The fault movement west of Kashmar has also a predominant subvertical component and the band of yellowish clay has been followed to Anabad (beyond Bardaskan, Figure 5.5b. In this region the block faulted appearance of older dislocations becomes complicated and the major trends align mostly NE-SW. This region is thought to mark the transition between the zone of block faulting to the east and the zone of shear faulting to the west, as discussed earlier. Many older conjugate shear faults in this region testify to a mainly N-S compressive direction (Figure 5.5 b).

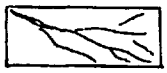
### 5.3.4 Sense of movement in the eastern section of the Great Kavir Fault

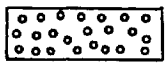
The fault system east of Torbat-e-Heidarieh (zones F and G) was visited by the author (in 1972) for the first time, and in several traverses along major river beds many parallel dip-slip faults with associated folding were recognised. One of the main characteristics of this region is the long continuous and parallel nature of the faults which are gently bent and always follow the axial plane of the symmetrical folds of the area.

The best cross section which gives a good direct view of the recent and former near surface structures is Kaleh-Sorkh (15 kilometers east of Torbat-e-Heidarieh). This is a river bed running almost N-S from Sibi on the north side of the mountain range to Malakabad in the southern side (Figure 5.5c).

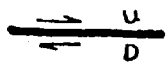
Fig. $5.5_b$. Structural map of the central section of the Great Kavir Fault( between Bardaskan and Doruneh ), based on 1:55,000 areal photograp

LEGEND


Recent alluvial fans mostly in process of formation.


Older alluvial fans and terraces.


Neogene Conglomerate and Marl.



Quaternary fault traces and inferred sense of movements.


Older faults.


Horizontal component of compressive stress, based on the pattern of the Pre-Quaternary faults.


Main roads.

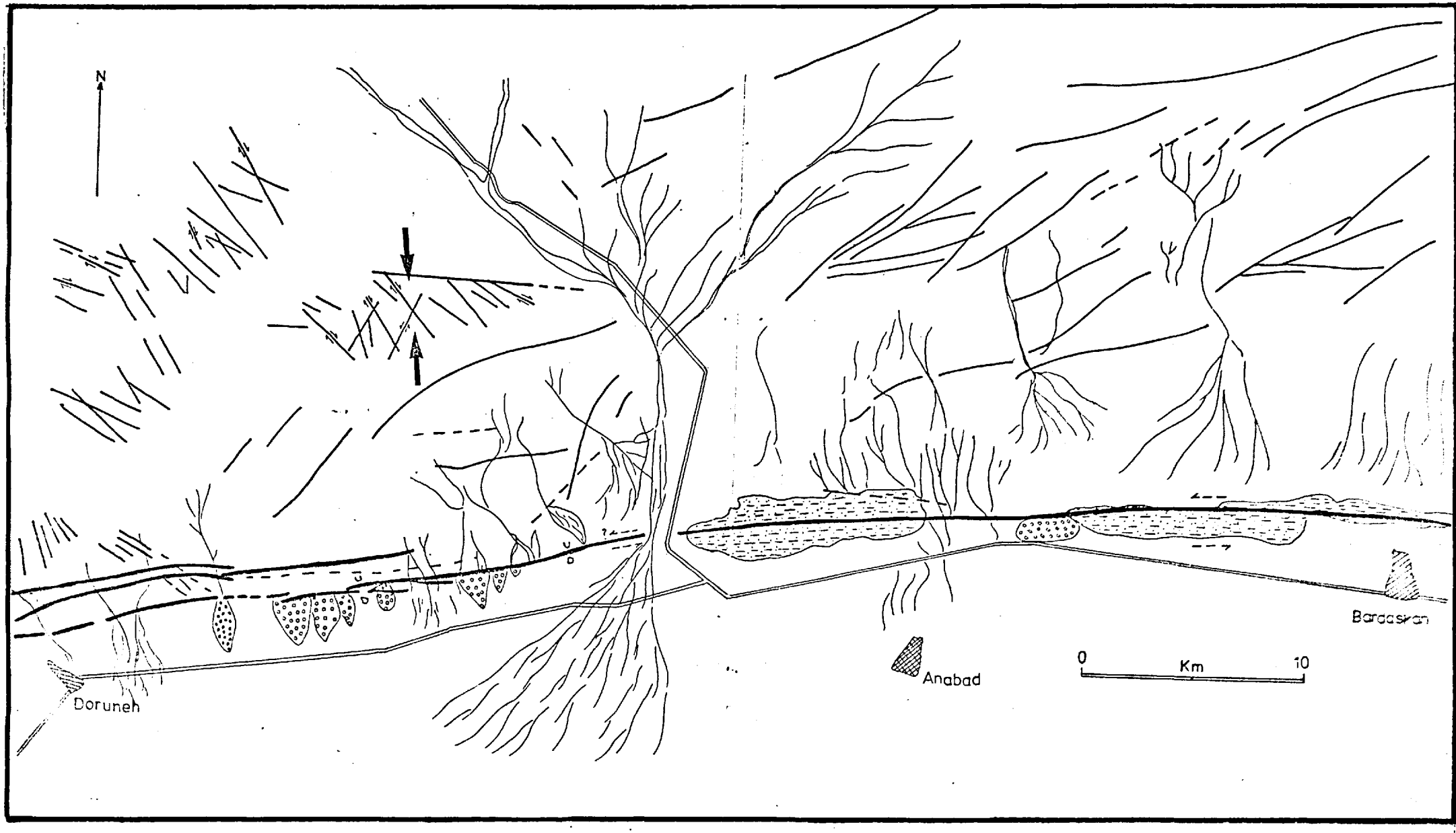
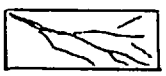
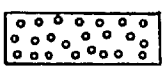

N
Doruneh
Anabad
Baraskan
0
Km
10

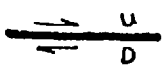
Fig. 5.5c. Structural map of a section of the eastern Great Kavir Fault (between Torbat-e-Heidarieh and Rushtkhar), based on 1:55,000 areal photographs.

LEGEND


Recent alluvial fans mostly in process of formation.


Older alluvial fans and terraces.


Neogene Conglomerate and Marl.

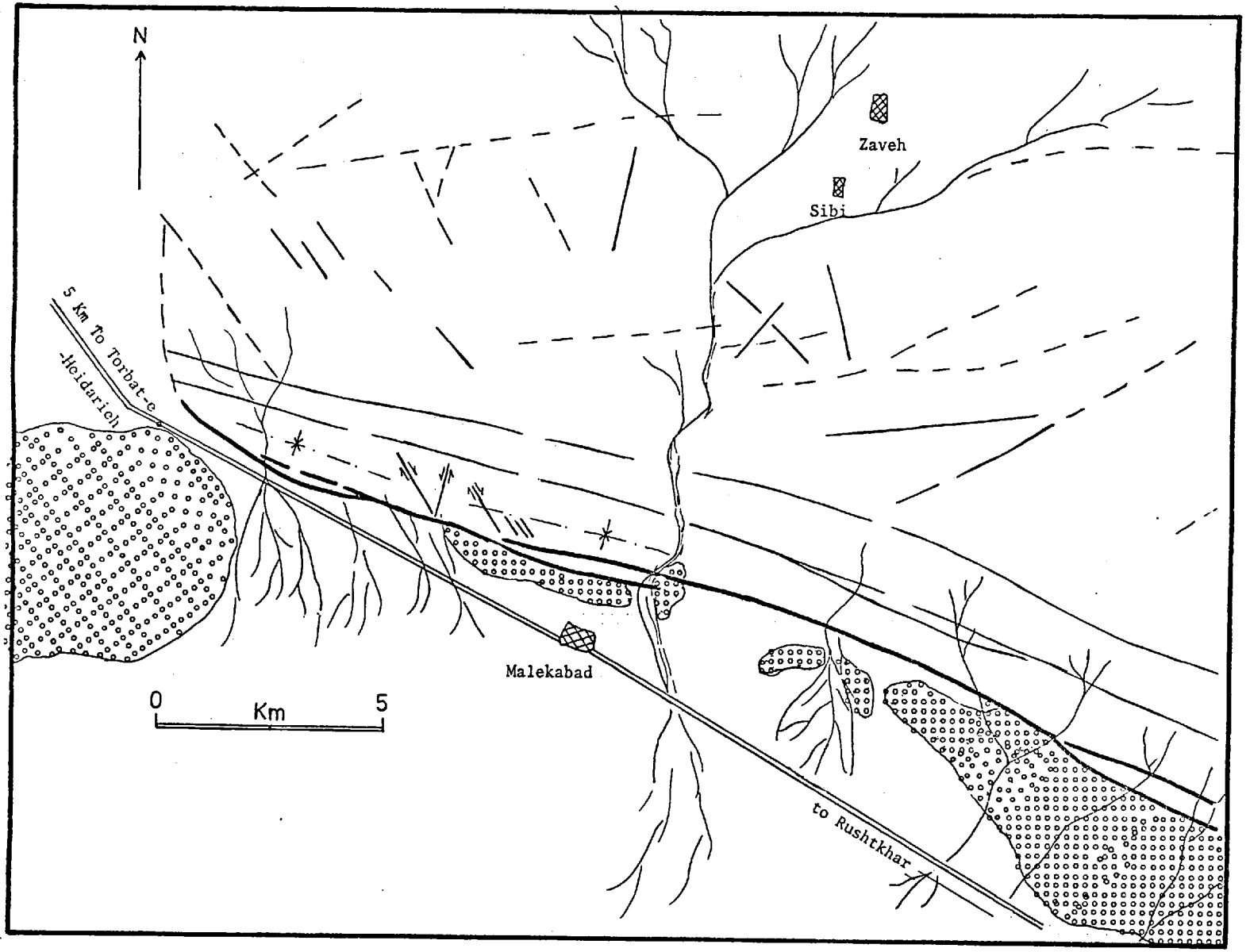


Quaternary fault traces and inferred sense of movements.


Older faults.


Horizontal component of compressive stress, based on the pattern of the Pre-Quaternary faults.


Main roads.


N
Zaveh
Sibi
5 Km To Torbat-e
-Heidarieh
Malekabad
0
Km
5
to Rushtkhar

In the river valley 3 km north of Malekabad, early Quaternary alluvial sediments ranging from boulders to fine sands, which have also produced distinct beddings, are strongly tilted toward the north (Figure 5.10). These consolidated alluvial deposits have gone through many phases of active tectonism which have resulted in high angle tilting and folding. In a later phase, sub-vertical fractures have been produced in them. These tilting and foldings are thought to relate to a syntectonic phase which is comparable to post-plio-pleistocene to pre-recent Zagros orogeny. This phase was followed by Late-Tectonic faulting and fracturing which does not continue into the recent river terraces, lying unconformably on the former deposits. On the top of this formation the most recent river terraces lies absolutely horizontally, indicating that the tectonic activity has ceased since the deposition of these young sediments.

Three hundred meters further north a fault scarp dipping $47^{o}$N is visible in this river valley. Along this fault the northern block thrusts over the southern block (Figure 5.11) and the striations on the fault mirror have a rake of about 90 degrees, and also being parallel to the fold axis in this area the fault is, therefore, a longitudinal high angle reverse with a very small component of left lateral movement. Here again the fault zone is covered by undisturbed young river terraces (Plate 5.2), a feature which might indicate that the fault activity did not continue to the present time. Two possible explanations exist for this observation, either the fault



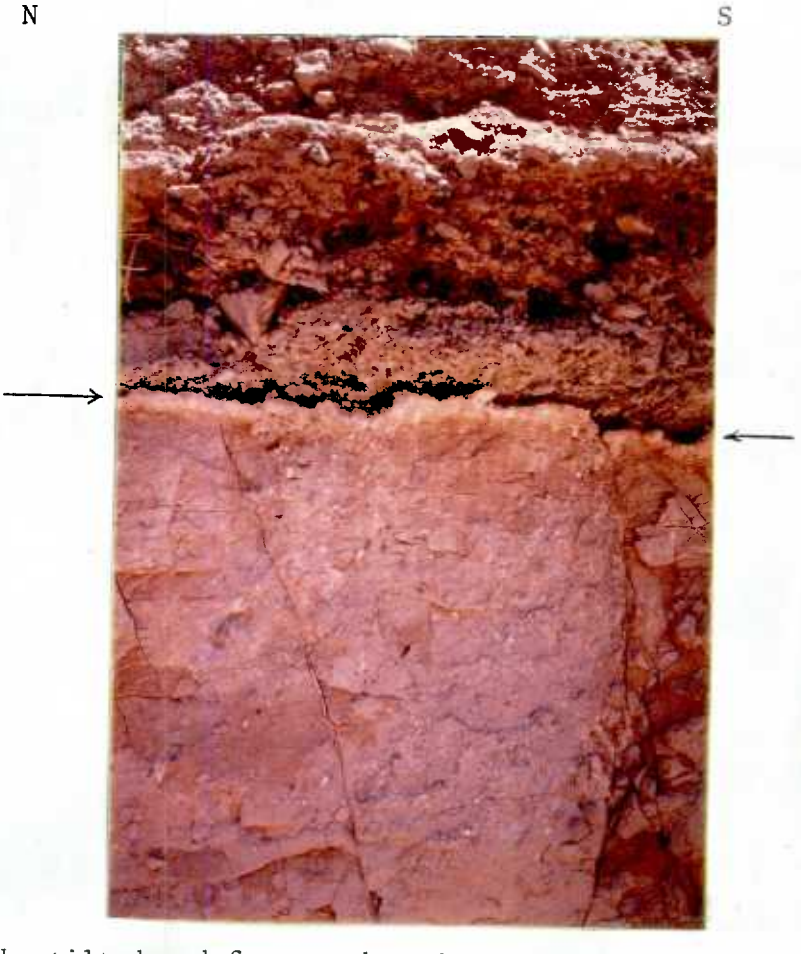




Fig. 5.10. Two views of the tilted and fractured early Quaternary alluvial deposites covered by undisturbed recent, horizontally lying, river terraces in Malekabad (15 Km east of Torbat-e-Heidarieh).




Fig. 5.11. The Great Kavir Fault scarp in Malekabad (15 Km east of Torbat-e-Heidarieh). At the bottom striations on the fault scarp are shown. The fault at this section is classified as a high angle reverse, dipping 47° to the north.



Plate 5.2. A panorama view of the Kaleh-Sorkh river valley 20 km east of Tobat-e-Heidarieh. Note the high angle reverse faulting at the left-hand side and horizontal river terraces to the right.



has ceased its activity completely since the late Quaternary, or strain is building up at low rates, or deformation is occurring in some other way.

This fault also serves as the southern limit of the limb of a syncline plunging west which consists of Eocene green tuff and well-bedded shale. In a cross-section presented in Figure (5.12) it is shown how this uplifted syncline is terminated by another south dipping fault. This fault also seems to be in the bedding plane of the northern limb of the syncline and does not bear any sign of recent activity (Figure 5.12, 5.13).

There are no reports of destructive earthquakes in the immediate vicinity of this region, although two shocks of moderate magnitude have been instrumentally located near this site. The nearest place to have experienced a devastating major shock is west of Torbat-e-Heidarieh (1923 earthquake) (see Chapter II and VI).

Another river valley similar to that of the Kaleh-Sorkh, which shows an informative cross-section normal to the fault traces was found 60 km east of Torbat-e-Heidarieh, north of Fath-Abad. There the main fault system also shows a high angle reverse movement.

Younger generations of faults in this area pass through the plain 2 km to the south and strike parallel to the older ones. Although it is difficult to distinguish their trend in the cultivated lands, the multiplication of normally single and linear ghanats

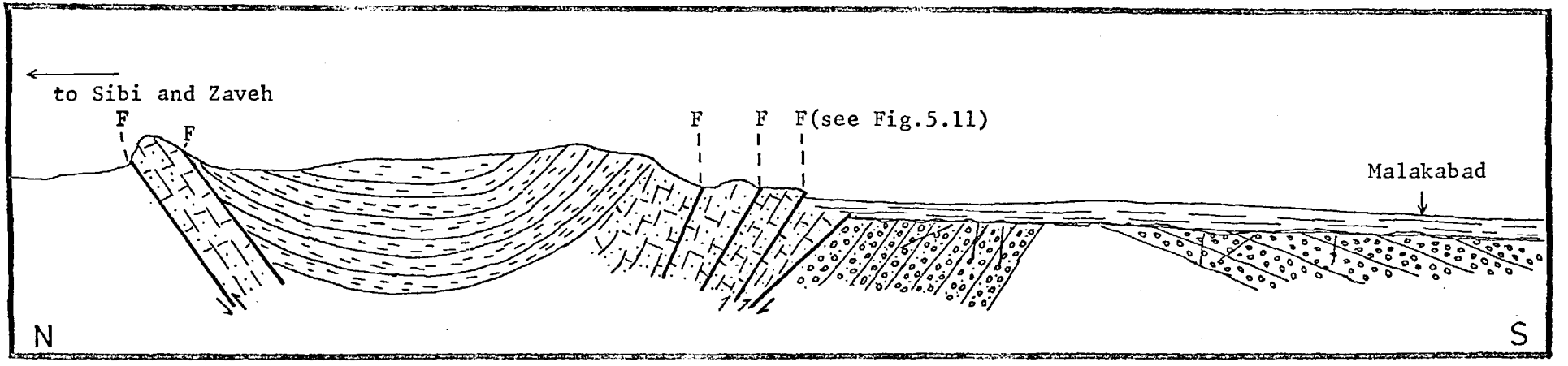



Fig. 5.12. Schematic cross section in the Kaleh Sorkh river valley.

LEGEND

Late Quaternary to Sub-Recent river terraces.

Early Quaternary alluvial deposites.

Paleogene thin bedded fine grain Sandstone.

Paleogene Green Tuffs.

N



S

Fig. 5.13. The high angle reverse fault, dipping to the south, which marks the northern limb of the Kaleh Sorkh syncline(15 Km east of Torbat-e-Heidarieh).

(traditional Persian underground irrigation systems which are connected to the surface through several vertical wells) at certain areas might signify fault zones. Also, it was evident on the 1:55,000 scale aerial photographs that there was a sudden bend of the ghanat lines when they reached that particular locality. Connecting the disturbed zone along all the ghanat lines resulted in a trend which coincided with a faint light coloured band noticeable on the aerial photographs. Local villagers complain of water supply interruptions from the ghanats, and their frequent repairs of the tunnels in the zone suggest either the existence of a narrow band of crushed and altered rocks along a fault trace which is susceptible to frequent collapses due to seasonal variations of climate and water flowage, or that rapid creep is taking place along this zone. The truth must be discovered by geodetic measurement.

## 5.4 Strike of the Great Kavir Fault

The abrupt changes in the strike of this fault system have hitherto been unexplained. These occur at Bardaskan, where the strike changes from NE-SW to E-W, and 200 kilometers further east at Rushtkhar, where it changes from E-W to WNW-ESE at which direction it continues eastwards (Figure 5.14).

Even if the above-mentioned trends had formed a single system in older geological time, they now seem to be dissociated and are probably displaced by various amounts where the sharp bending occurs.

## 5.5 The observed trend on the satellite imageries

There is an unmistakeable NE trend clearly visible on the ERTS-1 photographs which relates to the western section of the Great Kavir Fault and continues straight from central Dasht-e-Kavir through the village of Doruneh to Taknar, and finally bends eastward to Asadabad, a branch of which runs almost E-W about 40 km north of Kashmar (Kariz Fault), and is thought to be associated with a magnitude 5.5 earthquake in 1971 (see Chapter IV). The other E-W running fault system, corresponding to the eastern section of the Great Kavir Fault, meets the previous trend in a complicated pattern of N-S and NNW-SSE striking faults which are evident on both the aerial and the satellite photographs. This zone probably signifies an area of intense activity transitional between the two different systems of active faulting.

## 5.6 Evidence on a fossil Plate boundary

The NE-SW running fault system of the western Doruneh is associated with ophiolite bands (Eftekhar-Nezhad, 1973) which are generally thought to indicate the emplacement of an oceanic crust between two accreting continental plates (Ringwood, 1968, Takin, 1972). This band of contrasting ultrabasic material is lacking along the E-W striking section. This might suggest that the two fault systems have been disconnected at least since upper Cretaceous time when the ultrabasic material was emplaced in this area (Eftekhar-Nezhad 1974).

It is also suggested that such lines of active tectonics along which plate convergence has occurred might continue actively for quite a long time before becoming fossilised. Thus, if the ophiolite bands represent ancient plate boundaries a higher probability of continued activity could be expected from the western section than from the eastern part of this fault.

## 5.7 Discussion and Conclusion

The above-mentioned lines of evidence might indicate two identical and separable system of faultings such as the eastern and western Great Kavir Fault systems,with a trasitional zone at the middle (the area between Kashmar and Bardaskan). This inference, as already discussed, mainly relies on the changes in the pattern of faulting and the variations in sense of relative motion in these two sections.

Predominant sets of sub-parallel reverse faults, dipping opposite to each other (see Section 5.3.4, Figure 5.12), and vertical movement in the eastern part,manifests a regime of major horizontal compression which has been active and could have caused a general crustal shortening in the area, whereas the western ENE-WSW striking fault system shows a prevailing left-lateral shear movement (Section 5.3.3). Nevertheless, a single system of NE-SW compression could readily give rise to both of the observed senses of motion and, therefore, the whole deformation in this area could be considered

Fig. 5.14. A general NE directed compression in eastern Iran (also confirmed by pattern of faulting at N34E, as is discussed in Section 6.2) can be resolved into the normal stress and the shear stress acting on different segments of the Great Kavir (Dorumeh) Fault. In the western part, a b c, the normal stress is less than the shear stress ( $\tau > \sigma_n$ ) a left-lateral shear movement is the main component here, where as in the eastern part, b d, where shear stress is smaller ( $\tau' < \sigma_n'$ ) the dominant sense of movement is vertical.

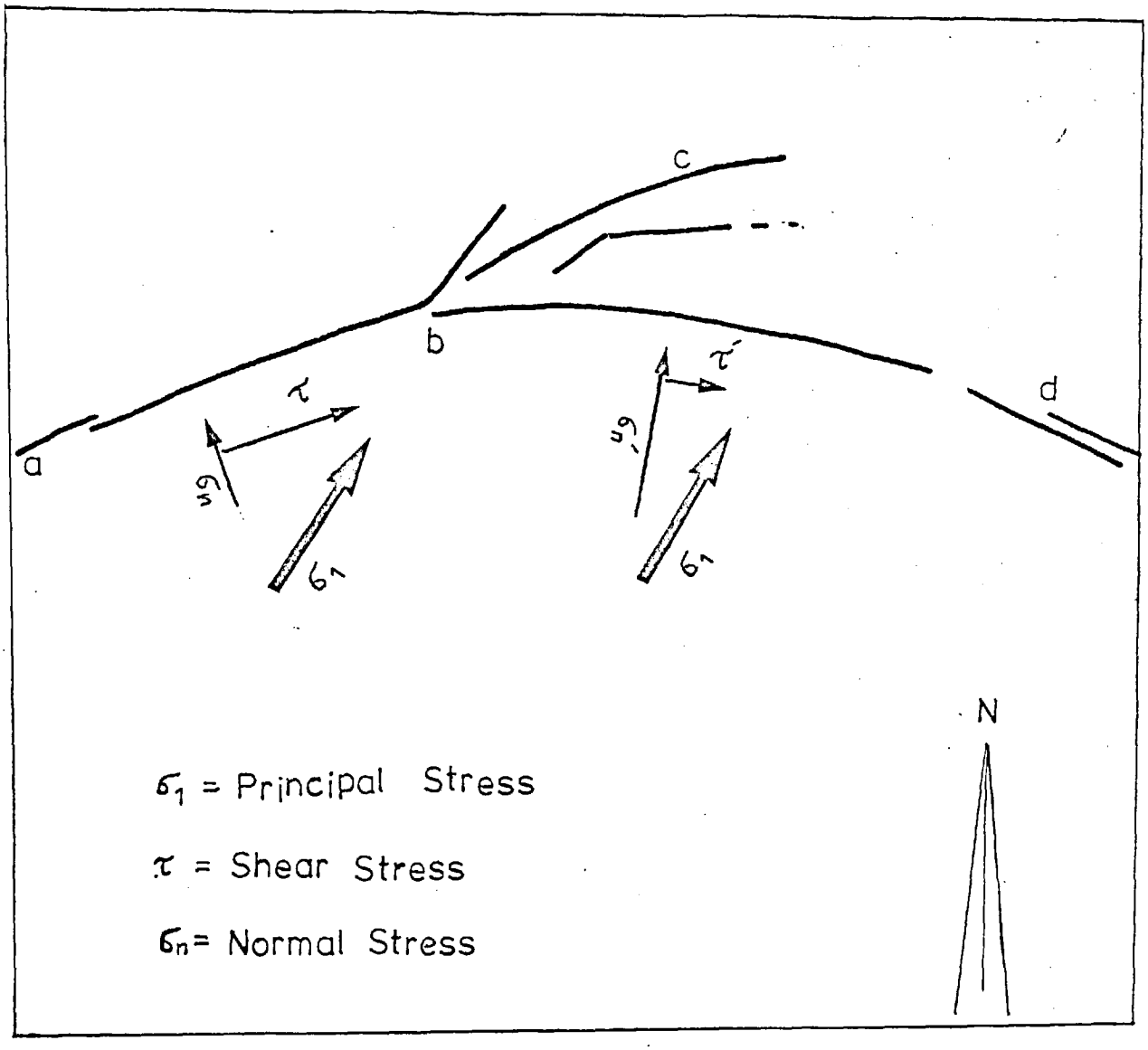

c
b
a
d
τ
σn
σ1
τ'
σn'
σ1'
N
σ1 = Principal Stress
τ = Shear Stress
σn = Normal Stress

Fig. 5.14.

as part of a unified stress system.

The general compression in this area is represented as a vector directed NE. By resolving it into two components, parallel and normal to the fault trace respectively, it is shown in Figure (5.14) that the sinistral shear component is much larger in the western section than in the eastern section of the fault, where the normal component has a larger value.

# CHAPTER VI

# DISCUSSIONS AND CONCLUSIONS

## 6.1 Reflection on the rigidity of the Lut Block

The east Iranian tectonic problem has been a matter of controversy for many years. Suggestions have been put forward as to why the structural trends of this part of Iran should be taken as indicating a separate and identifiable unit related to the prevailing tectonic regime in other parts of Iran (vid. Tectonic Map of Iran 1973; Gansser 1955; Stocklin 1968; Crawford 1972). These suggestions are more justified when examining the satellite photographs of the whole of Iran, in which the two main trends of the Elburz and Zagros at the north and the south-west of the country, respectively, seem to show different geomorphic features from the east Iranian structural trends. There are also differences in the Neotectonic models recently proposed by Nowroozi (1972) and McKenzie (1972) for this area, an account of which is given in Chapter I, and an attempt has been made in this thesis to arrive at a unifying model,at least for the recent and contemporary crustal deformation in eastern Iran.

The eastern part of central Iran is divided into two parts, a western stable part called the Lut Block, and a strongly folded eastern part which belongs to the larger system of the East-Iranian

ranges (also see Chapter II). The concept of a rigid Lut Block was originally developed by Stocklin et al., (1965) from their observations, in the Tabas-Ferdous area, of a contrast between the narrow fold and thrust structures of the Shotori range and the simple pattern of the structures in the adjoining area. According to Stocklin (1968) the Lut Block is an irregularly outlined, essentially north-south trending, rigid mass, smoothly surrounded by the ranges of central and eastern Iran. The remarkable north-south trend of the bordering ranges was apparently enforced by the rigid block. On the north, the Nayband Fault and the Shotori range split the block in two fractions, the Lut Block proper on the east and the Tabas Block on the west. The Shotori range is a part of eastern central Iran, with a nearly NNW-SSE to N-S trend (see Chapter II). Stocklin et al., (1965, 1972) suggested that the Shotori range appears as a cicatrice-like, fault bounded, strongly tectonized and uplifted feature between two regions of considerable rigidity.

Stocklin's definition of the Lut and Tabas rigid blocks (with low intensity of deformation) applied especially to the western part of the Lut with its widespread Tertiary volcanic formations, whereas, farther east, where Mesozoic formations occupy larger areas, the distinction between "low" and "high" degrees of deformation becomes rather vague.

Mohajer-Ashjai et al. (in press) have questioned the rigidity of the Lut Block in the light of a detailed study of satellite photographs aided by some field observations and other geophysical

evidence. As they pointed out, there are several major dislocations cutting through this proposed rigid block (Figure 6.1). This could be explained either by subdividing the Lut Block into many smaller rigid blocks, or by allowing for some internal deformation and dislocations within the Lut Block itself, which contradicts the basic assumption of its rigidity. Further north, east of the Nimblock Valley (Dasht-e-Bayaz area), the layered and folded early Paleogene extrusives are strongly refolded (Behzadi 1972). In the same area there are also paleogene extrusives without layering, which naturally could not represent the deformational features as clearly as the layered and folded rocks. However, they are extensively faulted, and this is thought to be related to the massive nature of these extrusive bodies. Similar massive rock types with extensive internal faulting and lack of folding are found in the Central Lut area (Stocklin et al. 1972). The same characteristics of the volcanic rocks have been observed for most parts of the Lut Block on the satellite photographs. Therefore, this apparent common deformational feature in the Lut area is not necessarily an indication of its rigidity, as has been proposed before (Stocklin et al. 1965; Stocklin 1968).

Other factors which cast doubt on the concept of rigidity of the Lut Block are the occurrence of numerous Quaternary volcanoes, and the internal seismicity of the area (Figure 6.4). There are over 50 tiny Quaternary volcanoes composed of pyroxene andesite in the northern Lut (Stocklin and Nabavi 1971) which have cut their way through the block and coincide with a north-striking zone of high

# NEOTECTONIC MAP OF EASTERN IRAN

N.B. Faults traced from ERTS-1 photographs & G.S.I. 1973 Tectonic map of Iran

By. A. Mohajer-Ashjai (1974)

0 100 km.
Approx. Scale

## KEY

- Neogene Foldings
- N — Taken from N.I.O.C. Geological Map 1957
- G — Taken from G.S.I. Geological Report
- S — Based on the ERTS-1 satellite photographs
- Direction of maximum horizontal shortening deduced from Neogene axes of folding
- Horizontal Component of the slip vector based on the focal mechanism of earthquakes
- Sense of relative horizontal movement
- Quaternary volcanoes
- Horizontal Component of the Compressional axis based on the focal mechanism of earthquakes
- Horizontal Component of the Compressional axis based on the geodetic measurements
- Generalized Compressive direction based on the pattern of the Quaternary faulting
- Fault active during Quaternary
- Fault trace ---- Uncertainty
- High angle reverse fault
- + − Vertical movement; up, down

seismicity (Nowroozi 1971). The magnitude 7.3 Dasht-e-Bayaz earthquake occurred in the northern Lut in 1968 (Ambraseys and Tchalenko 1969; Niazi 1969). There have been other large to moderate size earthquakes in central Lut since 1900 (Nowroozi 1971, Nabavi 1972 and see also Figure 6.4). Berberian (1973) has also presented some geological evidence questioning the rigidity of the Lut Block in earlier times.

These findings and the ERTS-1 observations presented by Mohajer-Ashjai et al., modify the original concept of the earlier authors and indicate that the Lut Block should not be considered as a rigid unity. This new argument could, in some ways, affect the interpretations of other authors who have based parts of their inferences on the proposed rigid Lut Block (Takin 1972; Crawford 1972; Nowroozi 1972 and Dewey 1973).

## 6.2 Dislocation theory and analysis of aftershocks in eastern Iran

As has been explained in Chapter IV, the high level of activity in the Dasht-e-Bayaz and N. Kashmar areas might be related to the late aftershocks phase of the large 1968 and 1971 earthquakes. If this is true, the following is an attempt to find some explanation regarding a few associated phenomena of these aftershocks, such as their distribution and mechanism.

Major shallow earthquakes are normally followed by aftershocks. Several papers deal with the aftershocks, but most of them are

concerned with the phenomenological side of the problem and only few authors have attempted explanations. Some of the early work on this subject belongs to Benioff (1951), Benioff and Gutenberg (1951) and Bath and Benioff (1958), who relate aftershocks to an elastic creep of the medium. Assumptions of this model were criticised by Richter (1958), Bath and Duda (1964) and Sykes (1966). Besides, the above model does not explain the space distribution and fault-plane solutions of aftershocks. Later, Mogi (1962; 1963) and Scholz (1968) presented another approach to aftershock investigation through laboratory experiments on the deformation of brittle solid samples. According to Rybicki (1973) Mogi's and Scholz's analysis lacks a detailed and conveincing physio-mathematical explanation for the aftershock process, and therefore, should be treated as the first step towards better knowledge of this phenomenon. Recently, Chinnery and Rodgers (1968) and Rybicki (1973) have utilized the dislocation theory to analyse the processes taking place in the source area of major shocks. This new hypothesis suggests that aftershocks are generated as a result of the action of stresses created in the medium after the main rupturing, on inhomogeneities existing in the medium. Some of these inhomogeneities can be described by means of physical dislocations or internal cracks. Intrusions, material failures, changes in internal structure and contacts between different media are examples of inhomogeneities which form additional local stress concentrations and subsequently are related to spatial distribution of aftershocks.

Different mathematical models based on dislocation theory have been developed and discussed by Chinnery (1961, 1963, 1964, 1969) and Rybicki (1973) to show stress trajectories associated with different dislocation geometry. A common conclusion based on different

models examined is that there is a concentration of stresses near the edges of the main crack (e.g. Figures 6.2, 6.3). Another important concentration of stress field might be produced by the swing of a fault, as shown in Figure (6.3).

If all the assumptions of the above hypothesis are true for the large scale dislocations of the earth's crust, then the greatest probability of aftershock generation should obviously be expected in the regions of concentration of stresses associated with a main-shock fault.

The high rate of microearthquake activity found at each end of the 1968 Dasht-e-Bayaz Fault, which (see Chapter IV) is thought to represent the late aftershock phase of that earthquake, is fully compatible with the latest hypothesis based on dislocation theory. Also, in the N. Kashmar region, where a complex pattern of faulting prevails (mostly changing direction from a NE to almost E-W direction) microearthquakes are very frequent, also in accordance with this hypothesis.

Furthermore, this hypothesis suggests that a negative stress concentration close to the edge of a fault is to be expected after the mainshock has occurred and that the new stress field might result an aftershock phase with a different fault plane solution (or CFPS) than that of the main shock.

Two composite fault plane solutions are presented in Chapter IV, one of which (in the Daht-e-Bayaz area) reveals a similar solution

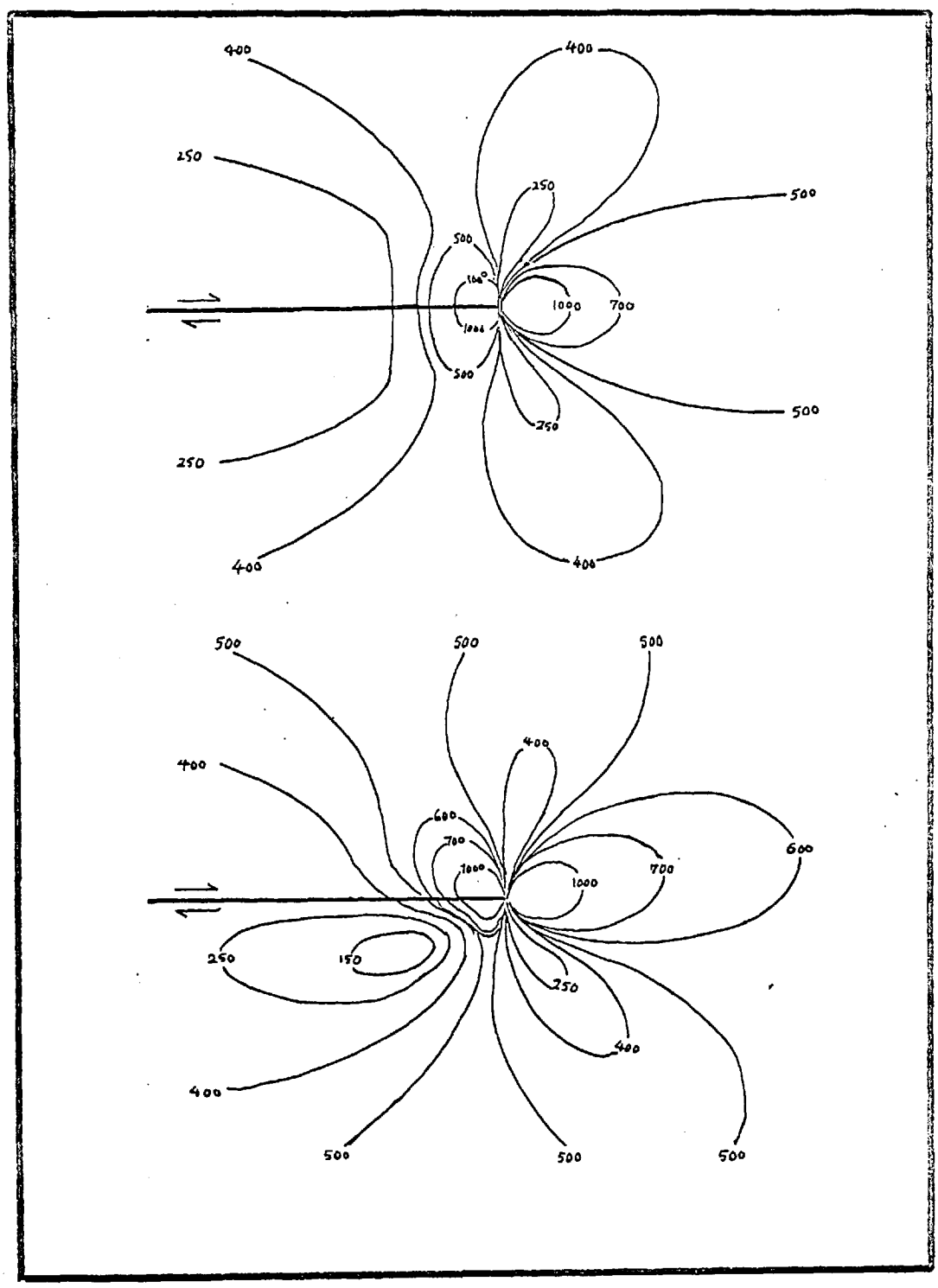



Fig. 6.2. Contours of equal maximum shear stress at the ground surface near the end of a fault, after faulting has occurred: above, for faulting under pure shear and below, for faulting under a uniaxial compression. (after Chinnery, 1966)

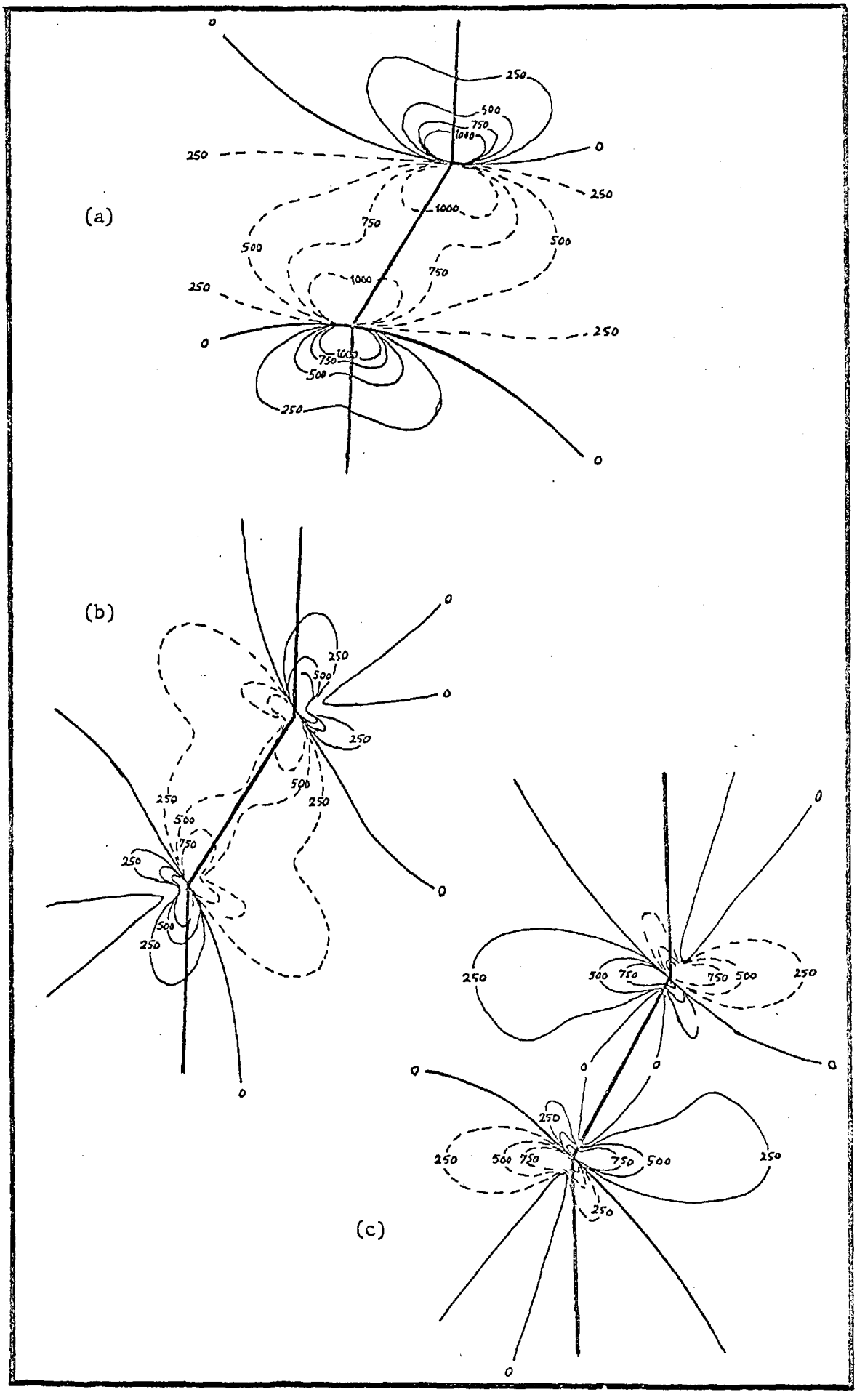



Fig. 6.3. (a) Contour lines of equal stresses $S_{11}$ in a fault swing model, (b) $S_{22}$ stress trajectories of the same model and (c) contour lines of equal shear stresses $S_{12}$ of the fault swing model. (after Rybicki, 1973)

to the main 1968 shock, showing strike slip mechanism with two nearly vertical nodal planes trending N-S and E-W (Figure 4.19). The N. Kashmar CFPS, however, revealed a completely different mechanism from the larger 1971 shock to the west of the area. The explanation of the above discrepancy must await further research though it may be connected with the negative stress concentration mentioned above. Other work however, has attempted to show how other theories, particularly that of dilatancy, can explain the differences between main shock and late aftershock mechanisms (Evison and Robinson 1973).

## 6.3 Significance of the observed low b values in the area

As demonstrated in Section 4.6, all the recurrence curves obtained for different localities in the area under study, and their combinations, revealed conspicuous low b values, which can be interpretated in the light of experimental work in laboratories and through comparison with observational data in other parts of the world.

It has been demonstrated by Mogi (1961, 1962a, 1962b, 1963) that during the deformation of rock in laboratory experiments there are striking similarities between the statistics of the microfracturing events observed and those of earthquakes. In the light of this observation, he suggested that rock deformation is a scale model of crustal deformation and interpreted his results accordingly. Scholz (1968) found small cracking events, i.e. microfractures, occur in rock specimens which radiate elastic waves in a manner similar to earthquakes. He detected these radiations during uniaxial and

triaxial compression tests and has shown that their frequency-magnitude relation obeys the Gutenberg and Richter relation of Log N = a + bm.

This analysis not only demonstrates the similarity between rock deformation experiments in the laboratory and deformation of the crust, but has also been used to infer the condition under which different b values are obtained. As a result, the dependence of the parameter b on rock type, stress and confining pressure was studied. It was found to depend primarily on stress, in a characteristic way. The frequency-magnitude relation for microfracturing events accompanying frictional sliding and deformations of a ductile rock was found to have a much higher b value than that observed for brittle rock.

It was further discovered that the state of stress, rather than the heterogeneity of the material, plays the most important role in determining the value of b. The b value for earthquakes has been extensively studied and has been found to be characteristic of the seismicity within a given region. Consequently, regional variations of b may reflect variations of the state of stress.

Sykes (1970) has determined the b values for two large earthquake swarms detected from the mid-Atlantic ridge. In both cases the b value was about 1.3 (relatively high) and concluded that along rift zones, where the temperature is high, earthquakes occur largely as cataclastic deformation with a high b value.

By analogy with results from the micro-fracturing experiments of Scholz (1968a, b), the low b values (about 0.5, see Section 4.6) found in the northern Lut Zone would signify a typical brittle fracturing under high level of stresses. This seismicity and deformational characteristic is identically different from the areas along creeping plate boundaries,where the occurrence of a large number of small shocks is responsible for most of the strain release so that larger magnitude earthquakes are rare.

Isacks and Oliver (1964) have shown the low level of activity around New York relative to that of a major plate boundary, such as the San Andreas Fault in California. Another example of intraplate low seismicity with a b value in the order of 0.6 (low) is presented by Lammlein et al. (1971) from south-eastern Missouri.

The above interpretation of the regional microseismicity of eastern Iran is in a good agreement with other inferences of this thesis (Sections 6.1 and 6.4), regarding the difficulties of applying microplate tectonic theories in this area. These low b values simply reject the possibility that either the Great Kavir or the Dasht-e-Bayaz Faults act as boundaries between two rigid plates in the way suggested by Nowroozi (1972).

## 6.4 A new interpretation of the seismicity of Eastern Iran

Figure 6.4 is a map of the East-Iranian region on which the epicentres (from both instrumental and macroseismic determinations) of all earthquakes, for which information is available, which have

occurred in the past 1100 years are plotted. Several different sources have been used in compiling this map (Nabavi 1972; Nowroozi 1971; Berberian 1971, 1972, 1973).

Even allowing for considerable uncertainty in the macroseismic and early instrumental locations it must still be apparent from the distribution of epicentres that there are no well defined axes of activity in the region, and that no one fault or fault system can be said to have been responsible for the activity. This, of course, is totally at variance with either the plate or microplate tectonic models proposed for the area (see Chapter I), both of which would require the seismicity to be well defined by narrow zones.

However, inspection of the seismicity map does suggest some areas where clusters of activity have occurred. Such clusters (centred at Lat. 30 N. Long. 57.7 E; Lat. 34 N. Long. 59 E; Lat. 35.2 N, Long. 58 E) seem to be associated with areas of complicated tectonics, where two or more major structural trends intersect. Such areas will be called tectonic knots.

Thus it is proposed that the current and historical seismicity of the region (at least from present data) is governed by these tectonic knots.

Another feature of the historical seismicity of the region (which is not apparent from Figure 6.4) is its temporal distribution.

Fig. 6.4. Seismicity of eastern Iran, based on macroseismic and microseismic information from 643 AD to 1974. Sources are Ambraseys 1961; Nowroozi 1971; Nabavi 1972 and newspaper clippings compiled by M. Berberian as internal reports of the Geological Survey of Iran since 1971.

LEGEND

◇ ○ ∘ ∘ Earthquake $M>7$, $6<M<7$, $5<M<6$ and $M<5$ respectively.

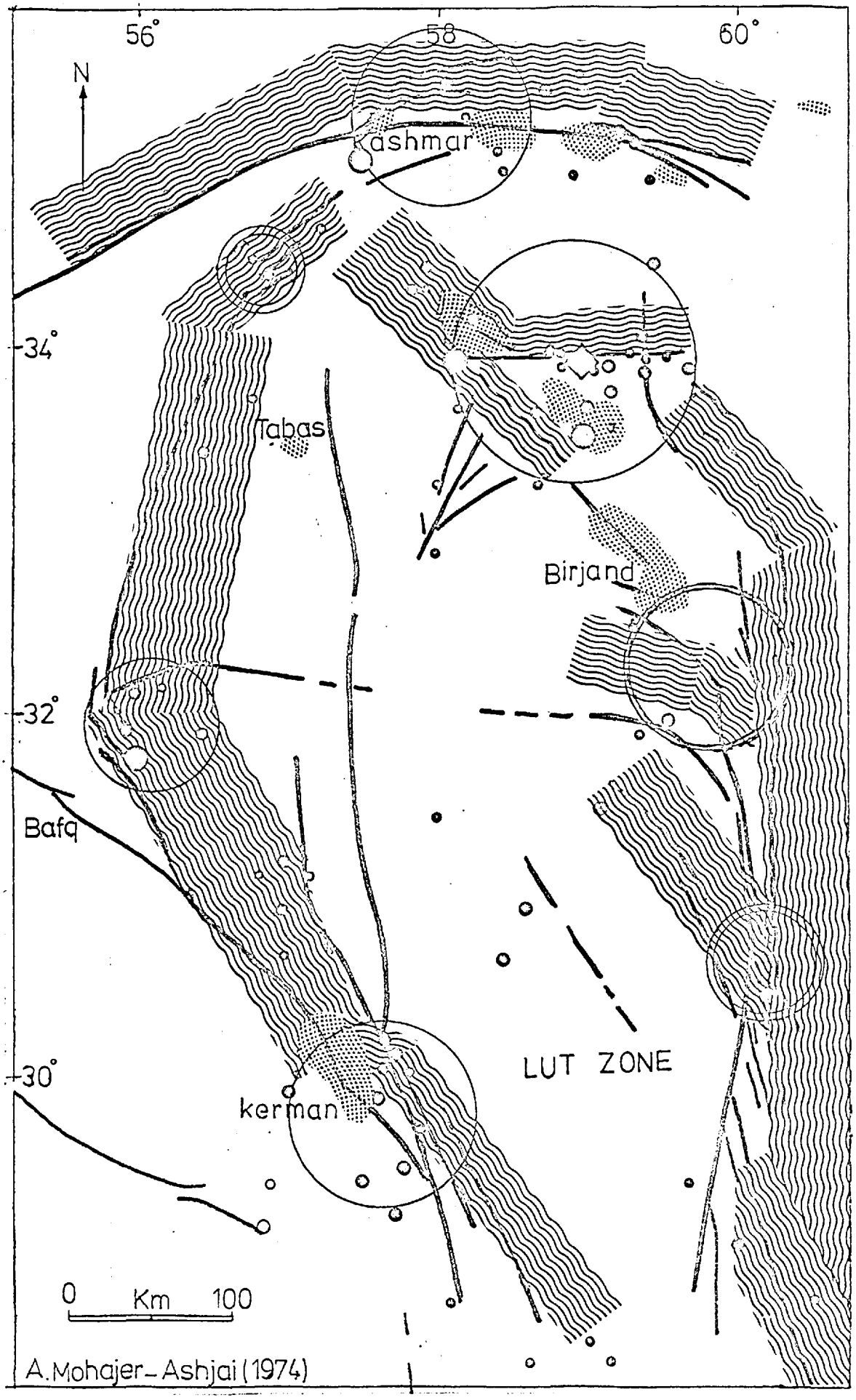
Extent of historical earthquakes or felt and reported shocks in recent years.

Fault trace based on the Tectonic Map of Iran G.S. . 1973 and satellite photographs.

Major structural trends, mostly axes of large scale folding.

A single circle signifies main tectonic knots (where several structural units meet) associated with large number of major earthquakes.

Double circles signify areas of potential future large shocks.


56°
58
60°
N
ashmar
34°
Tabas
Birjand
32°
Bafq
30°
kerman
LUT ZONE
0 Km 100
A. Mohajer-Ashjai (1974)

Certainly in recent years (and allowing for the incompleteness of the data, probably for much longer too) earthquakes have been infrequent and large, with fairly long intervals of complete quiescence between them. A good illustration of this is the record for this century: 1909 Turshiz; 1923 Torbat-e-Heidarieh and 1968 Dasht-e-Bayaz earthquakes. Such behaviour is, of course, indicative of low b values in the recurrence curves (frequency versus magnitude relationship).

Here it should be recalled that one of the most interesting findings of the microearthquake surveys described in Chapter IV was that the only areas of activity found both showed very low b values, just as is indicated by the record of the large earthquakes.

Possible reasons for low b values were discussed earlier in this Chapter, but it is perhaps worth pointing out that in a region such as eastern Iran, whose tectonics are undoubtedly governed mainly by compression and where much of the faulting contains at least a certain degree of thrusting (or reverse faulting), the friction forces acting on a fault are likely to be large in comparison with some other areas. Among such other areas might be mentioned the San Andreas Fault zone in California (with b values ranging from 0.8 to 1) or the Zagros region of south-west Iran where activity is more or less continuous and b values are conspicuously higher, in the order of 1.4 (Evernden 1970) (the Zagros area have been moving as a major dextral shear zone according to recent suggestions of Tchalenko et al. (1974) and Houshmand Zōdeh, personal communication).

The last feature of the seismicity of the area which is indicated by this study is the total lack of any area of high micro-earthquake activity which is not very probably related to an aftershock sequence. (In Chapter IV two regions of high micro-earthquake activity were described, both of which were related to at least intermediate sized earthquakes). In this respect too, the eastern Iranian regionis very different from the California San Andreas (central) area, where there is always a moderately high background level of microearthquake activity associated with continuous creep on the active faults. It thus seems possible to rule out such creep as a mechanism of strain release in this region of Iran, perhaps another indication of high friction on the faults.

It is worth finishing this section with a discussion of the influence of what has been said of the seismicity on the possibility of predicting major earthquakes in this area.

Firstly, it seems that tectonic knots are likely to be centres of future activity. Secondly, the high friction proposed for the region suggests that strain may accumulate to fairly high values before a major earthquake.

Thus it seems that an earthquake prediction programme could be sensibly based on vertical and horizontal strain measurements in areas of tectonic knots.

## 6.5 Variation of the maximum horizontal shortening and recent crustal deformation in eastern Iran

The structural analysis of the major tectonic features and the inference of their general strain pattern presented here is based on the interpretation of the fold axes, thrusting trends, conjugate shear faults, and shear and tension joints pattern. This analysis was carried out wherever possible on the basis of field observation, or directly inferred from the ERTS-1 photographs. As demonstrated in Figures (6.1), it allows us to reconstruct the generalized direction of the maximum crustal shortening for the area under study in pre-Neogene and post-Neogene times.

It is widely assumed (Lensen 1960 and Pavoni 1971) that these shortening directions coincide in principle with the direction of maximum horizontal pressure. The radial pattern of these axes in the northern part of the area under study in Pre-Neogene times is difficult to explain with the presently available geological information. However, several possibilities exist. They might signify the existence of several small blocks which have enforced their curved marginal configuration into the more deformable surrounding rocks. Another possibility might be a large system of parallel strike slip faults with different strain rates along their path. This could give rise to a curvature in the fault's strike which might subsequently bend other structural features running along its trace. An example of this type of development at the ends of major strike slip faults is given by Freund (1974).

In contrast to the pre-Neogene compressive directions in eastern Iran, the post-Neogene directions, particularly the Quaternary and Recent compression, are fairly consistent throughout the area, between NE-SW and NNE-SSW (Figure 6.1). This inference relies mainly on the following three lines of evidence:

a. The direction of maximum horizontal compression is taken perpendicular to the axis of normal Neogene folds. For en-echelon folds the criteria reviewed by Wilcox et al. (1973) was considered when drawing the compressive direction. Age of the rock formation is assigned on the basis of the N.I.O.C. Geological Map (1959) and the available geological maps published by G.S.I., and the fold axes are mostly traced from the ERTS-1 photographs.

b. The pattern of the Quaternary and Recent fault scarps, as summarized in Table 1 and shown in a circular diagram (top left of Figure 6.1), indicates that the major wrench faults striking N-S and N70$^{o}$E are dominant and could be considered as a set of conjugate first order faulting relative to the other trends. The angular relationship between first order and second order faulting with their subsequent folding and thrusting is suggested by Moody and Hill (1956) and Moody (1973). The pattern of east Iranian recent faults implies a general N35$^{o}$E compression, which is in full accord with the available sense of fault movements and trends of post-Neogene folds (at the top left of Figure 6.1).

c. There are eight reliable fault-plane solutions in the area covered by Figure 6.1, all taken from Nowroozi (1972) and Niazi (1969),

TABLE 1

Summary of the Nature of Movements Along the East-Iranian Major Faults

| Name of the Fault | General Trend | Sense of Movement | Quaternary & Recent Activity | Source |
|---|---|---|---|---|
| The Great Kavir (Doruneh) | E-W & ENE-WSW | N<br>R | S<br>N<br>D<br>R | Wellman (1966) Tchalenko et al. (1973), Mohajer-Ashjai (1974) |
| Dasht-e-Bayaz (Ferdows) | E-W | S<br>RT | S<br>1968 EQ | B.S.S.A.(1969) 59. 1751-1843 Behzadi (1972) Berberian (1973) |
| Eastern Neh | N-S | R | R<br>D | Berberian 1973 |
| Western Neh | N-S | R | R<br>D | Berberian 1973 |
| Nayband | N-S | D<br>N | D<br>N | Wellman 1966 Stocklin et al. (1965) |
| Sarvestan | NNW-SSE | D<br>N | D<br>N | Dimitrijevic (1973) |
| Kuh Banan | NW-SE | D<br>R | D<br>R | Huckride et al. 1962 Wellman 1966 |
| Chah Sorb | NNE-SSW | T<br>D | D | Rutner 1968 |
| Jabbar | N-S | D | D<br>CPM | Behzadi 1972 McEvilly & Niazi in press |
| Asadabad | NE-SW & E-W | R | S<br>R<br>FPS | Mohajer-Ashjai (1974) |

N = Normal Fault
R = Reverse Fault
S = Left-Lateral
RT = Rotational Fault
T = Thrust Fault
D = Right-lateral
FPS = Fault Plane Solution
CPM = Creepmeter
EQ = Earthquake

except for a solution showing a thrust mechanism with a left-lateral component, which belongs to a shock north of Kashmar in 1971 (McKenzie, personal communication). The inferred slip vectors of these shocks are consistent with a NE to NNE direction of movement, with one exception, the Dasht-e-Bayaz main shock, which shows a slip vector oriented toward the west. Niazi (1969) presented several lines of evidence on the complexity of the source mechanism of the Dasht-e-Bayaz earthquake and has suggested a multiple source for this shock, which might have some bearings on the observed slip vector. Other than that, the uniform slip throughout eastern Iran, and in particular across the major dislocations such as the Great Kavir (Doruneh) and the Kuh Banan Faults is remarkable, and supports the concept of continuum media subjected to a NE compression in eastern Iran, as proposed here.

Inaccuracies in the determination of the stress field based on the focal mechanism of earthquakes have been discussed by McKenzie (1969), who has shown that a wide range of stress directions could give rise to the same sense of movement on the fault plane. Since the range of possible variation of the azimuths of these directions is always less than $90^{\circ}$, for the purpose of comparison in this study, axes of compressive stress inferred from the fault plane solutions are also presented in Figure (6.1). Considering the limits for dispersion of these axes, a NE direction of compression again seems probable.

Additional evidence for this preferred and presently active direction of compression has recently become available through direct distance measurements across the Dasht-e-Bayaz Fault. Measurements made in 1971, 1972 with a Mekometer (see Chapter III) revealed a N54$^{o}$W extension axis, corresponding to a nearly N36$^{o}$E compression, that is responsible for the observed ENE-WSW running shear movement.

This consistent NE direction suggests that the forces acting in east central Iran have been distributed almost uniformly throughout the area in recent times, and that the localized variation of some compressive directions, such as around Tabas, might have been imposed by relatively small scale rigid masses in a matrix of more deformable rocks.

This idea disagrees with the existence of a large Lut Block or Lut Plate, proposed by other investigators and discussed earlier. On the other hand, it does not rule out the possibility of several other small rigid units, such as the Tabas Block or fractions of the former Lut Block, which might not change the overall picture of a continuum deformation in east central Iran.

The success of plate tectonics in explaining the geological features of oceanic areas has motivated many research workers to extend the concept to continental areas. But if we are obliged to consider a large number of independent plates such as in Iran, then it becomes rather difficult to explain many features associated with their relative movements, and in particular their driving mechanism.

It is customary to assess the rate and direction of relative motion between major plates by interpretation of magnetic anomaly patterns (Pitman, Talwani and Heirtzler 1971; McKenzie and Sclater 1971). The motion between Eurasia and Arabia is estimated by McKenzie (1972) to be in the order of 5 cm per year in a NNE direction.

The data derived from the magnetic strip anomalies also suggest that the rate and direction of this motion has remained almost constant at least for the past 10 m.y. This direction is in accord with the inferred direction of maximum horizontal compression based on the geomorphic and geological and seismological data presented here for eastern Iran since Neogene time. Tchalenko et al. (1974) have also suggested that a NNE compression would best fit their observed three fractures, which are related to historical earthquakes in different parts of Iran.

# CHAPTER VII

## SUMMARY OF THE CONCLUSIONS, AND SUGGESTIONS FOR FURTHER STUDY

### 7.1 Conclusions

The central part of eastern Iran has been studied to investigate the neotectonics of a region where mountain building is at present taking place, with a view to testing the applicability of the recently proposed microplate concept to explain crustal deformation in this area. This work involved measuring strain and slip using the Mekometer, microearthquake studies by three portable high gain short period smoked paper seismographs, and detailed mapping of the faults and fractures, in conjunction with geomorphic field studies, from which the following conclusions were reached:

1. The part of eastern Iran which is the subject of this thesis is an area of high stress, and differs from areas of rapid creep, such as in California and on boundaries between rigid plates on which differential movement is taking place with association of numerous small to moderate magnitude shocks. This conclusion is based principally on the nature of the seismic activity occurring on the active faults.

Microearthquake activity, exceeding 15 events per day, is currently occurring near the ends of the Dasht-e-Bayaz Fault, which was also responsible for the magnitude 7.3 shock in 1968, and in an area about 40km north of Kashmar on a newly found (Kariz) fault, thought to be associated with a magnitude 5.5 earthquake in 1971. This level of activity appears to be confined to these parts only of the respective faults and does not represent the general level of background activity on them. This suggests that the microearthquakes represent after-shock phases of the 1968 and 1971 major shocks, a conclusion which is compatible with the dislocation theory model regarding the localized stress concentrations due to fault movement.

By analogy with experimental studies of rock mechanics and observations in other parts of the world, the low b values (about 0.5) inferred from the magnitude distribution of microearthquakes in this area support the above-mentioned idea and lend additional support to the existence of high stresses in the area. These would be partially relieved locally through the occurrence of large shocks.

2. In contrast to the continuous seismicity of the Zagros area, the seismicity of eastern Iran seems to be sporadic and mostly associated with places where two or several major structural features meet or cross each other (tectonic knots).

3. Along the Dasht-e-Bayaz Fault, an elastic rebound type of strain release is taking place presently. This conclusion is based on the strain and slip measurements made with the mekometer in 1971, 1972 and 1974. The complicated pattern of strain variations in the periods 1971 to 1972 and 1972 to 1974, which are mostly in a reverse sense to that of 1971 to 1972, might have alternatively been caused by relaxation of dominant compressive stresses in a NE-SW direction.

4. The Great Kavir (Dorumeh) Fault is divided into two segments with a transitional area in between, on the bases of detailed 1:55,000 mapping of the aerial photographs and field studies. The western segment is a sinistral wrench fault, whereas the eastern part has moved in the form of a high angle reverse fault. Nevertheless, a single system of uniaxial compression oriented NE-SW could give rise to both observed senses of movement along this fault.

5. With reference to the tectonic map of Iran, the fault trends observed on the satellite photographs and field studies, the angular relationship of the recent fault traces in eastern Iran, together with their sense of movements, again imply a NE-SW (N34E) direction of compression, which is consistant with the axes of Neogene foldings and focal mechanism solutions of earthquakes in this area. This observation also suggests an almost uniform distribution of recent

deformational features across the major structural units and throws doubt on the suggested rigidity of the Lut Block, at least since Neogene time. This lack of rigidity in the Lut Block also directly challenges the microplate concept as an explanation of recent and contemporary crustal deformation in eastern Iran.

## 7.2 Suggestions for further studies

Although long period observation is required to illustrate the contemporary deformation taking place in the earth's crust, the systematic and combined approach presented in this study could serve as a means for quick assessment of the neotectonic development in an area and, therefore, should be extended to other parts of Iran in order to investigate the common characteristics of deformations, their differences, and in particular the mechanisms giving rise to them. Such studies are not only essential to pave the way toward substantiating a thorough programme of earthquake prediction, but are also crucial for a realistic evaluation of seismic hazards in regions of potential population growth, or areas proposed to construction of heavy industries, dams or atomic power plants, which could involve the risk of loss of life and capital.

If there is a true spatial connection between the tectonic knots and occurrence of major earthquakes, as discussed in section 6.4, it seems to be sensible and worthwhile to concentrate the

future effort on the areas of potential seismic hazard, the five localities mentioned in section 6.4, and particularly in the three regions centered at Lat. $32^{o}.4$, Long. $59^{o}.7$; Lat. $30^{o}.9$, Long. $60^{o}.0$ and Lat. $34^{o}.3$, Long. $56^{o}.8$. These three regions are classified as tectonic knots but,as far as the available records show, they have not been associated with many large earthquakes previously. Thus it is tentatively suggested here that the unrelieved strain accumulated through a long quiescent period in these regions might give rise to the future major shocks in eastern Iran. The nearest centres of population to the above-mentioned regions are Birjand, Neh, Zahedan, Tabas and Doruneh (see Figure 6.4).

Other geophysical methods such as gravity, magnetic and seismic refraction might be used to obtain details of sub-surface faulting associated with regional seismicity and might provide complementary information which would enable the seismic hazard to be assessed more realistically and contribute to a better understanding of fundamental tectonic relationships.

## APPENDIX I

Three well measured values for $\lambda'$ namely $\lambda'_i$ , $\lambda'_j$ and $\lambda'_k$ making unknown angles of $\theta_i$ , $\theta_j$ and $\theta_k$ with the principal axis of strain ellipse, will produce three equations which can be solved simultaneously by appropriate manipulation. These equations are:

$$\lambda'_i = \lambda'_1 \cos^2\theta_i + \lambda'_2 \sin^2\theta_i$$

$$\lambda'_j = \lambda'_1 \cos^2\theta_j + \lambda'_2 \sin^2\theta_j$$

$$\lambda'_k = \lambda'_1 \cos^2\theta_k + \lambda'_2 \sin\theta_k$$

First, we solve these equations in their general form then we put in the respective values.

Using $\cos^2\theta = 1 - \sin^2\theta$ we have $\lambda'_i = \lambda'_1 (1 - \sin^2\theta_i) + \lambda'_2 \sin^2\theta_i$

then $$\lambda'_i = \sin^2\theta_i (\lambda'_2 - \lambda'_1) + \lambda'_1 \qquad (6)$$

similarly $$\lambda'_j = \sin^2\theta_j (\lambda'_2 - \lambda'_1) + \lambda'_1 \qquad (7)$$

$$\lambda'_k = \sin^2\theta_k (\lambda'_2 - \lambda'_1) + \lambda'_1 \qquad (8)$$

Now from equation (6)

$$\lambda'_2 - \lambda'_1 = \frac{\lambda'_i - \lambda'_1}{\sin^2\theta_i} \qquad (9)$$

Substituting in equations (7) and (8),

$$\lambda'_j = \frac{\sin^2\theta_j (\lambda'_i - \lambda'_1)}{\sin^2\theta_i} + \lambda'_1 \qquad (10)$$

and

$$\lambda'_k = \frac{\sin\theta_k (\lambda'_i - \lambda'_1)}{\sin^2\theta_i} + \lambda'_1 \qquad (11)$$

Rearranging equation (10),

$$\lambda_j' \sin^2\theta_i = \lambda_i' \sin^2\theta_j - \lambda_1' \sin^2\theta_j + \lambda_1' \sin^2\theta_i$$

whence

$$\lambda_1' = \frac{\lambda_j' \sin^2\theta_i - \lambda_i' \sin^2\theta_j}{\sin^2\theta_i - \sin^2\theta_j} \qquad (12)$$

similarly equation (11) leads to

$$\lambda_1' = \frac{\lambda_k' \sin^2\theta_i - \lambda_i' \sin^2\theta_k}{\sin^2\theta_i - \sin^2\theta_k} \qquad (13)$$

equating (12) and (13)

$$\frac{\lambda_j' \sin^2\theta_i - \lambda_i' \sin^2\theta_j}{\sin^2\theta_i - \sin^2\theta_j} = \frac{\lambda_k' \sin^2\theta_i - \lambda_i' \sin^2\theta_k}{\sin^2\theta_i - \sin^2\theta_k}$$

then

$$\lambda_j' \sin^4\theta_i - \lambda_j' \sin^2\theta_i \sin^2\theta_k - \lambda_i' \sin^2\theta_j \sin^2\theta_i + \lambda_i' \sin^2\theta_j \sin^2\theta_k =$$
$$\lambda_k' \sin^4\theta_i - \lambda_k' \sin^2\theta_i \sin^2\theta_j - \lambda_i' \sin^2\theta_k \sin^2\theta_i +$$
$$\lambda_i' \sin^2\theta_k \sin^2\theta_j$$

omitting similar characters from both sides of this equation we end up with

$$\sin^2\theta_i \left[ (\lambda_j' - \lambda_k') \sin^2\theta_i + (\lambda_k' - \lambda_i') \sin^2\theta_j + (\lambda_i' - \lambda_j') \sin^2\theta_k \right] = 0 \qquad (14)$$

we can now solve this equation by reducing the three ($\theta_i$, $\theta_j$ and $\theta_k$) unknowns to one by rewriting them in terms of $\varphi$, the aximuth of the principal axis of the strain ellipse. Thus

$$\theta_i = \varphi - \alpha$$
$$\theta_j = \varphi - \beta$$
$$\theta_k = \varphi - \gamma$$

where $\alpha$, $\beta$ and $\gamma$ are the measured azimuths of $\lambda_i$, $\lambda_j$ and $\lambda_k$, three measured values of the longitudinal strain.

Since one of the solutions of equation (14) is $\sin^2\theta_i = 0$ this means $\varphi - \alpha = 0$ or $\varphi = \alpha$

similarly $\varphi = \beta$ and $\varphi = \gamma$ could be other solutions. Nevertheless,

from these three possibilities we can discard the ones with lower strain values since by definition the principal axis of the strain ellipse must correspond to the solution involving the largest value of strain.

However, the remaining part of equation (14) could be extended with respect to $\varphi$ in the form of

$$(\lambda'_j - \lambda'_k)\sin^2(\varphi-\alpha) + (\lambda'_k - \lambda'_i)\sin^2(\varphi-\beta) + (\lambda'_i - \lambda'_j)\sin^2(\varphi-\gamma) = 0$$

or

$$(\lambda'_j - \lambda'_k)(\sin\varphi\cos\alpha - \cos\varphi\sin\alpha)^2 + (\lambda'_k - \lambda'_i)(\sin\varphi\cos\beta - \cos\varphi\sin\beta)^2 + (\lambda'_i - \lambda'_j)(\sin\varphi\cos\gamma - \cos\varphi\sin\gamma)^2 = 0$$

then

$$(\lambda'_j - \lambda'_k)(\sin^2\varphi\cos^2\alpha + \cos^2\varphi\sin^2\alpha - 2\sin\varphi\cos\varphi\sin\alpha\cos\alpha) + (\lambda'_k - \lambda'_i)(\sin^2\varphi\cos^2\beta + \cos^2\varphi\sin^2\varphi - 2\sin\varphi\cos\varphi\sin\beta\cos\beta) + (\lambda'_i - \lambda'_j)(\sin^2\varphi\cos^2\gamma + \cos^2\varphi\sin^2\gamma - 2\sin\varphi\cos\varphi\sin\gamma\cos\gamma) = 0$$

this simplifies to

$$\sin^2\varphi\left[(\lambda'_j - \lambda'_k)\cos^2\alpha + (\lambda'_k - \lambda'_i)\cos^2\beta + (\lambda'_i - \lambda'_j)\cos^2\gamma\right] + \cos^2\varphi\left[(\lambda'_j - \lambda'_k)\sin^2\alpha + (\lambda'_k - \lambda'_i)\sin^2\beta + (\lambda'_i - \lambda'_j)\sin^2\gamma\right] - 2\sin\varphi\cos\varphi\left[(\lambda'_j - \lambda'_k)\sin\alpha\cos\alpha + (\lambda'_k - \lambda'_i)\sin\beta\cos\beta + (\lambda'_i - \lambda'_j)\sin\gamma\cos\gamma\right] = 0 \quad (15)$$

by accepting common constants such as

$$K = (\lambda'_j - \lambda'_k)\cos^2\alpha + (\lambda'_k - \lambda'_i)\cos^2\beta + (\lambda'_i - \lambda'_j)\cos^2\gamma$$

$$L = (\lambda'_j - \lambda'_k)\sin\alpha\cos\alpha + (\lambda'_k - \lambda'_i)\sin\beta\cos\beta + (\lambda'_i - \lambda'_j)\sin\gamma\cos\gamma$$

$$M = (\lambda'_j - \lambda'_k)\sin^2\alpha + (\lambda'_k - \lambda'_i)\sin^2\beta + (\lambda'_i - \lambda'_j)\sin^2\gamma$$

and by dividing both sides of equation (15) by $\cos^2\phi$ the solution simplifies to

$$K\tan^2\phi - 2L\tan\phi + M = 0 \qquad (16)$$

Using equation (16) and calculating values of K, L and M we have two solutions for $\phi$. Having found the azimuth of the principal axes of the strain ellipse, we proceed to calculate $\theta_i$, $\theta_j$ and $\theta_k$, and subsequently values of $\lambda_1$ and $\lambda_2$, using equations (12) or (13) and equation (9) and the maximum value of the finite shear strain can be found from (Ramsay 1967).

$$\gamma = \pm \frac{\lambda_1 - \lambda_2}{2(\lambda_1\lambda_2)^{1/2}}$$

ACKNOWLEDGEMENTS

It is a great pleasure to be able to acknowledge all those people who contributed to make this study possible.

I am grateful to Professor R.G. Mason for his guidance, generous financial support and critical review of the manuscript.

I am greatly indebted to Professor M. Niazi for his interest and encouragement throughout the course of this study, technical assistance and for making the Mashad University's seismographs available to me.

Dr. J. Brander contributed a great deal by assisting me with the Mekometer field work. I am also thankful to him for many fruitful discussions and critical review of the theses.

I have benefitted a lot from many discussions and field trips with Professor N. Ambraseys, Drs. D. McKenzie, G. King, R. Bilham, J.S. Tchalenko and their constant interest on the present study is highly appreciated.

Local transport and technical assistance provided by the University of Mashad and the Geological Survey of Iran and Centre for Planning of the Ministry of Science and Higher Education were crucial for the accomplishment of this work,which are acknowledged.

The Natural Environmental Research Council of the United Kingdom supported the east Iranian project and provided funds which enabled me to be employed as a Research Assistant for 2.5 years in the Geophysics Department of Imperial College, which is appreciated immensely.

I would like to thank greatly Dr. Froome, Mr. Bradsell and the Director of the National Physical Laboratory who kindly provided the prototype Mekometer used in 1971 and 1972 field work.

Aerial photographs and other unpublished geological maps were made available to me by the kind permission of Dr. Khadem, formerly Director of the Geological Survey of Iran, and great help was received from Dr. H. Nabavi, Dr. A. Houshmand-Zadeh and Mr. M. Berberian to whom I extend my sincere gratitude.

Thanks are due to Dr. Ariyi, Mr. H. Behzadi, Mr. Namdar, Mr. Ashori and Mr. Adabi of Mashad University for helping me with local preparations for several field trips, and to my colleague Mr. A. Hedayati, who assisted with part of the computing.

And last, but not least, I would like to appreciate my family for their support and tolerance in the years during which the deformation of eastern Iran dominated our lives. There are also special thanks due to my wife Minoo for typing the first draft and to Mrs. Flower for final typing of the manuscript.

List of other Contributions of the Author

Tchalenko, J.S., Iranmanesh, M.H. and A. Mohajer-Ashjai, 1972. The Babal-Kenar (1971) earthquake and the seismotectonics of the Central Alborz (Iran). Annali di Geofisica, XXV: 27-36.

Mahajer-Ashjai, A., 1974: Strain and slip measurements along active faults in the Tehran region, In, Materials for the study of seismotectonics of Iran, Geol. Surv. of Iran, Rep. No. 29: 139-155.

Mohajer-Ashjai, A., 1974. Determination of the polarity of unoriented basalt samples: A test of the anhysteritic and natural coercivity spectra comparative method. Can. J. Earth Sci., 11: 16 p.

Mohajer-Ashjai, A., Behzadi, H. and M. Berberian, 1975. Reflections on the rigidity of the Lut Block and recent crustal deformation in eastern Iran. Tectonophysics, 25: 19 p.

Mohajer-Ashjai, A. and G. Neilson in press. A study of microearthquake activity in Stirling area (central Scotland).

## CITED REFERENCES

Aggarwal, Y.P; L.R. Sykes, J. Armbruster and M.L. Sbar, 1973. Premonitory changes in seismic velocities and prediction of earthquakes. Nature, 24 : 101-104.

Aki, K., 1966. Earthquake generating stress in Japan for the years 1961 to 1963 obtained by smoothing the first motion radiation patterns. Bull. Earthquake Res. Inst. Tokyo Univ., 44 : 73-88.

Aki, K., 1969. Analysis ofthe seismic coda of local earthquakes as scattered waves. J. Geophys. Res., 74 : 615 - 631.

Allen, C.R., 1968. The tectonic environments of seismically active and inactive areas along the San Andreas Fault system in proceedings of conference on geologic problems of San Andreas Fault system. Editors W.R. Dickinson, A., Grantz.

Ambraseys, N. 1961 : The seismicity of southwest Asia. Revue pour l'etude des calamites 37, Geneva.

Ambraseys, N.N. and Tchalenko, J.S., 1969 : The Dasht-e-Bayaz (Iran) earthquake of August 31, 1968 : A field report. Bull. Seismo. Soc. Am., 59 : 1751-1792.

Asada, T., 1957. Observations of near-by microearthquake with ultrasensitive seismometer, J. Phys. Earth, 5 : 83-92.

Asada, T., Suyehiro, S. and K. Akomatu, 1958. Observations of near-by earthquakes with ultrasensitive seismometers at Matsushiro, Japan, J. Phys. Earth 6 : 23-33.

Bagdely, P.C., 1965. Structural and tectonic principles. Harper and Row, N.Y.

Barrel, E. and A. Sears, 1939. Phil. Trans. Royal Soc. London, Series A.

Bath, M. and H. Benioff, 1958. The aftershocks sequence of the Kamchatka earthquake of November 4, 1952. Bull. Seismo. Soc. Am., 48 : 1-15.

Bath, M. and S.J. Duda, 1964. Earthquake volume, fault plane area, seismic energy, strain deformation and related quantities.

Behzadi, H., 1972. Geological map of Dasht-e-Bayaz, University of Meshed. Internal rept.

Benioff, H., 1951. Earthquakes and rock creep. Bull. Seismo. Soc. Am., 41 : 31-62.

Benioff, H. and B. Gutenberg, 1951. Strain characteristics of the Earth's Interior in : Internal Constitution of the Earth. Dover publ., New York, N.Y., 439 PP.

Berberian, M., 1973 : Preliminary seismotectonic map of Iran. Geol. surv. Iran, Tehran.

Bisztricsany, E., 1958. A new method for the determination of the magnitude of earthquakes. Geofiz - Kozlemen., 7 : 69-96.

Bolt, B.A., 1960. The revision of earthquake epicenters, focal depths and origin times using a high-speed computer. Geophys. J., 3 : 433-440.

Brace, W.F. and J.D. Byerlee, 1970. California earthquakes; why only shallow focus? Science (AAAS), 168 : 1573-1575.

Brander, J.L., 1973. Geodetic measurements and the tectonics of Iceland. Ph.D. Thesis, University of London.

Bullard, E.C., J.E. Everett and A.G. Smith, 1965. The fit of the Continents around the Atlantic. A symposium on Continental drift, Phil. Trans. Roy. Soc. London, A, 1088 : 41-51.

Burford, R.D.,1968. Evidence of recent strain in the San Andreas Fault system from triangulation surveys. In proceedings of conference on geologic problems of San Andreas Fault system. Editors W.R. Dickinson and A. Grantz.

Cisternas, A., 1964. Percision determination of focal depths and epicentres of local shocks in California. Bull. Seism. Soc. Am., 53 : 1075-1083.

Chinnery, M.A., 1961. The deformation of the ground around surface faults. Bull. Seismo. Soc. Am., 51 : 355-372.

Chinnery, M.A., 1963. The stress changes that accompany strike-slip faulting. Bull. Seismo. Soc. Am., 53 : 921-932.

Chinnery, M.A., 1964. The strength of the earth crust under horizontal shear stress. J. Geophys. Res., 69 : 2085-1089.

Chinnery, M.A., 1966a. Secondary faulting, 1. Theoretical aspects. Can. J. Earth Sci., 3 : 163-174.

Chinnery, M.A., 1966b. Secondary faulting, 2. Geological aspects. Can. J. Earth Sci., 3 : 175-190.

Chinnery, M.A., 1969. Theoretical fault models. Publ. Dom. Astrophys. Obs. Ottawa, XXXVII., 7 : 211-223.

Chinnery, M.A. and D.A., Rodgers, 1968. The stress zone at the lower edge of a strike-slip fault. Trans. Am. Geophys. Union., 49 : 199.

Crampin, S., 1969. Aftershocks of the Dasht-e-Bayaz, Iran earthquake of August, 1968. Bull. Seism. Soc. Am., 59 : 1823-1843.

Crampin, S., 1970. A method for the location of near seismic events using travel times along ray paths. Geophys. J.R. astr. Soc., 21 : 535-539.

Crampin, S., A.W.B. Jacob, A. Miller and G. Neilson, 1970. The LOWNET radio-linked seismometer network in Scotland. Geophys. J.R. astr. Soc., 21 : 207-216.

Crampin, S. and P.L. Willmore, 1973. Small earthquakes observed with local seismometer networks. Phil. Trans. Ro. Soc. A : 383-387.

Crawford, A.R., 1972. Iran; continental drift and plate tectonics. 24th International Geological Congress, Section 3 : 106-112.

Crosson, R., 1972. Small earthquakes, structure and tectonics of Puget Sound region. Bull. Seism. Soc. Am., 62 : 1133-1173.

Dewey, J.F., Pitman, W.C., Ryan, W.B.F. and Bonnin, J., 1973. Plate tectonics and the evolution of the Alpin system. Bull. Geol. Soc. Am., 84 : 3137-3180.

Dimitrijevic, J., 1973. Geology of Kerman area. Geological Survey of Iran, Internal Rept. No. 1/4/52.

Brazangi, M. and J. Dorman, 1969. World seismicity map of ESSA coast and geodetic epicentre data for 1961-67. Bull. Seism. Soc. Am., 59 : 369-374.

Eftekhar-Nezhad, J., 1973. Kashmar quadrangle map, scale 1 : 250,000. Geol. Surv. of Iran, Tehran.

Eftekhar-Nezhad, J., 1974. A few speculations on the plate tectonics of eastern Iran and its relation with sedimentary basins of the region (in Persian), J. Tech. Faculty Tehran Univ. 2 : 218-227.

Evernden, J.F., 1970. Study of regions, seismicity and associated problems. Bull. Seism. Soc. Am., 60 : 393-446.

Evison, F.F., R. Robinson and W.J. Arabaz, 1973. Late aftershocks, tectonic stress and dilatancy. Nature, 246 : 471-472.

Flinn, E.A., 1960. Local earthquake location with an electronic computer. Bu-l. Seismo. Soc. Am., 50 : 467-470.

Frank, F.C., 1966. Deduction of earth strains from survey data. Bull. Seismo. Soc. Am., 56 : 35-41.

Freund, R., 1974. Kinematic of transform and transcurrent faults. Tectonophysics, 21 : 93-134.

Froome, K.D., and R.H. Bradsell, 1966. A new method for the measurement of distances up to 5000 feet by means of a modulated light beam. J. Sci. Instr., 43 : 129-134.

Froome, K.D., 1971. Mekometer III; E.D.M. with sub-millimetre resolution. Surv. Review, 21 : 98-105.

Furon, R., 1941. Geologic du plateau Iranian, Perse-Afghanistan-Beloutchiston. Meu Mus. Nat. Hist. Paris, N.S., 7 : 177-414.

Gansser, A., 1955. New aspects of the geology in central Iran. Proc. 4th world petrol. Congr. Sect. 1/A/5 : 279-300.

Gutenberg, B., 1941. Mechanism of faulting in South California indicated by seismograms. Bull. Geal. Soc. Am., 31 : 263-302.

Gutenberg, B., 1951. Summary of colloquium on plastic flow and deformation within the earth. J.R.B., 539-543.

Healy, J.H., W.H.K. Lee, L.C. Pakiser, C.B. Raleigh and M.D. Wood, 1972. Prospects for earthquake prediction and control. In : Forerunners of strong earthquakes. Tectonophysics, 14(3/4) : 319-332.

Hedin, S., 1918 1927. Eine Routenaufnahme durch Ostpersien: Stockholm (Generalst. Lit. Anst.), 1(1918) : 139 P., 2(1927) : 548 P.

Hess, H.H., 1962. History of the ocean basin, in petrologic studies, Buddington memorial volume, P. 599, Geological Society of America.

Hofman, R.B., 1968 : Geodimeter fault movement investigations in California. Calif. Dept. Water, Res. Bull., 6 : 116-121.

Howard, J.H., 1968. Recent deformation of the Cholame and Taft. Maricopa areas, California. In : proceedings of conference on geologic problems of San Andreas Fault system.

Huckridge, R., Kurstsen, M. and Venzlaff, H., 1962. Sur geologie des gebiets zwischen Kerman und Sagand (Iran). Beih, Geol. Jahrb., 51 : 197 p.

Institute of Geophysics, Tehran University, 1963. Bouguer gravity anomaly map of I ran., Tehran University. Publication No. 22, 1965.

Isacks, B. and J. Oliver, 1964. Seismic waves with frequencies from 1 to 100 cycles per second recorded in a deep mine in northern New Jersey. Bull. Seismo. Soc. Am., 54 : 1941-1955.

James, D.E., I.S. Sacks; L.E. Lazo; G.P. Aparico, 1969. On locating local earthquakes using small networks. Bull. Seismo. Soc. Am., 59 : 1201-1212.

Kaveh, H. and I. Solehi, 1972. The results of magnetic surveys in Iran, proceedings of 24th Intern. Geol. Long., Section 9 : 16-24.

Lammlein, D.R, M.L. Shar and J. Dorman, 1971. A microearthquake reconnaissance of southeastern Missouri and western Tennessee. Bull. Seismo. Soc. Am., 61 : 1705-1716.

Lee, W.H., R.E. Bennett and K.L. Meagher, 1972. A method of estimating the magnitude of local earthquakes from signal duration, U.S. Geol. Surv. Open file report.

Lensen, G.J., 1960. Principal horizontal stress directions as an aid to the study of crustal deformation. Publ. Dominion Obs. Ottawa XXIV310 : 389-397.

McKenzie, D.P. and R.L. Parker, 1967. The north pacific; an example of tectonics on a sphere. Nature, 216 : 1276-1279.

McKenzie, D., 1969. The relation between fault plane solutions for earthquakes and the directions of the principal stresses. Bull. Seismo. Soc. Am., 59 : 591-601.

McKenzie, D.P., 1970. The plate tectonic of the Mediterranean region, Nature, 226 : 239-242.

McKenzie, D., 1972. Active tectonics of the Mediterranian region. Geophys. J. R. astr. Soc., 30 : 109-185.

McKenzie, D. and Sclater, J.G., 1971. The evolution of the Indian Ocean since the Late Cretaceous. Geophys. J. R. astr. Soc., 241 : 437-528.

Mogi, K., 1962a. Study of elastic shocks caused by the fracture of heterogeneous materials and its relations to earthquake phenomena. Bull. Earthquake Res. Inst. Tokyo Univ., 40 : 125-174.

Mogi, K., 1962b. Magnitude frequency relation for elastic shocks accompanying fractures of various materials and some related problems in earthquakes. Bull. Earthquake Res. Inst. Tokyo Univ., 40 : 831-854.

Mogi, K., 1963. Some discussions on aftershocks, foreshocks and earthquake swarms. The fracture of a semi-infinite body caused by an inner stress origin and its relation to the earthquake phenomena, 3, Bull. Earthquake Res. Inst. Tokyo Univ., 41 : 615-658.

Mohajer-Ashjai, A., 1974. Strain and slip measurements along active faults in the Tehran region. In, Material for the study of seismotectonics of Iran. Geol. Surv. of Iran. Rep. No. 29 : 139-155.

Mohajer-Ashjai, A., Behzadi, H. and M. Berberian, 1975. Reflections on the rigidity of the Lut Block and recent crustal deformation in eastern Iran. Tectonophysics, 25 : 19 P.

Mohajer-Ashjair, A., and G. Neilson (in press). A study of micro-earthquake activity in Stirling area (central Scotland).

Moody, J.D., 1973. Petroleum exploration aspects of wrench-fault tectonics. Am. Assoc. pet. Geol. Bull., 57 : 449-476.

Moody, J.D. and Hill, M.J., 1956. Wrench fault tectonics. Bull. Geol. Soc. Am., 67 : 1207-1215.

Morgan, W.J., 1968. Rises, trenches, great faults and crustal blocks. J. Geophys. Res., 73 : 1959-1982.

Nabavi, M.S., 1972. The seismicity of Iran. M. Phil. Thesis, Imperial College, University of London.

National Iranian Oil Company, 1959. Geological map of Iran 1 : 2,500,000 with explanatory notes, Nat. Iran. Oil Co. Tehran.

Nersesov, I.L., A.N. Semonova and I.G. Simbireva, 1969. In the physical basis of foreshocks (Nauka, Moscow).

Niazi, M., 1969. Source dynamics of the Dasht-e-Bayaz earthquake of 1968 August 31. Bull. Seismo. Soc. Am., 59 : 1843-1862.

Nordquist, J.M., 1962. A special purpose programme for earthquake location with an electronic computer. Bull. Seismo. Soc. Am., 52 : 431-437.

Nowroozi, A.A., 1971. Seismotectonics of the Persian plateau. Bull. Seismo. Soc. Am., 61 : 317-341.

Nowroozi, A.A., 1972. Focal mechanism of earthquakes in Persia, Turkey, West Pakistan and Afghanistan and plate tectonics of the Middle East. Bull. Seismo. Soc. Am., 62 : 823-850.

Pavoni, N., 1971. Recent and late Cenozoic movements of the earth's crust. Recent crustal movement. A symposium. Roy. Soc. New Zealand Bull. 9 : 7-17.

Pitman, W.C., Talwani, M. and Heirtzler, J.R., 1971. Age of the North Atlantic Ocean from magnetic anomalies. Earth planet. Sci. Lett., 11 : 195-200.

Ramsay, J.G., 1967. Folding and fracturing of rocks. McGraw Hill, N.Y., 568 p.

Real, C.R. and T.L. Teng, 1974. Local richter magnitude and total signal duration in southern California. Bull. Seismo. Soc. Am., 63 : 1809-1827.

Reid, H.F., 1910. The mechanics of earthquakes in the California earthquake of April 18th, 1906, report of the state earthquake commission 2; Carnegie Institute of Washington D.C.

Richter, C.H., 1935. An instrumental earthquake scale. Bull. Seismo. Soc. Am., 25 : 1-35.

Richter, C.H. and B. Gutenberg, 1956. Seismicity of southern California. Calif. Div. of Min. Bull. 170 : 19-25.

Ringwood, A.E., 1968. Composition and evolution of the upper mantle. In; the earth's crust and upper mantle, editor P.J. Hart, geophysical monograph 13. A.G.U.

Ruttner, A., Nabavi, M. and Hajian, J., 1968. Geology of the shirgesht area (Tabas area, east Iran). Geol. Survey Iran Rept. No. 4, 113 p.

Rybicki, K., 1973. Analysis of aftershocks on the basis of dislocation theory. Physics of the earth and planetary interiors., 7 : 409-422.

Rikitake, T., 1974. Probability of earthquake occurrence as obtained from crustal strain. Tectonophysics, 23: 299-312.

Savage, J.C. and R.O. Burford, 1970. Accumulation of tectonic strain in California. Bull. Seismo. Soc. Am., V.60, P. 1877.

Savage, J.C. and R.O. Burford, 1973. Geodetic determination of the relative plate movement in central California. J. Geophy. Res., 78 : 832-836.

Scholz, C.H., 1968a. Micro-fracturing and the inelastic deformation of rock in compression, J. Geo. Phys. Res. 73 : 1417-1432.

Scholz, C.H. 1968b. The frequency-magnitude relation of microfaulting in rock and its relation to earthquakes, Bull. Seismo. Soc. Am., 58 : 399-415.

Scholz, C.H. and T.J. Fitch, 1969. Strain accumulation along the San Andreas Fault, J. Geophys. Res. 74 : 2049-2060.

Scholz, C.H., L. Sykes and Y. Aggarwal, 1973. Earthquake prediction; a physical basis, Science, 181 : 803-810.

Seeber, L., M. Barazangi and A. Nowroozi, 1970. Microearthquake Seismicity and tectonic of coastal northern California. Bull. Seismo. Soc. Am., 60 : 1669-1699.

Stocklin, J., 1961. Lagoonal formations and salt domes in eastern Iran. Petrol. Inst. No. 3 : 22-46.

Stocklin, J., 1968. Structural history and tectonics of Iran. A review. Am., Assoc. petrol. Geol., 52 : 1229-1258.

Stocklin, J. and Nabavi, M.H., 1971. Boshruyeh quadrangle map, scale 1 : 250,000 with explanatory text. Geol. Survey Iran, Tehran.

Stocklin, J., Eftekhar-Nezhad, J. and Hushmand-Zadeh, A., 1965. Geology of the Shotori range (Tabas area, eastern Iran). Geol. Survey Iran Rept. No. 3, 69 p.

Stocklin, J., Eftekhar-Nezhad and Hushmandzadeh, A., 1972. Geological reconnaissance map of Central Lut., Geol. Survey Iran Rept.

Sykes, L.R., 1966. The seismicity and deep structure of island arcs. J. Geophys. Res., 71 : 2981-3006.

Sykes, N.R., 1970. Earthquake swarms and sea-floor spreading. J. Geophys. Res., 75 : 6598-6611.

Takin, M., 1972. Iranian geology and continental drift in the Middle East. Nature, 235 : 147-150.

Tchalenko, J.S., 1973. The Kashmar (Turshiz) 1903 and Torbat-e-Heidariyeh (South) 1923 earthquakes in central Khovassan (Iran). Ann. Geophy. 10 : 250-255.

Tchalenko, J.S., Berberian, M. and Behzadi, H., 1973. Geomorphic and seismic evidence for recent activity on the Doruneh Fault, Iran. Tectonophysics 19 : 333-341.

Tchalenko, J.S., J. Braud and M. Berberian, 1974. Discovery of three earthquake faults in Iran. Nature, 248 : 661-663.

Tectonic map of Iran, 1971, 1973, scale 1 : 250,000. Geological Survey of Iran, Tehran.

Tsumura, K., 1967. Determination of earthquake magnitude from total duration of oscillation., Bull. Earthquake Res. Institute, Tokyo Univ., 15 : 7-18.

Vialon, P., M. Sabzehi and A. Houshmand-Zadeh, 1972. Proposition of a petro-structural evolution model of some Iranian mountains, as a consequence of plate tectonics. Int. Geol. Congr., 24 : 104.

Wadge, J., 1974. Volcanic deformation and eruption mechanism on Mont Etna. Ph.D. Thesis, University of London.

Wegener, A., 1924. The origin of continents and oceans, 4th edition, Methuen, London.

Wellman, H.W., 1966. Active wrench faults of Iran, Afghanistan and Pakistan, Geol. Rdsch., 55 : 716-735.

Whitcomb, J.H., J.D. Garmany and D.L. Anderson, 1973. Earthquake prediction : variation of seismic velocities before the San Fernando earthquakes. Science, 180 : 632-635.

Whitten, C.A., 1948. Horizontal earth movement in the vicinity of San Francisco, Calif., Trans. Am. Geophys. Union, 29 : 318-328.

Whitten, C.A., 1955. Measurements of Earth movements in California. Calif. Div. Mines Bull. 171 : 75-83.

Whitten, C.A., 1958. Notes on remeasurement of triangulation net in the vicinity of San Francisco. Calif. Div. of Mines. Spec. Rep., 57 : 56-59.

Whitten, C.A., 1960. Horizontal movement in the earth's crust. J. Geophys. Res., 65 : 2839-2849.

Whitten, C.A. and C.N. Claire, 1960. Analysis of geodetic measurements along the San Andreas Fault. Seismo. Soc. Bull. Am., 50 : 404-415.

Wilcox, R.E., Harding, T.P. and Seely, D.R., 1973. Basic wrench tectonics. Am., Assoc. pet. Geol. Bull. 57 : 74-96.

Yanshin, A.L., 1966. Tectonic map of Eurasia. Int. Geol. Congr., 22nd, India. Comm. Geol. Map World, Sci. Commun: 103-109.